FULL–SCALE FLOOR SYSTEM TESTING FOR FUTURE HOT-ROLLED ASYMMETRIC STEEL I-BEAMS

A Thesis

by

SHEYENNE DAVIS

Submitted to the Graduate and Professional School of
Texas A&M University
in partial fulfillment of the requirements for the degree of

MASTER OF SCIENCE

Chair of Committee,	Matthew Yarnold
Committee Members,	Peter Keating
	Zofia Rybkowski
Head of Department,	Zachary Grasley

May 2022

Major Subject: Civil Engineering

ABSTRACT

The residential building market has long been dominated by concrete floor systems due to their shallow depth, which allows for more floors in multi-story buildings. However, hot-rolled asymmetric I-beams, or A-shapes, are a path forward to enable structural steel into the residential market. The wider bottom flange allows for their use in shallow-depth steel-concrete composite floor systems since the bottom flange can support precast concrete panels. Overall, this type of floor system is shallower than traditional steel-concrete composite floor systems and faster to construct.

This research study involved the design and experimental testing of a shallow-depth steel-concrete floor system to further the knowledge of A-shapes in such systems. This information will eventually lead to standardized A-shapes. The floor system concept consists of A-shapes, precast hollow-core concrete panels, and a cast-in-place concrete slab. The testing involved taking measurements during construction, which included the placement of the panels and concrete pour, service loading, and loading of the system to failure.

The major unknown parameters included the system's constructability, the system's stability during construction, how well the system would perform under live load, and the level of composite action. This experiment revealed the system was constructed easily and quickly and remained stable during construction. The system performed well under service live load (100 psf), experiencing deflections equivalent to L/3000. The system failed due to the bond breaking between the concrete and steel,

going non-composite after experiencing partially composite behavior. This occurred at an actuator load equivalent to 500 psf, or five times the service live load. All of this indicates the floor system proposed in this test is a legitimate path forward to faster construction and shallower floor systems for use in steel residential floor system design. This validates the need for the research and development of standardized A-shapes in the United States.

DEDICATION

I would like to dedicate this thesis to all the women in engineering I have had the pleasure of meeting over the past six years. Thank you for your wisdom, encouragement, and friendship, and thank you for inspiring me to never give up.

ACKNOWLEDGMENTS

I would like to thank my committee chair, Dr. Yarnold, for his guidance and support throughout this research. I cannot thank him enough for allowing me to be a part of such a unique and interesting project and for giving me the resources to succeed. My committee members, Dr. Keating and Dr. Rybkowski, also deserve thanks for providing their expertise to this research. I would also like to thank everyone at the RELLIS High Bay Lab, including Charlie and Kirk, for their help with the testing and teaching me.

Thanks also go to Eric Stoddard for being a great teacher and letting me borrow many books. To all my friends, thank you for cheering me on and listening to me talk about my research.

Thank you to my family, but especially Mom and Dad, for your love and encouragement and for teaching me to aim high. Finally, thanks to my fiancé, Ryan, for being my biggest supporter, for making me laugh when I want to cry, and for believing in me every step of the way.

CONTRIBUTORS AND FUNDING SOURCES

Contributors

The work of this thesis was supervised by a committee consisting of Dr. Matthew Yarnold, the committee chair, and Dr. Peter Keating from the Department of Civil and Environmental Engineering, as well as Dr. Zofia Rybkowski from the Department of Construction Science.

The work previously done on this project, referenced in Section 4.3, was conducted by Eric Stoddard, a Ph.D. student, and Dr. Matthew Yarnold, an assistant professor of the Department of Civil and Environmental Engineering. The lab testing was conducted in the High Bay Lab in the Center for Infrastructure Renewal on the Texas A&M RELLIS campus. The testing was made possible by the Lab Director, Dr. Peter Keating, Lab Manager Charlie Droddy, and Facilities Manager Kirk Martin.

Funding Sources

This work is part of the project "Behavior of Hot Rolled Asymmetric Steel I-Beams," which is funded by the 2020 American Institute for Steel Construction (AISC) Milek Fellowship. The Graduate Diversity Excellence Fellowship from Texas A&M University also helped fund this work.

NOMENCLATURE

AIB	Asymmetric I-beam (built-up or hot-rolled)
ASB	Asymmetric *Slimflor*® Beam
A-shape	Hot-rolled asymmetric I-beam
AISC	American Institute of Steel Construction
CoSFB	Composite Slim-Floor beam
E	Modulus of elasticity
e	Location of the eccentric load from the beam centerline
EI	Flexural rigidity
F_y	Yield strength
f'c	Concrete compressive strength
G	Shear modulus
I_x	Second moment of area about the x-axis
IBC	International Building Code
kN/m^2	Kilonewtons per square meter
ksi	Kips per square inch
LTB	Lateral-torsional buckling
pcf	Pounds per cubic foot
psf	Pounds per square foot
W-shape	Hot-rolled doubly symmetric wide-flange I-beam

TABLE OF CONTENTS

Page

LIST OF FIGURES

Page

LIST OF TABLES

Page

1. INTRODUCTION

Structural steel is a reliable building material used for a variety of projects, from high-rise buildings to sports stadiums. Steel members used as beams and columns come in a variety of shapes, with a common one being an I-shape, which can include W-, M-, S-, and HP-Shapes [1]. A general I-shape is shown in Figure 1.1a, which is doubly symmetric. Asymmetric I-beams (AIBs), shown in Figure 1.1b, have two flanges and a web like its doubly symmetrical counterpart, but its top flange is narrower than its bottom flange.

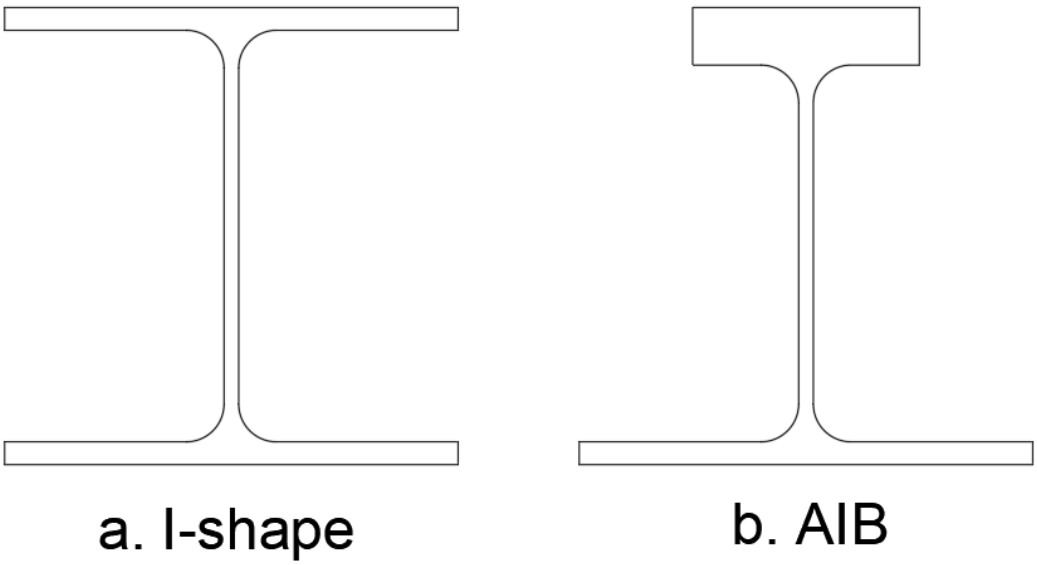

Figure 1.1: Cross-section of (a) a General I-shape and (b) an AIB

AIBs are especially advantageous when used in composite floor systems. Steel floor systems are typically composite, consisting of I-shaped beams, a steel deck, and a concrete slab, as shown in Figure 1.2. Steel floor systems are not common in residential

buildings because their floor systems typically need to be on the shallower side. Concrete floor systems are preferred because their lack of decking allows for a shallow floor system.

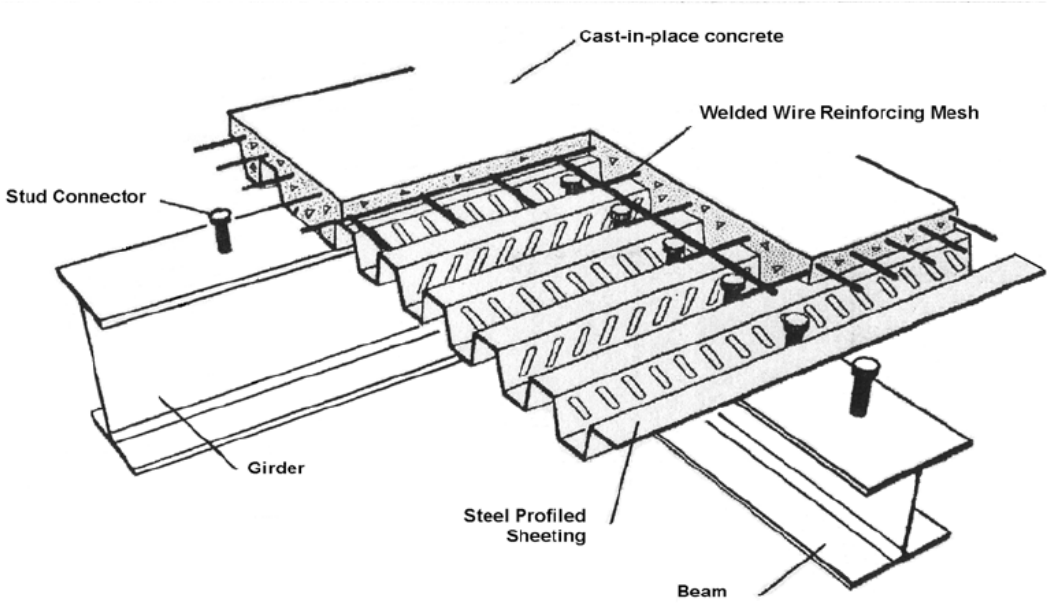

Figure 1.2: Typical composite steel floor system [2]

AIBs are a path forward for steel floor systems to be used in residential buildings. The smaller top flange allows for the use of a less conventional floor system, shown in Figure 1.3. Rather than the traditional composite floor system, this one consists of precast hollow-core concrete panels (termed precast panels herein) set on the bottom flange with a cast-in-place concrete slab. As discussed in Section 3.1.3, there are floor systems that take advantage of this arrangement, but most use built-up AIBs rather than a hot-rolled asymmetric beam (termed A-shapes herein).

This new configuration is both shallower and faster to construct than the traditional steel composite floor system. The American Institute of Steel Construction

(AISC) has a “need for speed” initiative to “increase the speed at which a steel project (either a building or a bridge) can be designed, fabricated, and erected by 50% by the end of 2025” [3]. The use of A-shapes in a configuration like Figure 1.3 can help accomplish this goal.

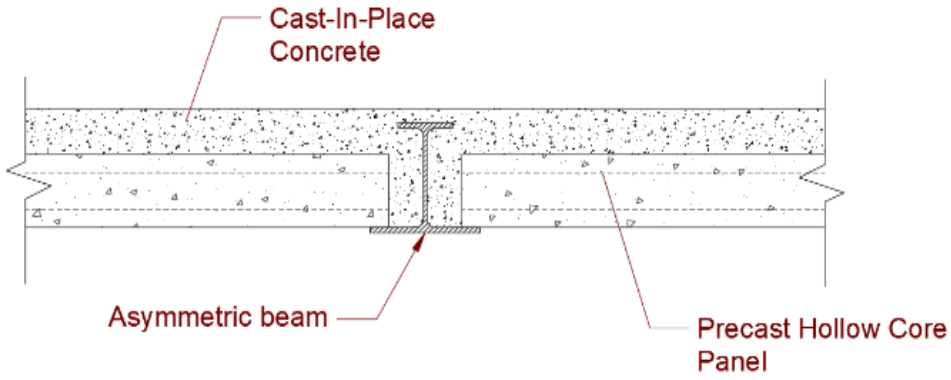

Figure 1.3: Shallow composite steel floor system

This research is part of the 2020 AISC Milek Fellowship project “Behavior of Hot Rolled Asymmetric Steel I-Beams.” The overall goal of this project is to develop future standardized A-shapes for use in the United States. This research specifically aims to further the knowledge of shallow-depth steel-concrete floor systems utilizing A-shapes, which will influence the development of standardized shapes. This was accomplished through the design and execution of a full-scale floor system test and subsequent analysis. The floor system was of the configuration shown in Figure 1.3, and the experimental testing consisted of 3 stages: construction, service live loading, and failure loading. The specific research objectives are discussed in the following section.

2. RESEARCH OBJECTIVES

This research investigates shallow-depth steel-concrete floor systems utilizing A-shapes, with a focus on their use in residential buildings. This work addresses the knowledge gaps in such systems, which will aid in the development of standardized A-shapes. The methods of this research are both experimental and numerical. A full-scale floor system was designed, built, and tested, and the results from the testing were compared with theoretical calculations. The information gathered from this research is measured per the following objectives.

1. Evaluate the constructability of the system for speed and ease of assembly for each of these stages:
    - Fabrication
    - Steel erection
    - Panel placement
    - Deck casting
2. Evaluate the system structural performance during construction (panel placement and concrete pour) through characterization of A-shape behavior, including:
    - Beam stability
    - Bending and torsional restraint
    - Controlling limit states
3. Evaluate the system structural performance under service live load
    - Identify the flexural rigidity of the system

- Verify linear composite behavior

4. Evaluate the ultimate strength of the system under vertical loading
    - Determine the failure mechanism
    - Quantify the ultimate capacity

3. LITERATURE REVIEW

This literature review is split into two main sections: asymmetric I-beams and floor system testing. The information on asymmetric I-beams includes why they are used, what problems there are to consider, and their use in floor systems. The floor system utilizing Asymmetric *Slimflor*® Beams, discussed in Section 3.1.3.4, is especially interesting as it is similar to the floor system design in this research. The second main section covers various floor system tests with a focus on their configurations and loading.

3.1. Asymmetric I-Beams (AIBs)

3.1.1. Advantages and Disadvantages

A big advantage of AIBs is that they are more efficient than standard I-beams in terms of flexural strength. Conventional composite floor systems like the one shown in Figure 1.2 normally have a neutral axis in or close to the top flange of the steel beam when subject to bending [4]. In this configuration, the top flange has minimal contribution to the flexural capacity of the system, which means the area of the top flange can be reduced without a significant reduction in how the system performs. In this configuration, asymmetric shapes are more efficient in terms of the strength per amount of steel.

AIBs are also advantageous to use in composite floor systems like the one shown in Figure 1.3. As discussed later in Section 3.1.3, these floor systems have been primarily made with built-up AIBs, but hot-rolled AIBs (termed A-shapes) have been

utilized as well. The advantage of using the A-shape is that it reduces the time in manufacturing and construction.

One of the biggest disadvantages of an AIB is the local and global stability. When the AIBs are in their non-composite states of construction, they are subject to large unbraced lengths, making lateral-torsional buckling (LTB) and local buckling of particular concern due to the smaller compression flange [4, 5]. Additionally, the bottom flange can experience local transverse bending. The AIBs should be designed so that they can resist the combined torsion and bending load experienced during construction [6].

3.1.2. Hot-Rolling Challenges

The major mills in the United States (e.g., Nucor, Steel Dynamics, and Gerdau) do not hot-roll A-shapes. Stoddard and Yarnold searched for mills around the world that do and found only one, British Steel, which hot-rolls ten A-shapes [4]. These A-shapes are referred to as ASB, or Asymmetric *Slimflor*® Beams, which is a registered trademark of Corus Construction and Industrial [6, 7]. These are A-shapes with a 0.6 ratio of the area of the top flange to the area of the bottom flange.

There are challenges with hot-rolling an A-shape. Due to the asymmetric nature, the beams will cool unevenly, which can induce deformations and residual stresses into the beam [4]. Residual stresses are something that have to be dealt with in conventional hot-rolled beams as well, but those patterns are well-understood. For example, Alpsten found that the major factors that affect the formation of residual stresses are the geometry of the shape as well as the cooling factors [8]. Additionally, Quayyum and

Hassan developed an advanced numerical technique that can accurately simulate residual stresses in hot-rolled wide-flange members [9]. Meanwhile, residual stresses of A-shapes are not well-studied. Residual stresses can affect the LTB behavior of the beam, which is especially concerning with A-shapes since LTB is a critical limit state.

Before the work of this thesis began, Yarnold and Stoddard met with Nucor and Steel Dynamics, and later, met with Gerdau. Representatives from all three expressed what challenges they anticipate experiencing with hot-rolling A-shapes. The big takeaways were: (1) a large difference in flange areas make it more difficult to roll the shapes, (2) a thicker top flange could help with cooling, and (3) the workability and rolling of the shape would be a trial and error process [10-12]. As evidenced by the ASB sections British Steel rolls, it is definitely possible to hot-roll A-shapes, but standardizing the process in the United States may take time.

3.1.3. Use in Floor Systems

There are certain floor systems that take advantage of AIBs in a configuration similar to the one shown in Figure 1.3. The ones produced in the United States, including GIRDER-SLAB®, Slim-Floor, and COMSLAB®, use built-up AIBs, while companies in the United Kingdom use ASB.

3.1.3.1. GIRDER-SLAB® [13]

Girder-Slab Technologies, LLC has developed the D-BEAM® Girder, a manufactured AIB used with precast concrete panels to create a shallow composite floor system [13]. The D-BEAM®, shown in Figure 3.1, is constructed by first cutting a traditional wide-flange beam in half through the web, producing two identical tee

sections. In order to have openings in the web, the beam is cut in a castellated pattern, as shown in Figure 3.2. A flat bar is then welded to the top of the web to create a smaller top flange. The precast panels can then sit on top of the bottom flange, and concrete topping may be used, if desired. A rendering of the system can be seen in Figure 3.3.

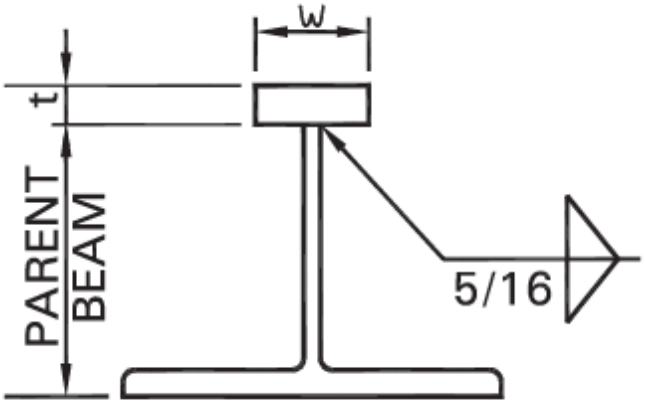

Figure 3.1: D-BEAM® Girder [13]

Figure 3.2: Castellated pattern cut to make D-BEAM® girder [13]

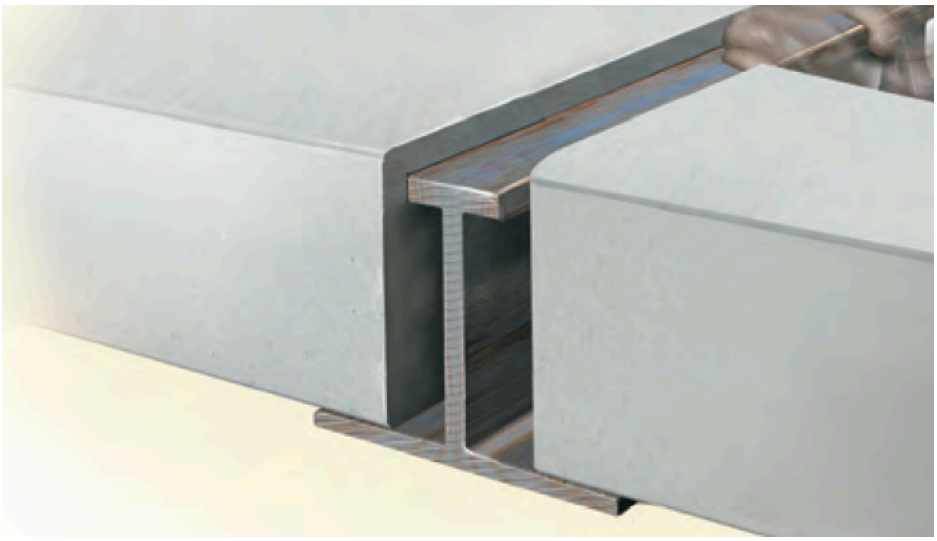

Figure 3.3: Floor system using D-BEAM® girder [13]

3.1.3.2. Slim-Floor by ArcelorMittal

ArcelorMittal has developed both their Slim-Floor beam and their Composite Slim-Floor beam (CoSFB) [14]. Their Slim-Floor beam configuration, shown in Figure 3.4a, consists of a conventional wide-flange beam with a plate welded to its bottom flange. This plate is wide enough to support a slab element, and the entire system is topped with cast-in-place concrete. The CoSFB configuration, shown in Figure 3.4b, is similar but has dowels connecting the steel to the cast-in-place concrete to ensure composite action and increase the strength of the system. The Slim-Floor beam can span up to 26.2 feet (8 meters), while the CoSFB can span up to 45.9 feet (14 meters).

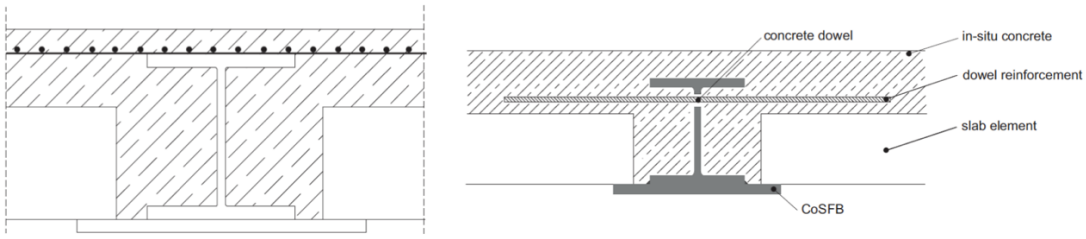

(a) Slim-Floor Beam Configuration

(b) CoSFB Configuration

Figure 3.4: (a) Slim-Floor Beam and (b) CoSFB [14]

3.1.3.3. COMSLAB®

Bailey Metal Products Ltd. has developed COMSLAB®, shown in Figure 3.5 [15]. Similar to ArcelorMittal's Slim-Floor beam configuration, COMSLAB® consists of a wide-flange beam with a plate welded to its bottom flange, as well as a deck sitting on that plate and a cast-in-place slab to hold it all together. There is mesh and rib reinforcement, and the deck is fastened to the steel plate.

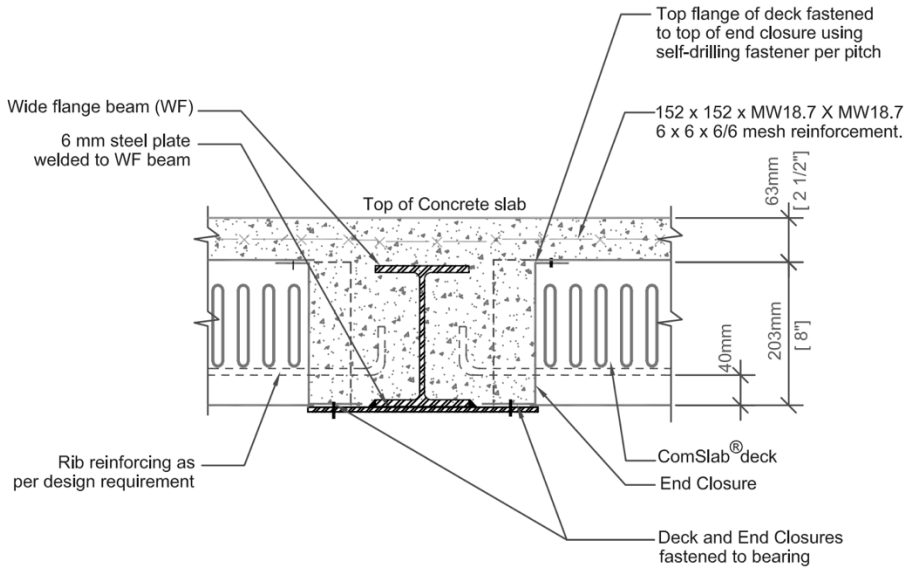

Figure 3.5: COMSLAB® [15]

3.1.3.4. Asymmetric *Slimflor*® Beams

Since this floor system uses hot-rolled AIBs, it is similar to the floor system designed in this research and is of particular interest. This floor system, developed by Corus Construction and Industry, is comprised of ASB with precast concrete slabs and can be constructed in two ways [6]. Type 1 construction, shown in Figure 3.6, does not include a concrete topping, but still requires an infill of cast-in-place concrete. Type 2 construction, shown in Figure 3.7, includes a concrete topping and tie reinforcement to connect the steel and cast-in-place concrete.

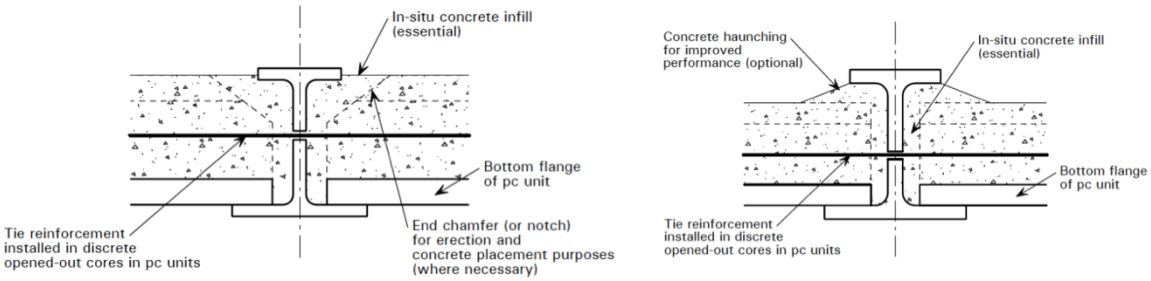

Figure 3.6: ASB Floor System: Type 1 construction [6]

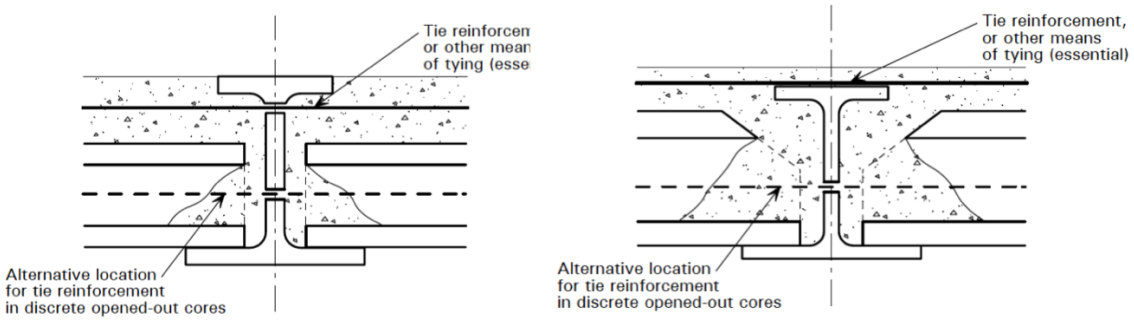

Figure 3.7: ASB Floor System: Type 2 construction [6]

Rackham et al. published a paper on the design of ASB with precast panels [6]. This contained plenty of information regarding ASB and the floor system itself, but the practical considerations and design loading cases were the most integral aspects of designing our own system.

3.1.3.4.1. Practical Considerations

The following are considerations that must be made when designing such a floor system:

1. **Nominal bearing length of the concrete panel on the ASB flange:** If there isn't enough of a bearing length, there is a risk of the panels falling off the

bottom flange. The amount of bearing length will depend on each system, but for ASB spaced between 4.9 to 36.1 feet (1.5 to 11 meters), the practical nominal bearing length is 3.2 inches (80 millimeters), and the minimum is 1.6 inches (40 millimeters).

2. **Geometric limitations and end preparations of precast panels:** The concrete panels are installed by placing one side on one flange and then lowering the other side, as shown in Figure 3.8. In order to fit the panel in, there needs to be at least 2.7 inches (60 millimeters) between the panel and ASB, and the ends of the panels may need to be chamfered or notched, as shown in Figure 3.9.
3. **Transverse tying reinforcement placement:** When needed, the transverse reinforcement is installed through the cores in the precast panels. This is done by opening part of the top of a core so the reinforcement can be placed and the cast-in-place concrete can fill the space, as shown in Figure 3.9. In order to block the wet concrete from filling entire voids, polystyrene bung or something similar is used to block the holes.

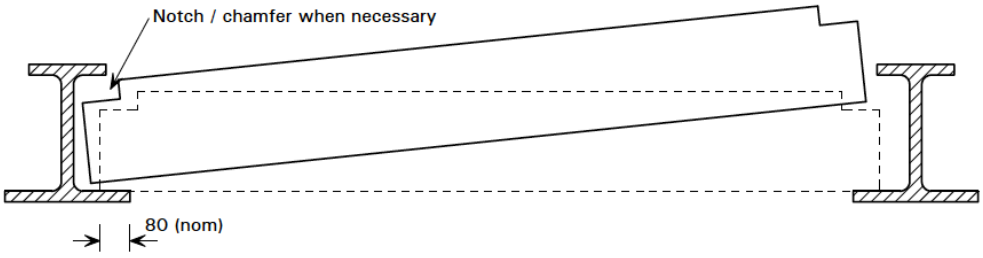

Figure 3.8: Concrete panel installation [6]

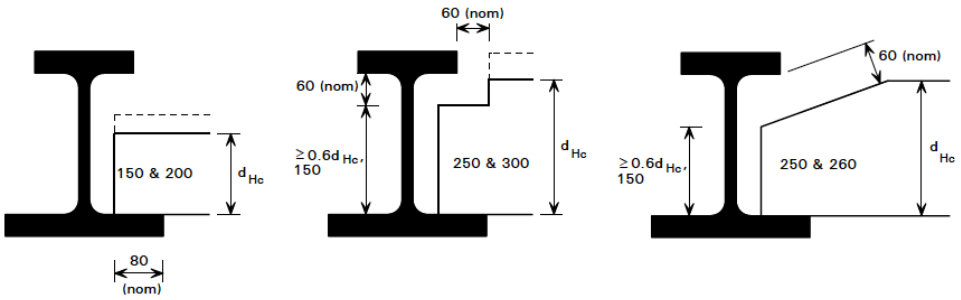

Figure 3.9: Concrete panel end preparations [6]

4. **Type and detailing of edge beams:** Special consideration must be made for the edge beams for a few reasons, notably because they experience eccentric loading and transfer diaphragm forces into columns. ASB beams may be used, but other beams are also allowed, including rectangular hollow sections (RHS) or built-up asymmetric shapes.
5. **Stability of ASB during precast panel installation:** The installation of the precast panels can cause eccentric loading on the beams that must be considered. Temporary restraints can be used if necessary; however, they are usually not needed because the beams are designed to resist these construction loads. Severe torsion will be induced if one side of an ASB has precast panels and topping while the other side has nothing. This instance of construction loading should be avoided.

3.1.3.4.2. Design Considerations

The following are the design cases and requirements that must be considered to ensure the strength and stability of such a floor system.

3.1.3.4.2.1. Construction Design Loading Cases

For Type 1 construction (no concrete topping):

(i) Precast panels and construction live loading on one side

(ii) Precast panels on both sides, construction live loading on one side (unlikely to be critical unless span lengths are different)

(iii) Precast panels and construction live loading on both sides

The following are the principal design checks for each design case:

- Cases (i) and (ii)
    - LTB: bending and torsion
    - Local capacity: bending and torsion
    - Twist
- Case (iii)
    - LTB: bending
    - LTB: torsion (only if span lengths are different)
    - Local capacity: bending and torsion (only if span lengths are different)

For Type 2 construction (concrete topping):

(i) Precast panels and construction live loading on one side

(ii) Precast panels on both sides, topping and construction live loading on one side

(iii) Precast panels and topping on both sides, construction live loading on one side (unlikely to be critical unless span lengths are different)

(iv) Precast panels, topping, and construction live loading on both sides

(v) Precast panels, topping, and construction live loading on one side

The following are the principal design checks for each design case:

- Cases (i), (ii), (iii), and (v)
    - LTB: bending and torsion
    - Local capacity: bending and torsion
    - Twist
- Case (iv)
    - LTB: bending
    - LTB: torsion (only if span lengths are different)
    - Local capacity: bending and torsion (only if span lengths are different)

3.1.3.4.2.2. Normal Stage Design Loading Cases

For Type 1 construction (no concrete topping):

(i) Precast panels and superimposed dead load on both sides and imposed load on one side

(ii) Precast panels, superimposed dead load, and imposed load on both sides

The following are the principal design checks for each design case:

- Case (i)
    - LTB: bending and torsion (unnecessary if restraint is assumed)
    - Local capacity: bending and torsion
- Case (ii)

- LTB: ending (unnecessary if restraint is assumed)
- Shear capacity check on ASB and precast panel
- Bending capacity
- Fire resistance
- Dynamic response
- Deflections
- Irreversible deformation/stress check

For Type 2 construction (concrete topping):

(i) Precast panels, topping, and superimposed dead load on both sides and imposed load on one side

(ii) Precast panels, topping, superimposed dead load, and imposed load on both sides

The following are the principal design checks for each design case:

- Case (i)
  - Local capacity: bending and torsion
- Case (ii)
  - Bending capacity
  - Shear capacity check on ASB and precast panel
  - Fire resistance
  - Dynamic response
  - Deflections
  - Irreversible deformation/stress check

3.1.3.4.2.3. Requirements for Limited Composite Behavior

For Type 1 construction or edge beams in Type 2 construction, non-composite behavior is assumed since there is insufficient concrete encasement to create the composite bond. Type 2 construction has sufficient concrete encasement, but due to the lack of test data, it is safer to assume non-composite behavior. However, for serviceability calculations for Type 2 construction internal beams, composite behavior can be assumed. Figure 3.10 shows the geometric concrete encasement requirements for assuming composite behavior.

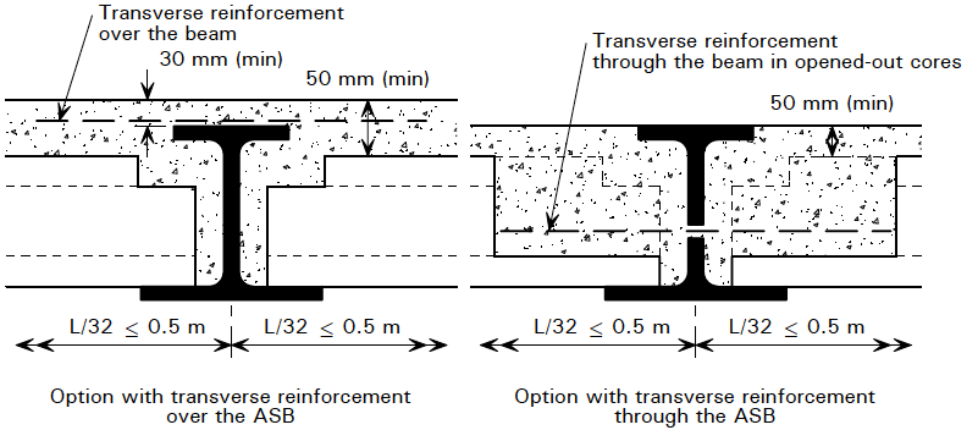

Figure 3.10: Minimum geometric encasement requirements for composite behavior [6]

3.2. Floor System and Beam Testing

When designing a floor system test, the two biggest components to think about are the set-up of the floor system and what loading will be applied. The following literature was used to collect information in order to properly design the full-scale floor system test as part of this research study. Even though some of the tests were conducted

on beams rather than floor systems, they were still useful to consider for designing the loading of the system.

Nadaskay and Buckner conducted tests in order to determine if the behavior observed in an isolated specimen is indicative of the behavior that the specimen will experience in a floor system [16]. The test specimens included a single stub girder as well as a full-scale model of a stub girder floor system. The full-scale model consisted of three parallel stub girders spaced at 53 inches on center along with a reinforced concrete slab and transverse members to act as intersecting floor beams. The middle girder was loaded to failure using a two-point concentrated load. When the two specimens were compared, there was a significant difference in the longitudinal shear strength as well as the failure mode of the slab.

Ahmad et al. tested two full-scale modified stub girder specimens in order to compare the conventional girder-to-column connection to the modified connection with an extended end stub [17]. The specimens consisted of modified stub girder configurations with transverse floor beams and a deck slab spanning 7.4 feet (2.25 meters) wide. Since there were no edge beams to support the systems, they were laterally braced by three rigid frames, two at each end and one at midspan. The systems were loaded vertically through the floor beams. Two tests were conducted: a 28-day sustained load to simulate live loading conditions and an ultimate load test to failure. The specimen with the modified connection was shown to be as structurally efficient as the conventional specimen and had a 14% increase in ultimate strength.

Pantelides et al. tested a full-scale prefabricated composite floor-building system that could reduce construction time and material costs as well as allow for more efficient mechanical ductwork placement [18]. Each panel of this system consisted of a wide-flange steel beam connected to a concrete T-section with mechanical block-outs by headed concrete anchors and welded reinforcing bars. The total depth was 3.5 feet, the span length was 45 feet, and the deck width was 8 feet. Three panels were used to make a floor system 24 feet wide, shown in Figure 3.11. The loading for the test was done per IBC requirements: for 24 hours, a superimposed load greater than or equal to twice the design load is applied; after the load is removed, wait 24 hours before measuring the deflection. The structure can then be reloaded until failure occurs, up to a load greater than or equal to twice the design load. All three panels were loaded to twice the design load for the first test. For the ultimate test, only the outer panels were loaded to failure.

Figure 3.11: Prefabricated composite floor-building system [18][1]

Barbero et al. studied the ultimate bending strength of composite box and I-beams made with glass-fiber-reinforced plastic (GFRP) [19]. These composite materials are lightweight and resistant to corrosion. Simply supported boundary conditions were simulated through supporting the ends of the beam specimens on concrete blocks through cylindrical rollers. Three and four point tests were conducted by applying an actuator load at midspan. Theoretically, the failure mode of these beams is caused by the local buckling of the thin walls, which was confirmed experimentally.

---

[1]Figure 3.11 reprinted with permission from "Short-Span and Full-Scale Experiments of a Prefabricated Composite Floor-Building System" by C. P. Pantelides, B. A. Burkhart, L. D. Reaveley, and D. Platt, 2016. Journal of Performance of Constructed Facilities, Volume 30, p. 04015018, Copyright 2016 by Chris Pantelides.

With the need for reduced floor-to-floor heights in high-rise buildings, Ju et al. conducted a flexural test of a proposed composite beam that used an asymmetrical steel section with web openings [20]. The asymmetrical steel section was comprised of an inverted structural tee with a plate welded to the web. Channels were attached to the bottom flange of the shape to support the deck during construction, and cast-in-place concrete fills either side of the asymmetrical shape and the deck. No shear connectors were used, with the shear strength developed through the bond strength between the concrete and steel and the bearing strength of the opened web area. The T-shape composite beams are 16.4 feet (5 meters) long and loaded in four-point bending. The beam was loaded by putting the actuator onto a loading beam on two rollers 3.9 feet (1.2 meters apart on the beam, while the beam was supported on either end. The beam failed due to concrete crushing, with complete composite action up until yielding and partial composite action afterward.

Sheehan et al. studied the flexural behavior of an asymmetric composite beam with a low degree of shear connection, assembled using unpropped construction [21]. Composite beams can be overdesigned for the degree of shear connection, and using unpropped construction methods can reduce construction time. The asymmetric beam consisted of a built-up section with a thicker bottom flange than top flange, with an area ratio of 1:1.5. The steel beam is connected to decking and a concrete slab by shear studs through the top flange. This configuration is shown in Figure 3.12. The 39.4-foot (12-meter) beam was supported on each end by rollers. Uniform loading was simulated by loading at eight points along the beam using three actuators. The load was applied up to

62.7 psf (3 kN/ m^2), 104 psf (5 kN/ m^2), 157 psf (7.5 kN/ m^2), 209 psf (10 kN/ m^2), 251 psf (12 kN/ m^2), 313 psf (15 kN/ m^2), and finally, up to failure, which occurred by beam yielding. Since no shear stud failure occurred, it can be concluded that the design limits on the degree of shear connection can be revised.

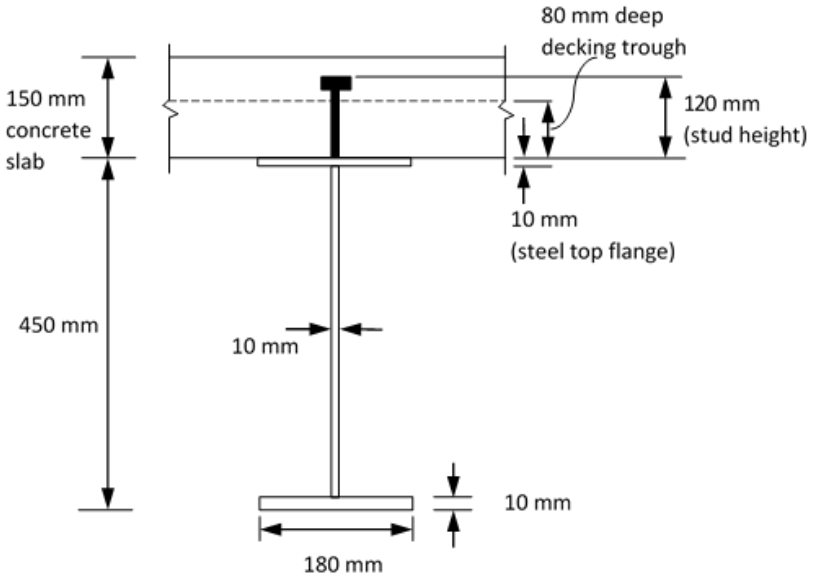

Figure 3.12: Asymmetric composite beam floor system [21][2]

In order to determine its structural performance, Hechler et al. conducted shear and flexural tests on CoSFB, ArcelorMittal's beam discussed in Section 3.1.3.2 [22]. For the flexural tests, two beams spanning 26.2 feet (8 meters) with an effective slab width of 8.2 feet (2.5 meters) were tested. The outer edges of the slab were supported to

[2]Figure 3.12 reprinted with permission from "Flexural behaviour of asymmetric composite beam with low degree of shear connection" by T. Sheehan, X. Dai, and D. Lam, 2018. Journal of Constructional Steel Research, Volume 141, pp. 251-261, Copyright 2018 by Therese Sheehan.

stabilize the system during testing. The beams were loaded in four-point bending by an actuator, using deflection control. This testing revealed CoSFB has sufficient load-bearing capacity and ductile behavior.

3.2.1. Floor System Configuration

The types of floor systems in these studies can be split into two categories: with edge beams and without edge beams. The configurations without edge beams, seen in the work by Ahmad et al. and Hechler et al., had to be laterally braced or otherwise supported during testing [17, 22]. The advantage of no edge beams is that you can solely load that beam, while the advantage of the edge beams is a more realistic system.

3.2.2. Loading

The floor systems with edge beams, seen in the work done by Nadaskay and Buckner and Pantelides et al., were loaded in two different ways [16, 18]. Nadaskay and Buckner loaded their middle girder only, while Pantelides et al. loaded all three of their beams for the service loading tests and the outer two beams for the ultimate loading tests [16, 18]. Nadaskay and Buckner used the justification that local failure of one beam is more likely than all three beams failing simultaneously [16].

The loading in all three beam tests was done through point-loading; although there are notable differences. Barbero et al., Ju et al., and Hechler et al. all used four-point loading, while Sheehan et al. used ten-point loading shown in Figure 3.13 [19-22]. With any of these configurations, the goal is to simulate uniform bending as much as possible. Obviously, the ten-point loading is a better way to do that, but it also requires more resources and coordination.

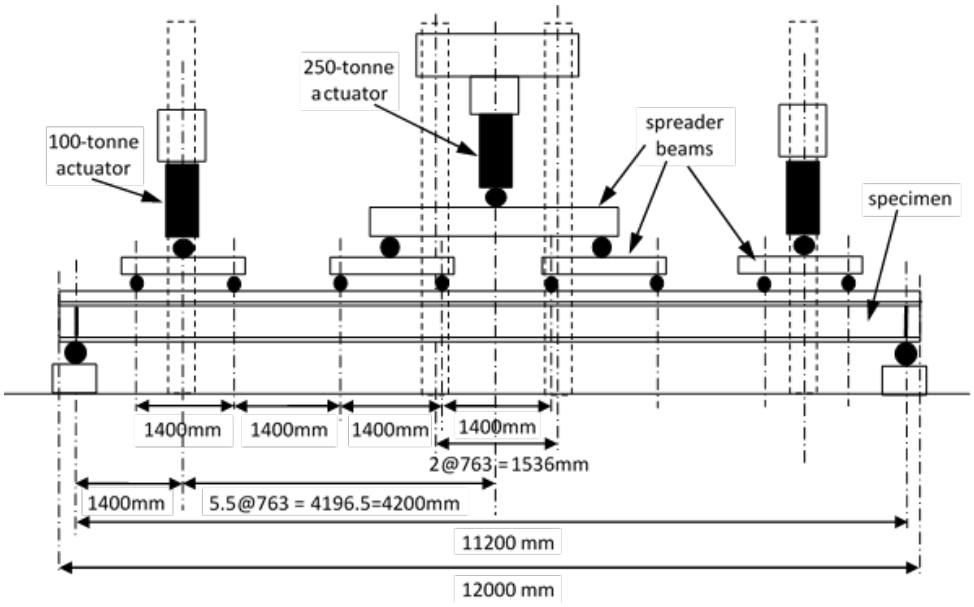

Figure 3.13: Ten-point bending [21][3]

Sheehan et al. used load control while Hechler et al. used deflection control [21, 22]. The difference is in how the actuator applies the load: with load control, the actuator applies a specified amount of load to the system while deflection control means the actuator applies a certain amount of deflection or stroke. With deflection control, you know how far your actuator is going to push whereas with load control, the amount of stroke will depend on the stiffness of your system.

[3]Figure 3.13 reprinted with permission from "Flexural behaviour of asymmetric composite beam with low degree of shear connection" by T. Sheehan, X. Dai, and D. Lam, 2018. Journal of Constructional Steel Research, Volume 141, pp. 251-261, Copyright 2018 by Therese Sheehan.

4. TESTING APPROACH

The overall objective of this research is to further the state of knowledge for shallow-depth steel-concrete floor systems utilizing A-shapes. In order to do this, a full-scale floor system test had to be designed, which is explained in Section 4.1. Section 4.2 details the instrumentation used in the test, while Section 4.3 covers the initial assembly before testing. The three tests in the experiment are outlined in Sections 4.4, 4.5, and 4.6.

4.1. Floor System Design

The work of this research began with designing the full-scale floor system to be tested. The configuration of the shallow floor system chosen can be seen in Figure 1.3. First, a preliminary design was chosen based on constraints and engineering judgment. That design was then tweaked after conducting calculations to confirm the validity of the design.

Prior to work done in this thesis, Stoddard and Yarnold obtained three proof-of-concept hot-rolled AIBs from Nucor [4]. These A-shapes were A12x53 beams, which were W12x65 beams with top flanges six inches wide rather than twelve inches. The W12x65 and A12x65 shapes can be seen in Figure 4.1. Since A-shapes are not regularly hot-rolled in the United States, it was preferable to use as many of these proof-of-concept beams as much as possible, which largely drove the design.

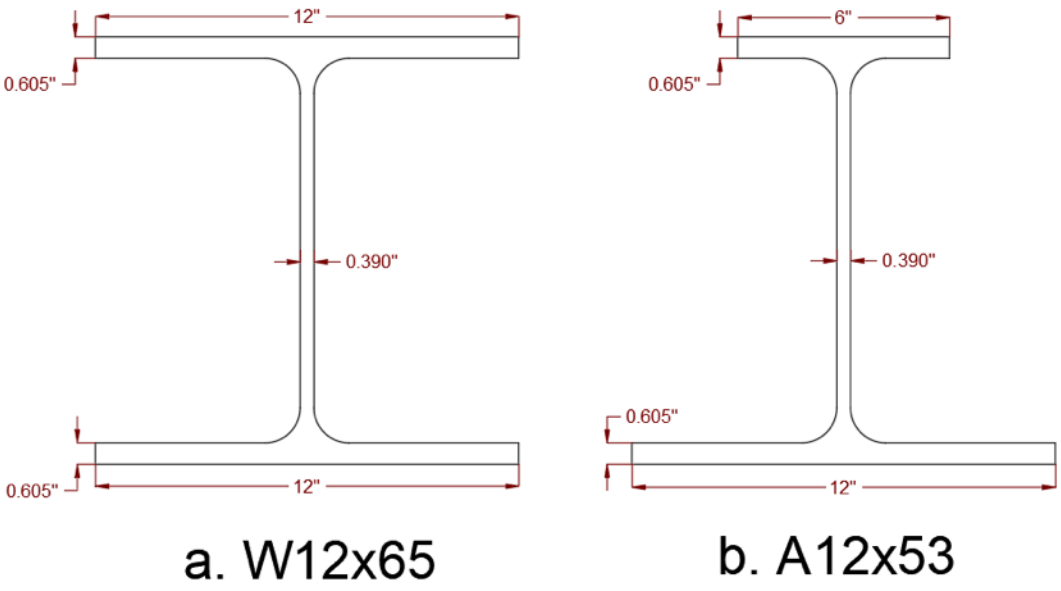

Figure 4.1: (a) W12x65 shape and (b) A12x65 shape

4.1.1. Preliminary Design

As discussed in Section 3.2.1, the common configuration for floor system testing is a two-bay system, either with edge beams or without edge beams. For this full-scale test, a two-bay floor system with three A-shapes was chosen. This allows for a look at the behavior of the A-shape under full loading (the middle beam) in a more realistic system. In a full building floor system, the edge beams would be larger to resist the considerable rotation they will undergo from the one-sided weight of the precast panels and wet concrete. For this test, A-shapes were used because it gives the most accurate view of the behavior of the middle beam. Much of the load would have been taken on by those stiffer beams, and there would not have been a clear picture of the capacity of the center A-shape. The selected configuration can be seen in Figure 4.2.

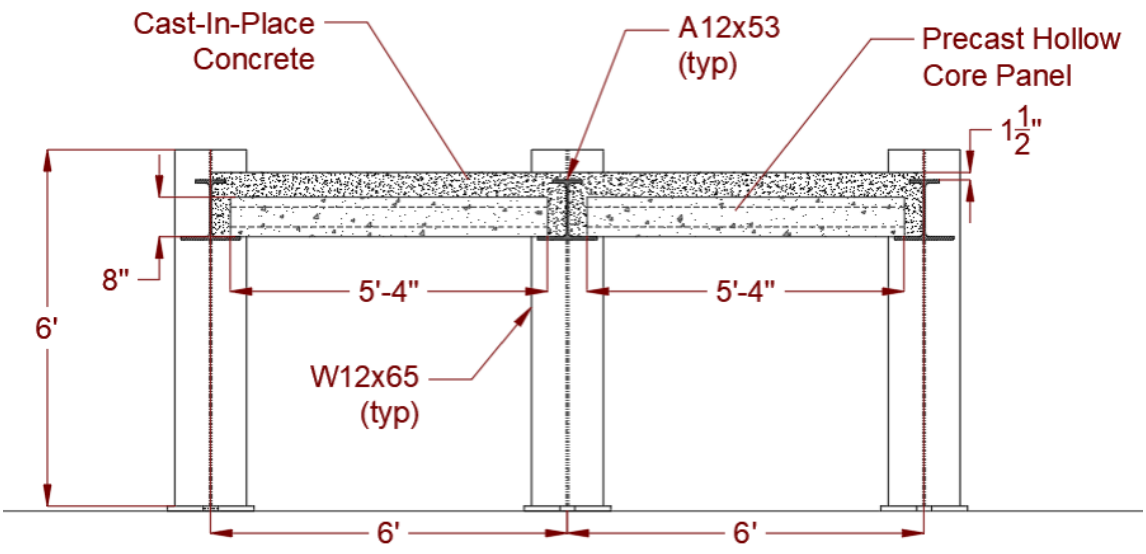

Figure 4.2: Floor system elevation view

The columns were chosen to be W12x65 sections because it was a larger section than needed, and it made the steel order simpler. In order to have easy access to the floor system and keep the columns stiff, the columns were chosen to be six feet tall. Much of the floor system, excluding the A-shapes, was overdesigned so that the failing mechanism would be related to the beams. Simple shear connections were chosen to attach the beams to columns on each end.

The dimensions of the floor in the high-bay lab presented some constraints for the floor system. The tie-down holes in the floor are three feet apart, meaning the baseplates for the columns had to adhere to that spacing, and beam spacing and span were limited to increments of three feet. The layout chosen is shown in Figure 4.3. Although it is unrealistic, a beam spacing of 6 feet was chosen due to the constraint of

the loading frame width. The spacing between columns was chosen as 24 feet, which made the beam span 22’ – 10-7/8”.

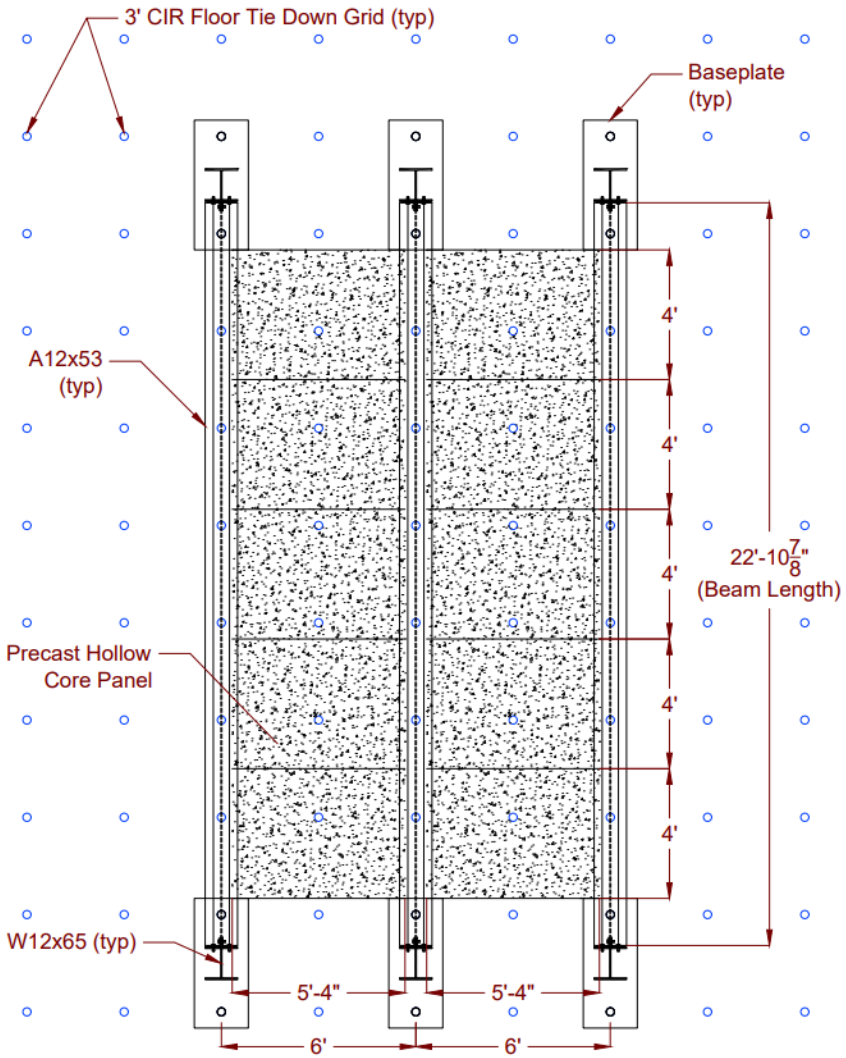

Figure 4.3: Floor system plan view

The precast panels had a width of 4 feet, so 10 panels were used to make a floor system 20 feet long. The panel length of 5’ – 4” was chosen per the bearing length on the bottom flange of the beam. It should be noted that these panels can span much greater lengths, but as discussed earlier, the constraints of the lab limited the beam spacing. The

difference between the bottom and top flange on one side is three inches, so a two-inch bearing length was chosen in order to have one inch of tolerance on each side as the precast panels were lowered in. 8-inch precast hollow-core concrete panels were chosen. These allowed for sufficient room between the top flange of the beam and the panels, making it easier to put wet concrete in the void by the beam webs.

4.1.2. Calculations and Design Adjustments

Calculations were conducted with this preliminary design to verify its performance. Many of the calculations were done on the A-shapes, as they were intended to be the controlling mechanism for the test. The following are the loading tests that had to be designed for:

1. Test 1: Precast Panel Placement
2. Test 2: Concrete Pour
3. Test 3: Actuator Loading

From these tests, the following critical design stages needed to be checked, as shown in Figure 4.4, Figure 4.5, and Figure 4.6:

Test 1: Precast Panel Placement

(i) Precast panels on one side

Test 2: Concrete Pour

(ii) Precast panels and wet concrete on both sides

(iii) Precast panels and wet concrete on one side

Test 3: Actuator Loading

(iv) All the dead and live loads on both sides

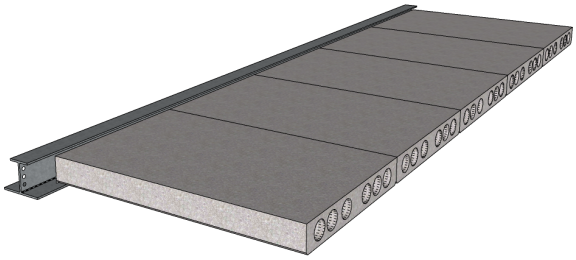

Figure 4.4: Test 1 design stage: precast panels on one side [23][4]

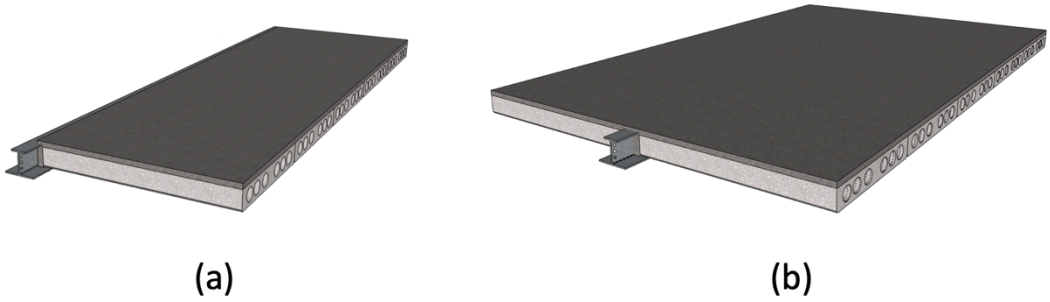

Figure 4.5: Test 2 design stages: (a) precast panels and wet concrete on one side and (b) precast panels and wet concrete on both sides [23][4]

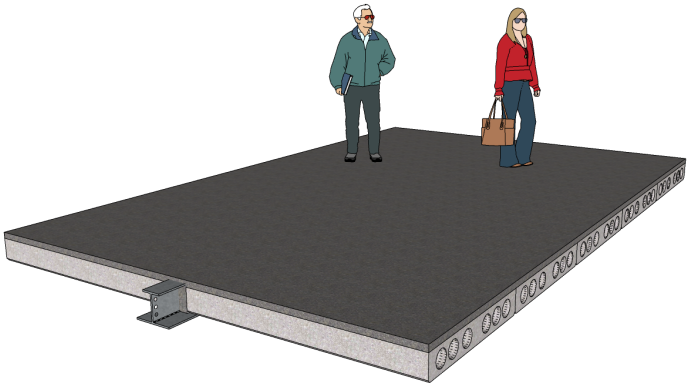

Figure 4.6: Test 3 design stage: all dead and live load on both sides [23][4]

[4]Figures 4.4, 4.5 and 4.6 reprinted with permission from "Behavior of Hot Rolled Asymmetric Steel I-Beams: Concept to Construction" by E. A. Stoddard, 2022. Copyright 2022 by Eric Stoddard.

The critical limit states were LTB and rotation of the edge beams for Tests 1 and 2 and yielding under normal stress for Test 3. The rotation of the edge beams was close to four degrees. There is not a specific limit on the rotation in the specifications, but four degrees was decided to be a practical limit. Therefore, the connection of the edge beams to the columns was changed to a fixed connection in order to reduce the rotation. The simple shear connection was changed to a fixed connection by adding two bolted/welded angles to the top and bottom flanges of the beam.

4.2. Instrumentation

To capture the behavior of the system during the tests, thirty-nine strain gauges and five displacement gauges were used in the locations shown in Figure 4.7. The strain gauges were placed at midspan as well as three feet in either direction. The greatest strains will occur at midspan, but the other cross-sections were chosen for measurement redundancy. Many of the strain gauges were encased in concrete, which can cause issues with the readings. The vertical displacement gauges were placed at each beam's midspan to measure the deflection the beams experienced. The lateral displacement gauges were placed on the leftmost beam, or Beam 1, to measure rotation. As shown in the midspan cross-section in Figure 4.8, strain gauges were placed at each corner of the beam in order to get a complete picture of the behavior at that cross-section. The center beam had an additional strain gauge in the center of its top flange since that was the critical beam. The other cross-sections have the same strain gauge arrangement as Figure 4.8, but they do not have any displacement gauges.

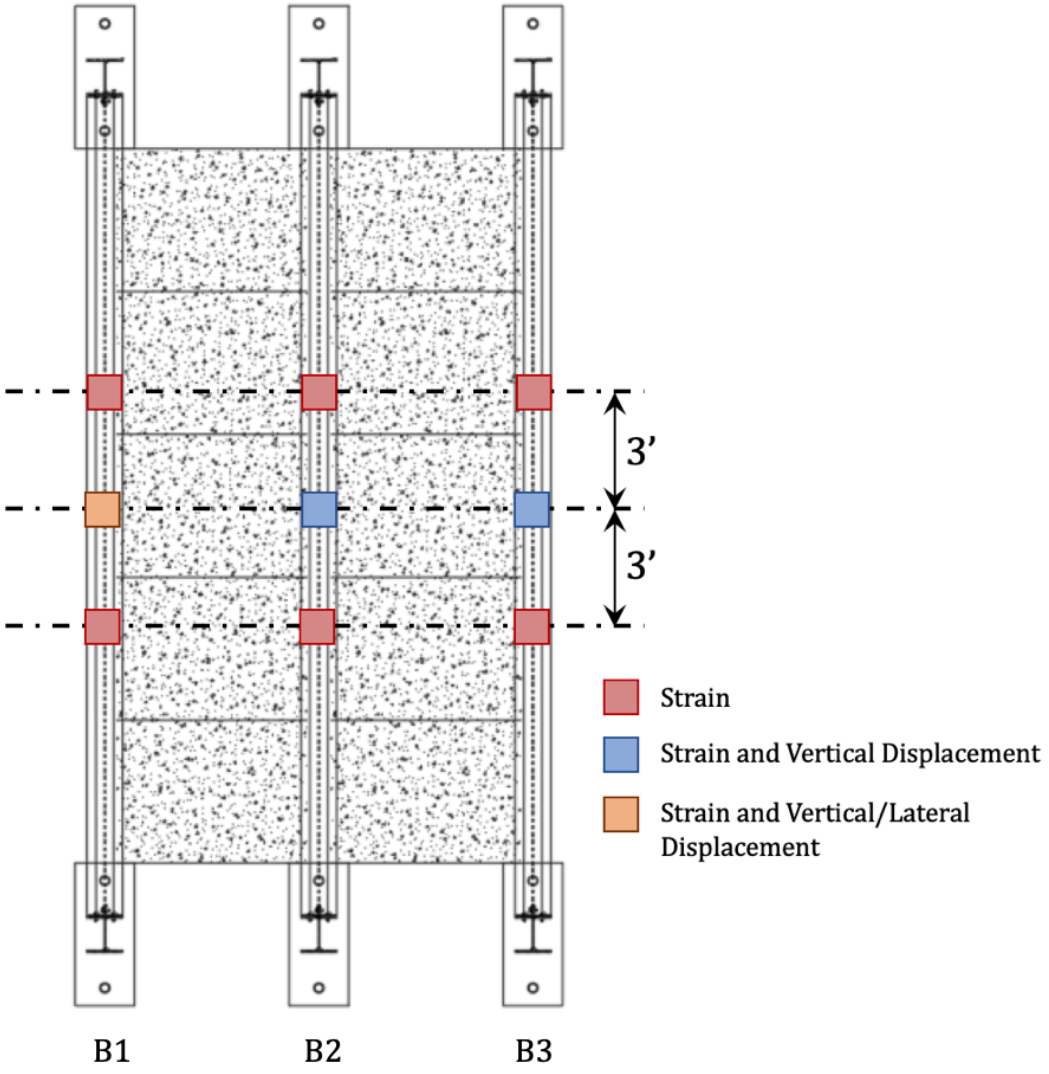

Figure 4.7: Instrumentation locations for the floor system test

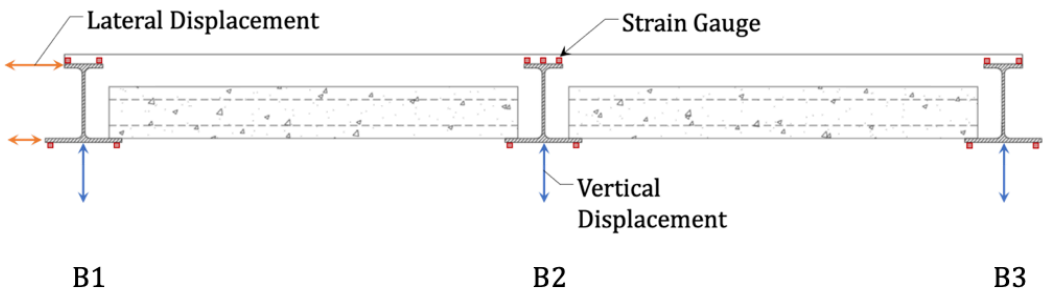

Figure 4.8: Instrumentation at midspan cross-section

4.3. Steel Erection

As discussed in Section 4.1, three A-shapes were obtained and were to be used in this test. Unfortunately, during the cooling process, one of the A12 beams had issues with deformations. One of the two straightest beams was picked to be used as the center beam in the test. The beam had to be flame-cut to the correct length of 22' – 10-7/8". The rest of the steel used for this test was donated through the coordination of AISC and fabricated by Davis Iron Works. The two edge beams were W12x65 beams with their flanges cut to six inches to make A12x53 beams. Unfortunately, cutting the flanges adds heat to the hot-rolled shape, and some deformation to the top flanges occurred. The width of the flanges of the edge beams ranged from 5.75 inches to the intended 6 inches.

Erection began by putting the steel columns in place and tying them down to the lab floor. The strain gauges were properly attached to the beams on the top and bottom flanges, as shown in Figure 4.9. Because many of the strain gauges would be encased in concrete, they were sealed and covered to protect them. The A-shapes were then bolted to the columns as discussed in Section 4.1.2, with the center beam having a pinned

connection, shown in Figure 4.10, and the edge beams having fixed connections, shown in Figure 4.11. The angles for these connections had slotted holes for the column bolts for ease of construction. The vertical string pots were assembled as shown in Figure 4.12. The lateral string pots were attached as shown in Figure 4.13 and Figure 4.14. The lateral string pots themselves were attached to the white column while the end of the strings were tied to steel angles affixed to the top and bottom of the beam. The steel framing is shown in Figure 4.15.

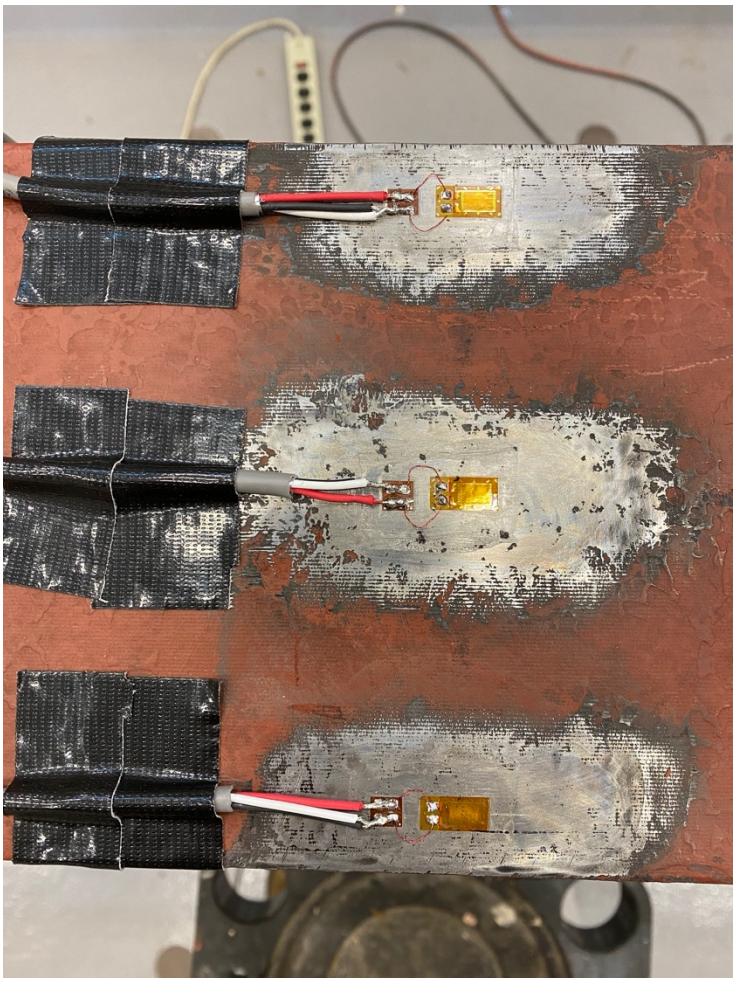

Figure 4.9: Strain gauge instrumentation (Photo by Sheyenne Davis)

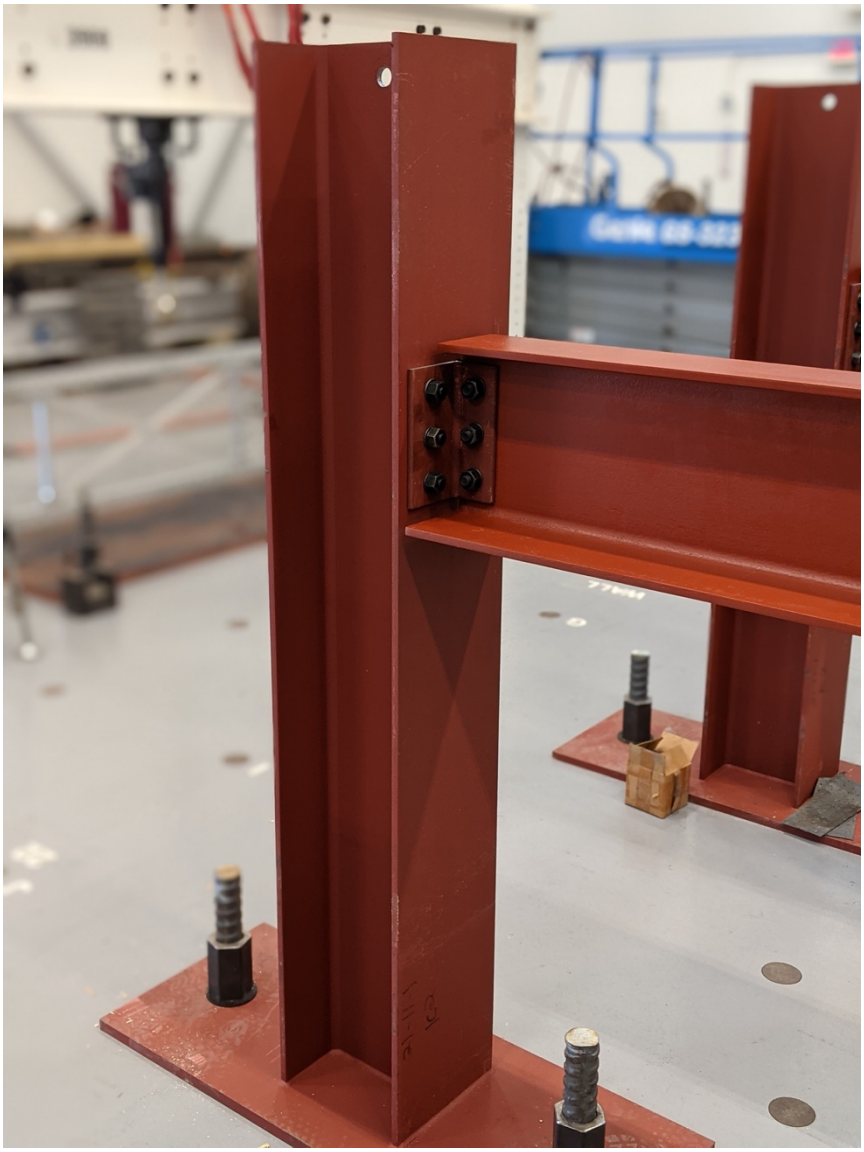

Figure 4.10: Pinned beam-to-column connection (Photo by Matthew Yarnold)

Figure 4.11: Fixed beam-to-column connection (Photo by Matthew Yarnold)

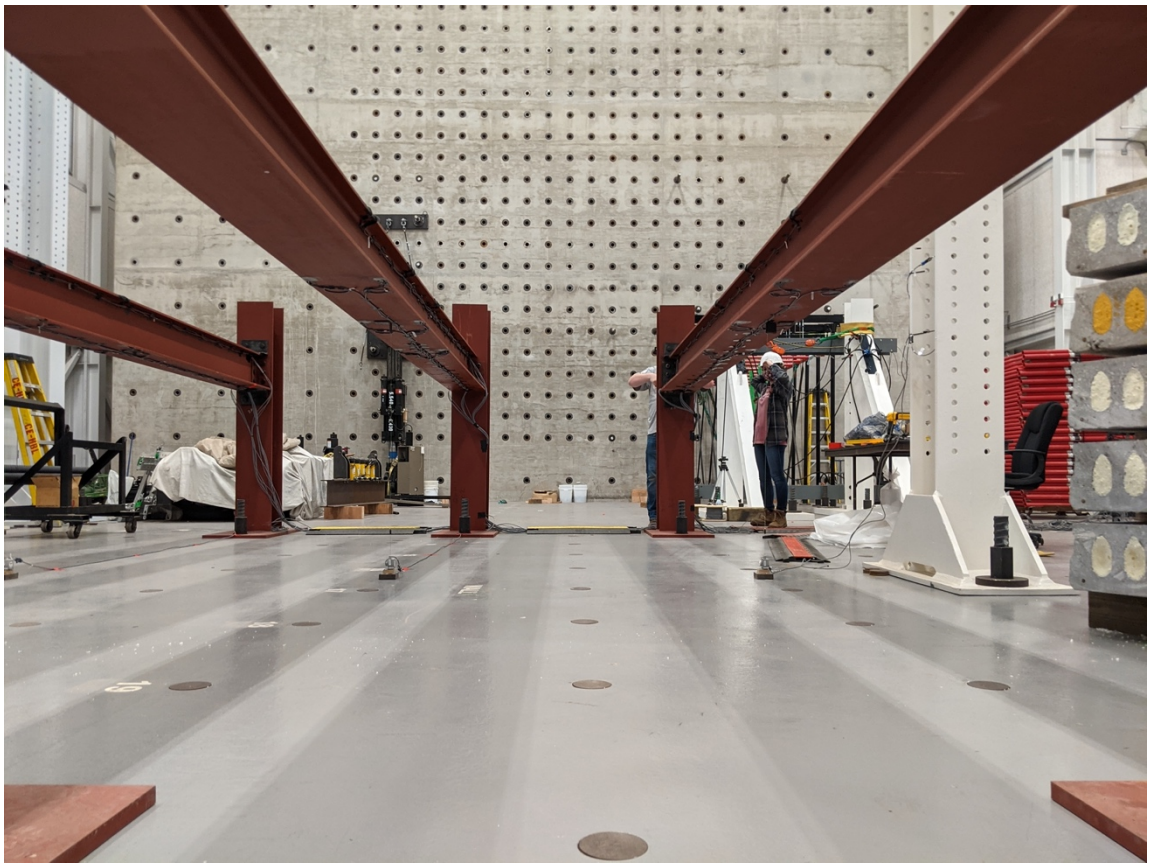

Figure 4.12: Vertical deflection string pots (Photo by Matthew Yarnold)

Figure 4.13: Lateral deflection string pots (Photo by Matthew Yarnold)

Figure 4.14: Top lateral deflection string pot (Photo by Sheyenne Davis)

Figure 4.15: Steel framing (Photo by Matthew Yarnold)

4.4. Test 1: Precast Panel Placement

The first construction loading test was setting the precast panels onto the bottom flanges of the beams. These tests were conducted by using a forklift to lift the panels above the system and place them on the beams' bottom flanges (this could have also been done using the overhead crane). Since the precast panels could be easily taken on and off the flanges by the forklift, three different cases were tested, as shown in Figure 4.16:

a. Load one bay, then the other bay

b. Load one bay with simple shear connections on the edge beam

c. Load bays alternately

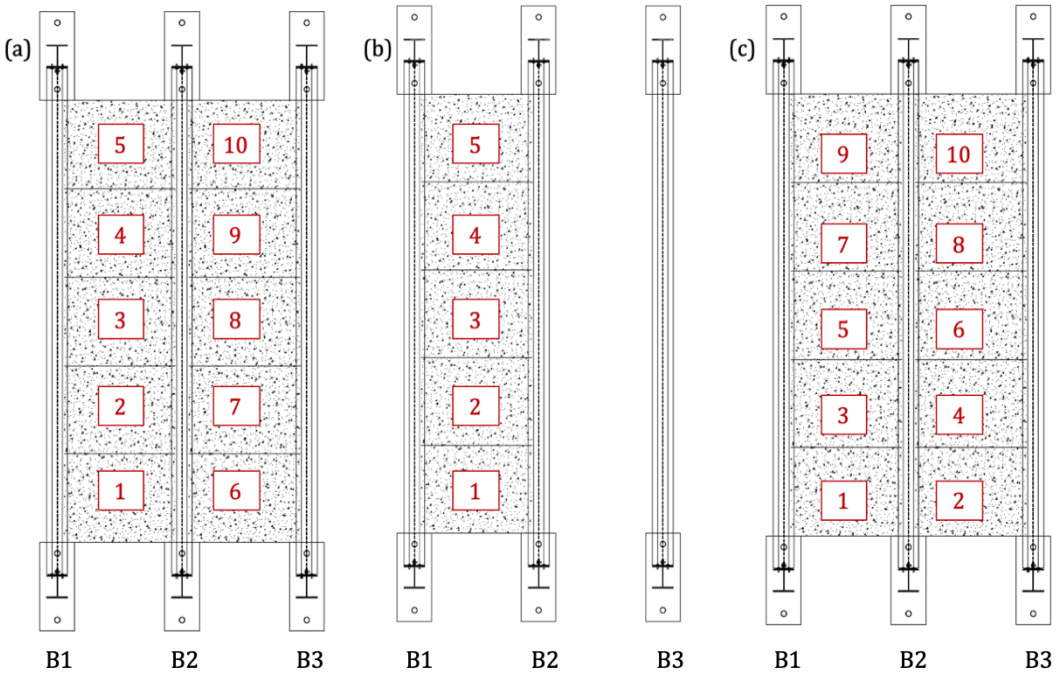

Figure 4.16: Precast panel loading cases (a), (b), and (c)

Before the test, the voids in the hollow-core panels had to be filled. As previously discussed in Section 3.1.3.4.1, the voids in the ASB floor system are filled with polystyrene bung or something similar. For ease of application, the voids were filled using Great Stuff™ Insulating Foam, as shown in Figure 4.17.

There was an issue with the precast panels during the test. Two of them cracked down the middle as the forklift lifted them, as shown in Figure 4.18. This was due to a design issue having the reinforcement only running in one direction. The cracked panels were still able to be placed onto the flange and not to be considered a problem for the intended purpose of the test.

Figure 4.17: Filled hollow-core panels (Photo by Sheyenne Davis)

Figure 4.18: Forklift lifting precast panel (Photo by Matthew Yarnold)

4.5. Test 2: Concrete Pour

The second loading test was pouring the concrete to make the slab. The cast-in-place concrete was mixed and delivered by Knife River. This test consisted of taking measurements as the slab was poured. Before this test occurred, steel rebar, shown in Figure 4.19, was installed to reinforce the concrete slab, consisting of #3 rebar spaced at approximately 18 inches on center. Additionally, wood was used to create forming for the slab, shown in Figure 4.20, and the interface between the precast panels were grouted, which was done using Great Stuff™ Insulating Foam.

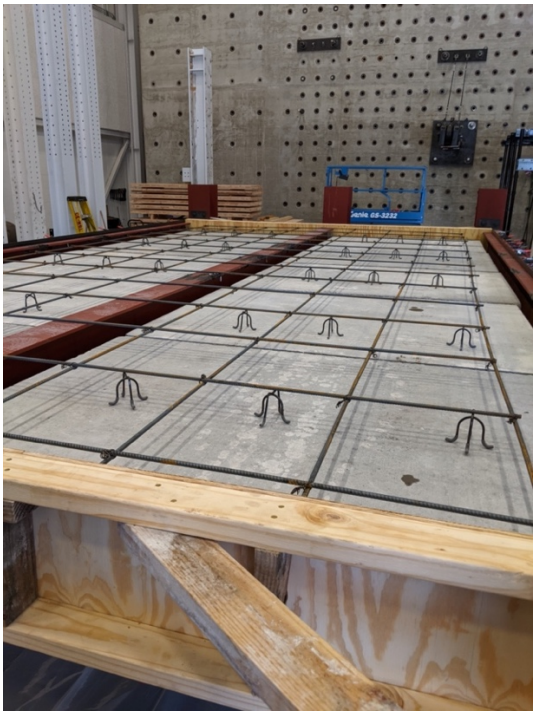

Figure 4.19: Steel mesh (Photo by Matthew Yarnold)

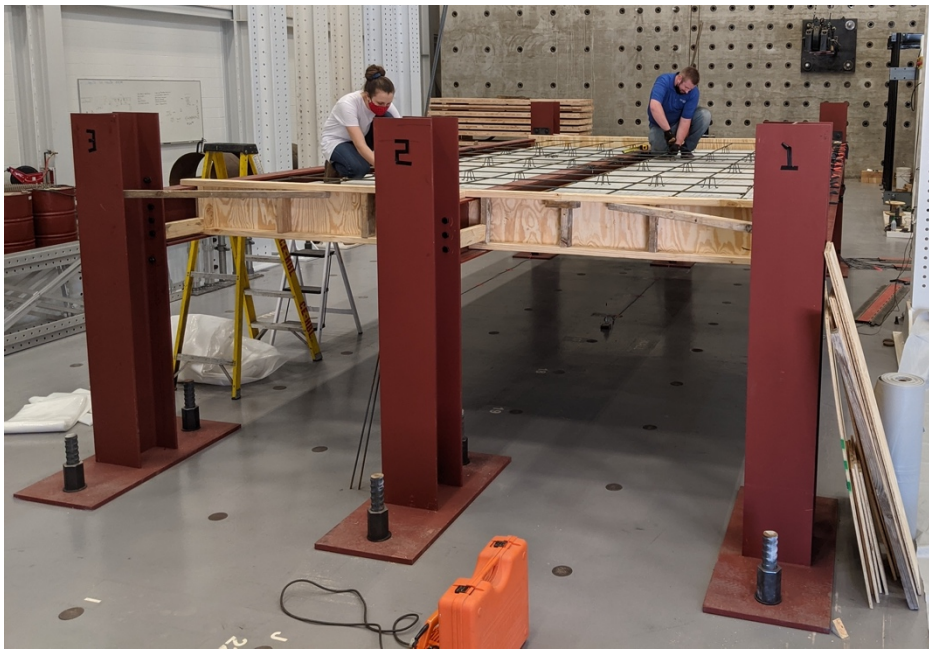

Figure 4.20: Wood forming (Photo by Matthew Yarnold)

4.6. Test 3: Actuator Loading

The last test was conducted by using a 200-kip actuator in the configuration shown in Figure 4.21. As discussed in Section 3.2.2, point-loading is generally used for floor system testing. Since it is critical and carrying the most load, the loading was designed to primarily load the center beam. Four-point bending was chosen, with the force applied by the actuator being distributed onto the system by the spreader beam and rockers. The actuator was programmed using force control such that it would apply the inputted amount of force onto the system. Displacement control was considered, but force control was ultimately chosen, as the desired data was the response of the system per how much force it was under.

Figure 4.21: Actuator loading configuration (Photo by Matthew Yarnold)

The following are the cases that were tested using the actuator:

- 35 psf equivalent service loading (or 6.6 kips)
- 85 psf equivalent service loading (or 15.9 kips)
- Ultimate loading to failure

The first two cases were the service loading tests that simulated equivalent 35 pounds per square foot (psf) and 85 psf loading conditions. This floor system is proposed for use in residential buildings, which are designed at most for a live load of 100 psf, so

these were conservative loading conditions. The actuator load needed to simulate the live loading conditions was back-calculated. Case A used an actuator load of 6.6 kips, which is equivalent to 35 psf, while Case B used 15.9 kips, which is equivalent to 85 psf. The live loading tests were conducted as follows:

1. Load at 1 kip/minute until 6.6 kips is reached
2. Unload at 2 kips/minute until 0.2 kips is reached
3. Load at 2 kips/minute until 15.9 kips is reached
4. Unload at 2 kips/minute until 0.2 kips is reached

The first loading was done at 1 kip/min out of an abundance of caution; after seeing the system respond as expected, the loading was increased to 2 kips/min to speed the test up. The test was unloaded to 0.2 kips rather than 0.0 kips so that the actuator could stay in contact with the spreader beam. If it came completely off, it would have to be readjusted between each test.

The last case was the ultimate loading test, which consisted of loading the floor system to failure. The ultimate load was more difficult to estimate because the nature of the composite characteristics of the system was unknown. This is further discussed in Section 5.5.4, but the problem can be estimated by calculating the steel beam's yield and plastic moment capacity, and the system's capacity if it were fully composite, shown in Appendix A.

The yield moment capacity of the beam is 209 kip-ft, the plastic moment capacity of the steel beam is 274 kip-ft, and the fully composite capacity is 375 kip-ft. When accounting for the dead load and assuming all the load is going to the center

beam, the yield moment translates to an actuator load of 37 kips, the plastic translates to 52 kips, and fully composite translates to 76 kips. Assuming all of the load is going to the center beam is a conservative assumption, but these values were used to get a low-end idea of when the system fail. It is more likely that about half of the load would go to the center beam, which translates to an actuator load of 74 kips for yielding, 104 kips for plastic, and 152 kips for fully composite failure.

Since it was possible the system could fail at a lower load, this test was conducted in stages that were decided as the test proceeded, shown below. The system failed during loading stage 8 at 94.0 kips.

1. Load at 2 kips/minute until 15.9 kips is reached
2. Load at 2 kips/minute until 25 kips is reached
3. Load at 2 kips/minute until -33.8 kips is reached
4. Load at 2 kips/minute until 49.3 kips is reached
5. Load at 2 kips/minute until 65 kips is reached
6. Load at 2 kips/minute until 80 kips is reached
7. Load at 2 kips/minute until 93.5 kips is reached
8. Load at 2 kips/minute until 100 kips is reached

5. RESULTS

The results of the test described in Section 4 are outlined here. Section 5.1 summarizes the naming convention used in communicating the results, while Section 5.2 summarizes the data collection for each test. Section 5.3 covers the test data and initial conclusions, while Sections 5.4 and 5.5 discuss more of what was learned from the experiment.

5.1. Naming Convention

As the results are laid out, it is important to be clear which test, case, beam, and gauge the data is associated with. The sections herein lay out this information.

5.1.1. Test Cases

The following is a summary of the tests and cases that will be analyzed in the subsequent sections. A detailed overview of how these tests were performed can be found in Sections 4.4, 4.5, and 4.6.

- Test 1: Precast Panel Placement
    - Case A: Load one bay, then the other bay
    - Case B: Load one bay with simple shear connections on the edge beam (pinned)
    - Case C: Load bays alternately
- Test 2: Concrete Pour
- Test 3: Actuator Loading
    - Case A: 85 psf equivalent service loading

- Case B: 100 psf equivalent service loading
- Case C: 200 psf equivalent service loading
- Case D: Failure

It should be noted that the cases listed for Test 3 are different than the intended cases for testing as outlined in Section 4.6. The design service live load for residential buildings is 100 psf, so data from the ultimate loading case was taken so that values at 100 and 200 psf equivalent loading could be evaluated. The 35 psf case was not used for analysis because its magnitude was so small compared to the other cases that it proved to be inconsequential to the results of this experiment. Because of this, the 200 psf case was included so that more data could be assessed.

5.1.2. Beam Numbering

Figure 5.1 shows the beam numbering for this experiment, with the beams numbered 1 – 3 going left to right and Beam 1 containing the lateral deflection string pots. Figure 5.2 and Figure 5.3 in future sections show how the beams are numbered relative to the strain gauges and string pots.

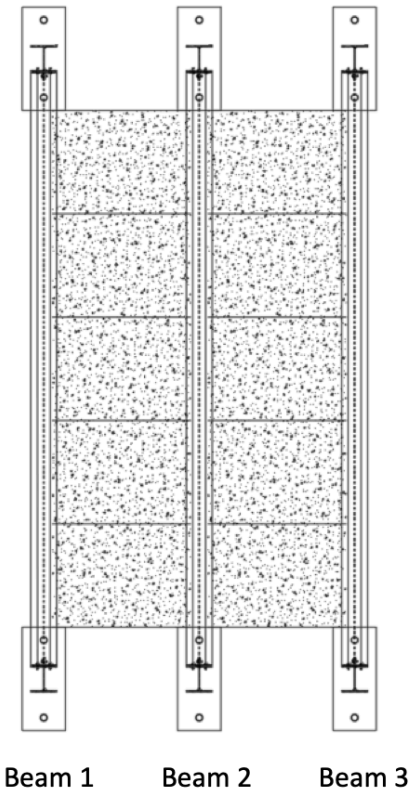

Figure 5.1: Beam Numbering

5.1.3. Gauge Numbering

5.1.3.1. Strain Gauges

As discussed in Section 4.2, the beams were instrumented with strain gauges at midspan and two other cross-sections. This was to capture as much data as possible in case of strain gauge failure, but the stresses are highest and most critical at midspan. Only one of the strain gauges at midspan proved to be unreliable, as further discussed in Section 5.2.1, so only the data collected at midspan is used for analysis. The strain gauges were originally numbered 1 – 39, but since only a third are being referenced, the notation shown in Figure 5.2 will be used. A specific strain gauge will be referred to by

SG (strain gauge), followed by the beam number and letter. For example, the top right strain gauge on Beam 3 will be SG 3-C.

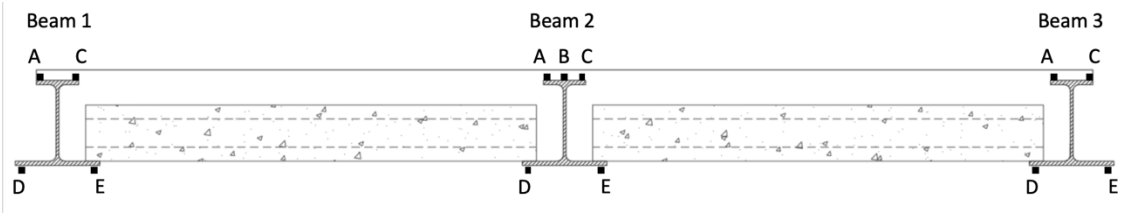

Figure 5.2: Midspan Cross-Section: Strain Gauge Notation

5.1.3.2. String Pots

As discussed in Section 4.2, a total of five string pots were installed. Three were under the midspan of each beam in order to capture the maximum vertical deflection for each test, while two string pots on Beam 1 measured the lateral deflection, which was used to determine the rotation of the beam. These string pots use the notation shown in Figure 5.3, where V denotes "vertical," L denotes "lateral," and top and bottom refer to which flange the string pot is on.

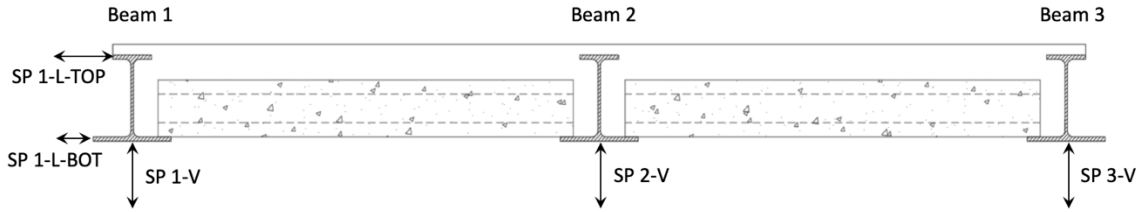

Figure 5.3: String Pot Notation

5.2. Data Collection

The data collected included microstrain and deflection data for all the tests as well as the actuator load and stroke for Test 3. Each data type is covered in the following

sections, including the details of data collection, the quality of the data, and how each is used in the analysis.

5.2.1. Stress Data

The majority of the data collected during the experiment were microstrains. The units for strain are in/in, and microstrain is strain with an increase of 10^6. The microstrains collected during the test were converted to stress in kips per square inch (ksi) for purposes of data reporting using Equation 1, where E is the modulus of elasticity, σ is the stress, and ε is the microstrain. The value of E for structural steel is 29,000 ksi.

$$\sigma = \frac{E \times \varepsilon}{10^6} \quad (1)$$

Before the microstrains were converted into stresses, they were zeroed at the beginning of each test so that the stresses analyzed were only for the loads on the structure during that test. For example, the stresses reported for Test 2 are only from the load of the wet concrete. Zeroing the data is especially important with the stresses as the magnitude that the strain gauges measure can drift between tests. The stresses reported are an average over which the data was steady, except for Test 3 Cases B and C, which is further explained in Section 5.3.3.

The quality of the stress data is relatively good, except for one faulty strain gauge. As mentioned in Section 5.1.3.1, only the midspan stresses are considered for the purposes of data analysis because all but one of the strain gauges failed. During Test 2, SG 2-A failed and reported stresses that were clearly not accurate, as shown in Figure 5.4. Although the appropriate precautions were taken as discussed in Section 4.3, this

was likely due to the wet concrete reaching the strain gauge. This means that SG 2-A was not reliable for Tests 2 or 3, so its stresses are not reported.

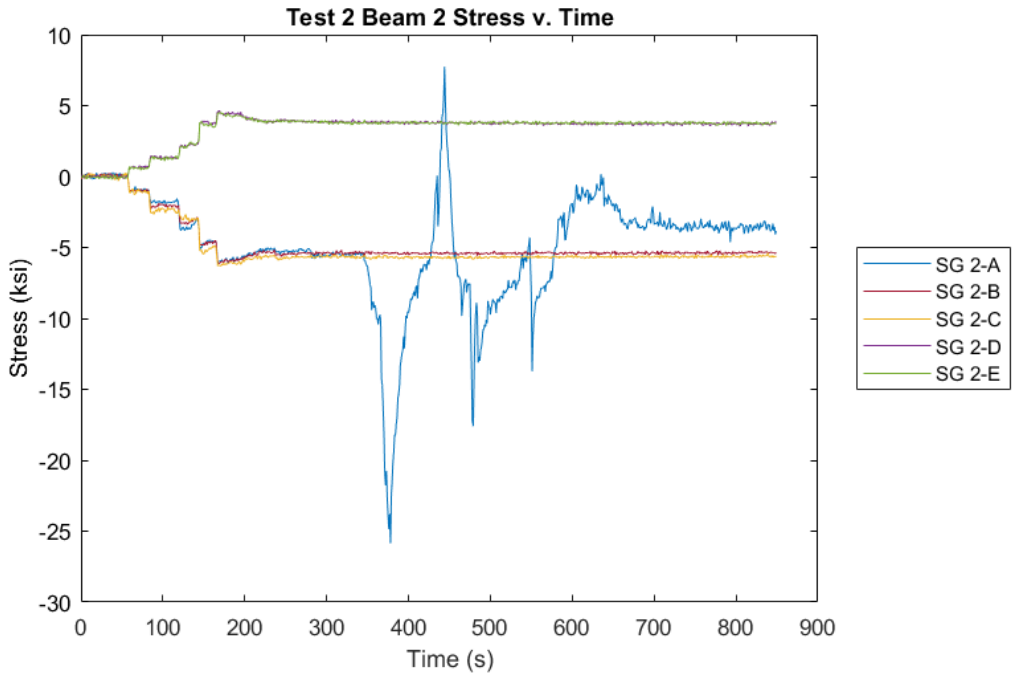

Figure 5.4: Test 2 Beam 2 Stress v. Time with Faulty Strain Gauge SG 2-A

Other than SG 2-A, the strain gauges reported data accurately. Figure 5.5 through Figure 5.12 show the time histories during Test 1 for all three beams during all three cases. There is not a figure for Beam 3 during Case B since it was not loaded, and the stresses were near zero. Figure 5.5, Figure 5.6, and Figure 5.7 show the stresses for Case A, where the precast panels were loaded into one bay and then the other. Figure 5.8 and Figure 5.9 show the stresses for Case B, where the precast panels were only loaded into the bay between Beam 1 and 2. Figure 5.10, Figure 5.11, and Figure 5.12 show the stresses for Case C, where the precast panels were loaded into the bays alternately.

For all of these cases, there was an increase in stress magnitude each time a panel was placed onto the system and a decrease each time a panel was removed. This is especially clearly seen for SG 1-A in Figure 5.5, Figure 5.8, and Figure 5.10. Note that there is not a decrease in stress back to zero for Case C because the panels stayed on. The noise in each figure is relatively minor, except in Figure 5.7, especially SG 3-E. The reason for this is not obvious, but it could be as simple as the beam getting hit during the test. Since the noise is not constant for all of the tests, it is not considered an issue.

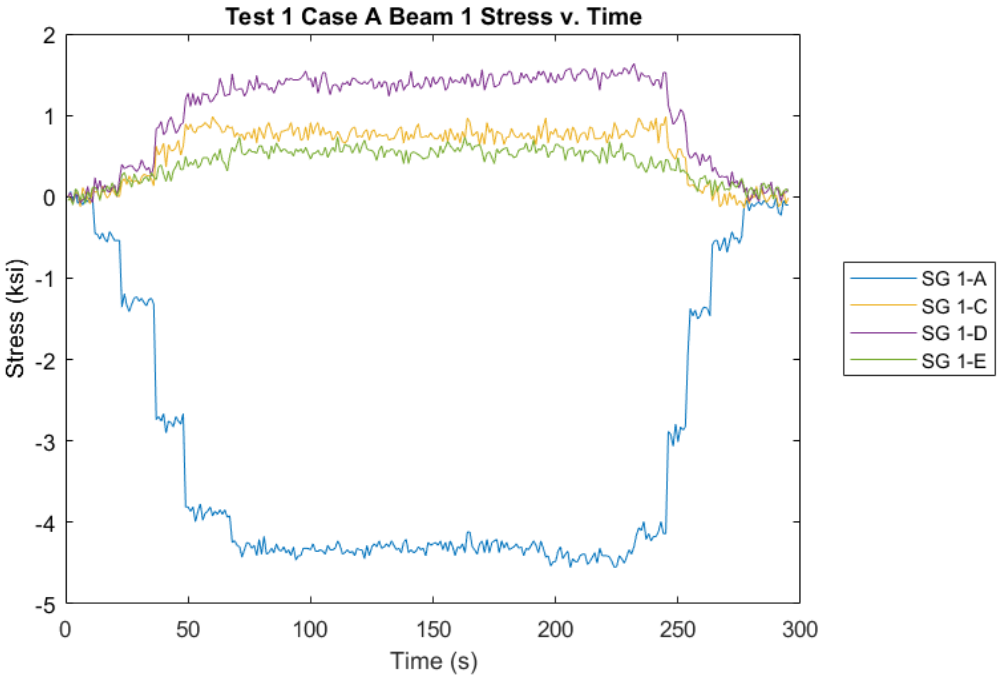

Figure 5.5: Test 1 Case A Beam 1 Stress v. Time

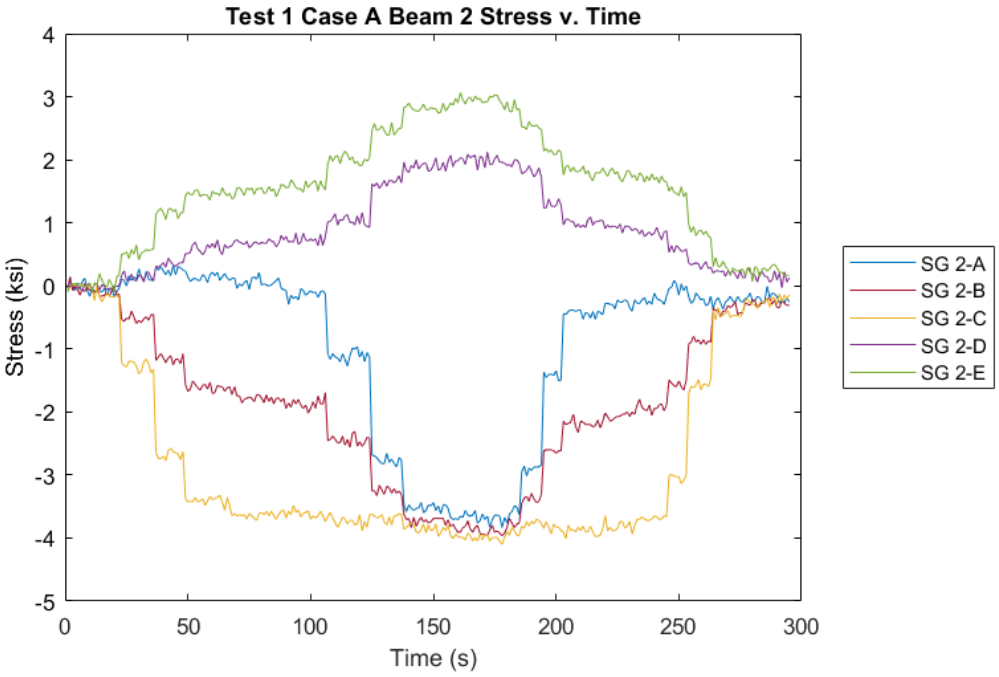

Figure 5.6: Test 1 Case A Beam 2 Stress v. Time

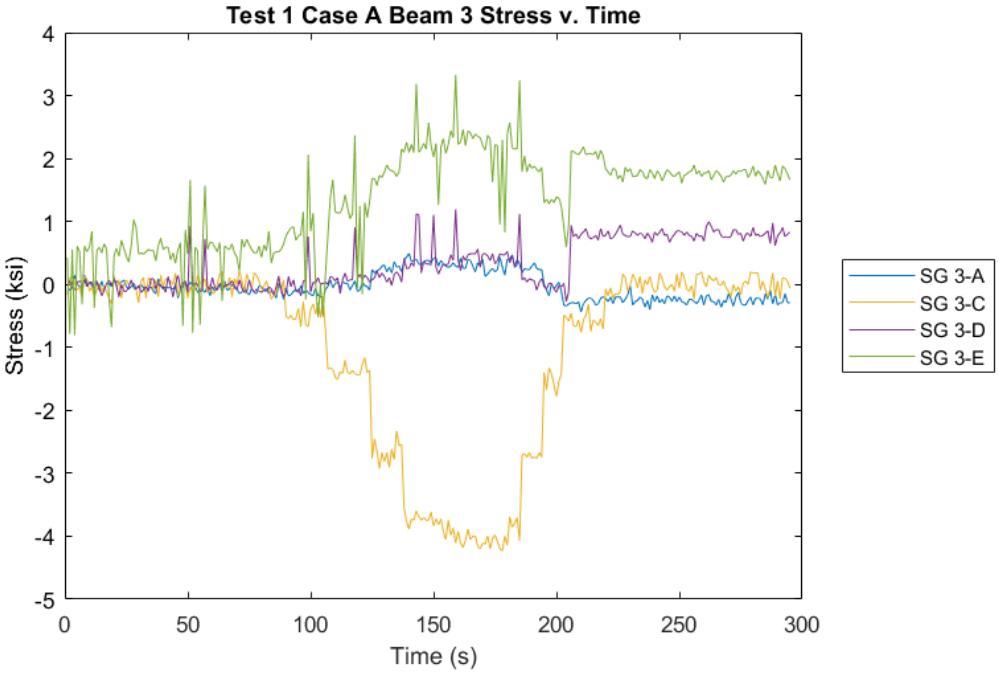

Figure 5.7: Test 1 Case A Beam 3 Stress v. Time

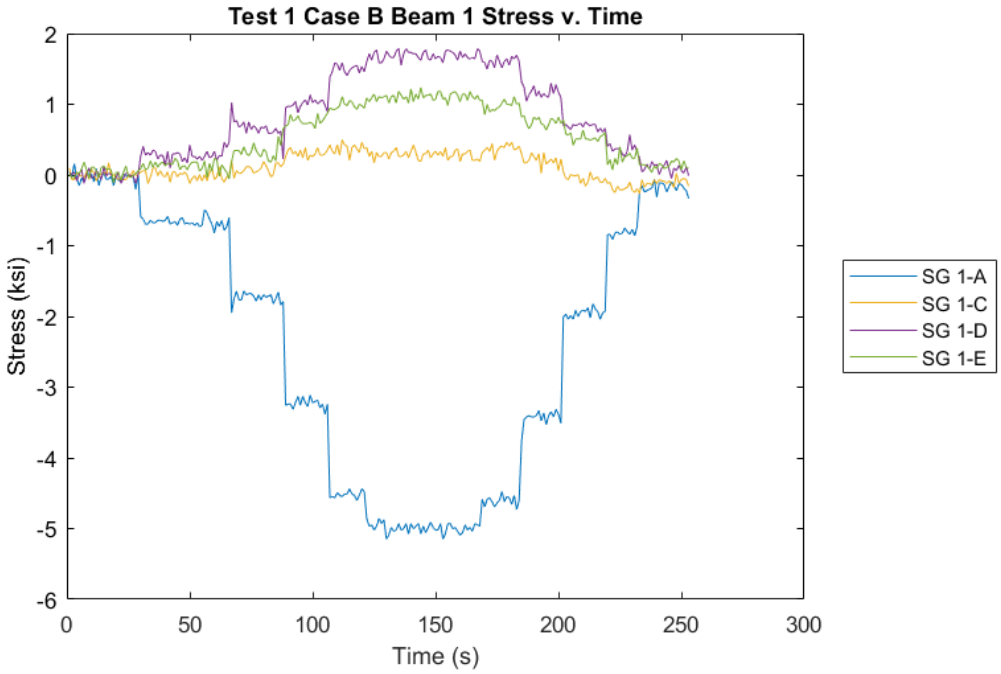

Figure 5.8: Test 1 Case B Beam 1 Stress v. Time

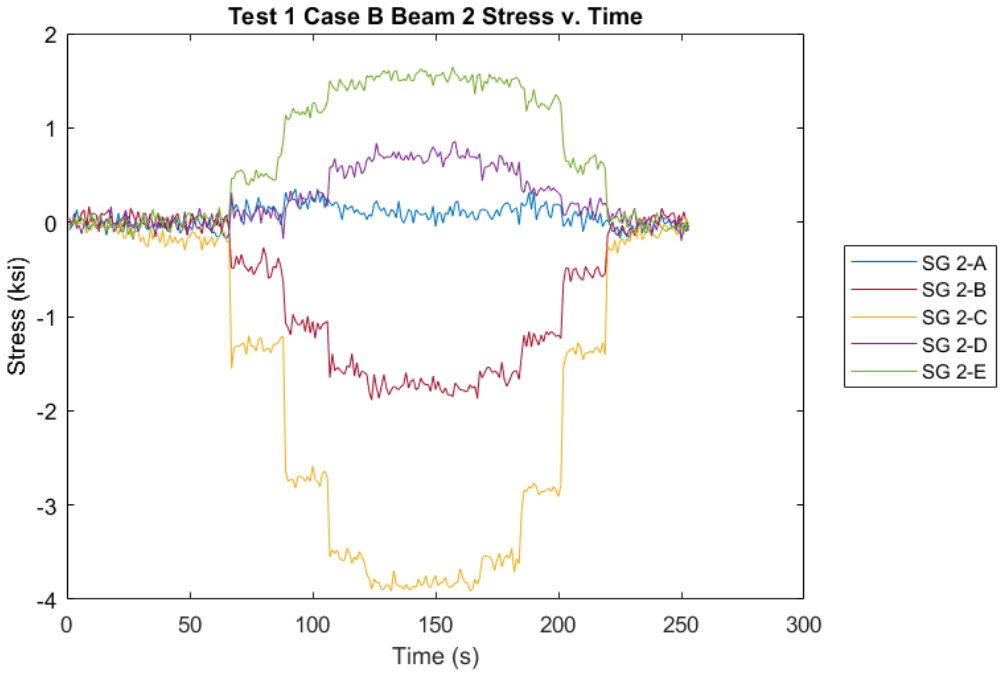

Figure 5.9: Test 1 Case B Beam 2 Stress v. Time

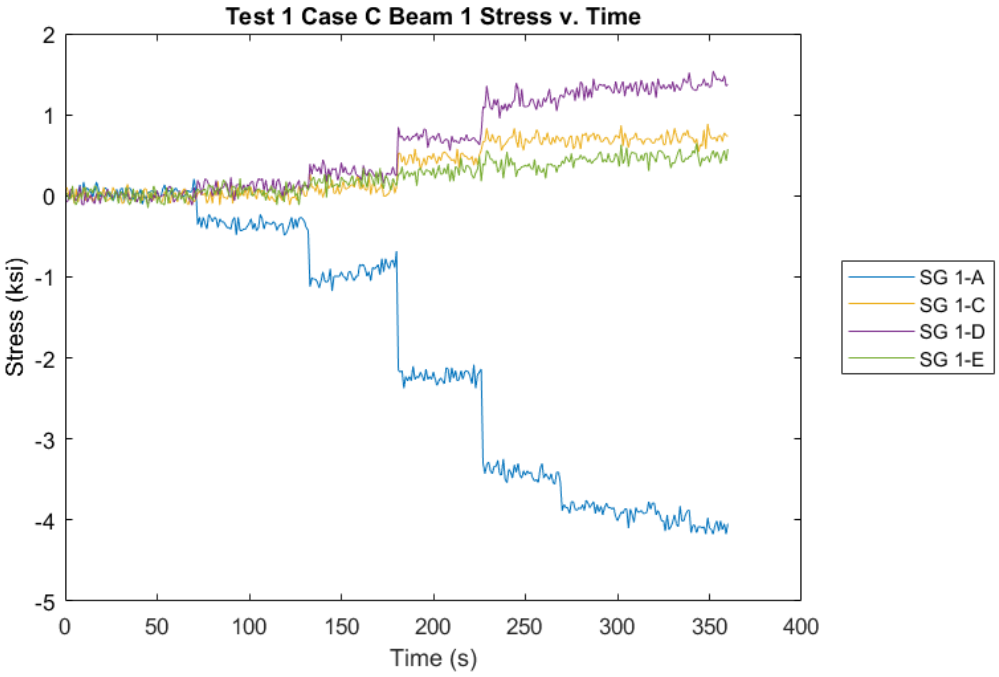

Figure 5.10: Test 1 Case C Beam 1 Stress v. Time

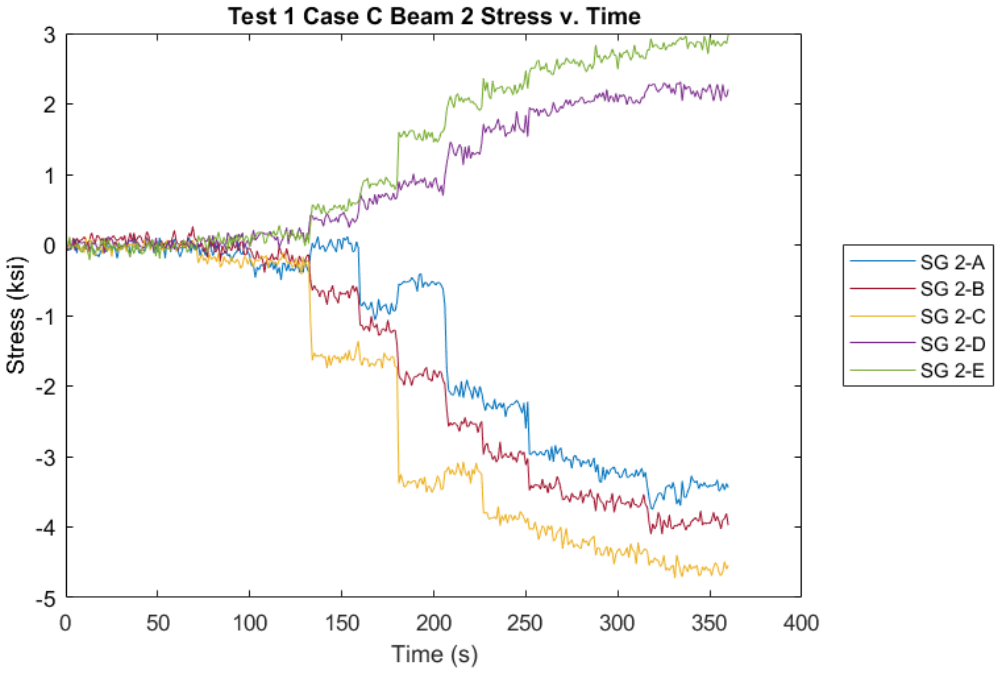

Figure 5.11: Test 1 Case C Beam 2 Stress v. Time

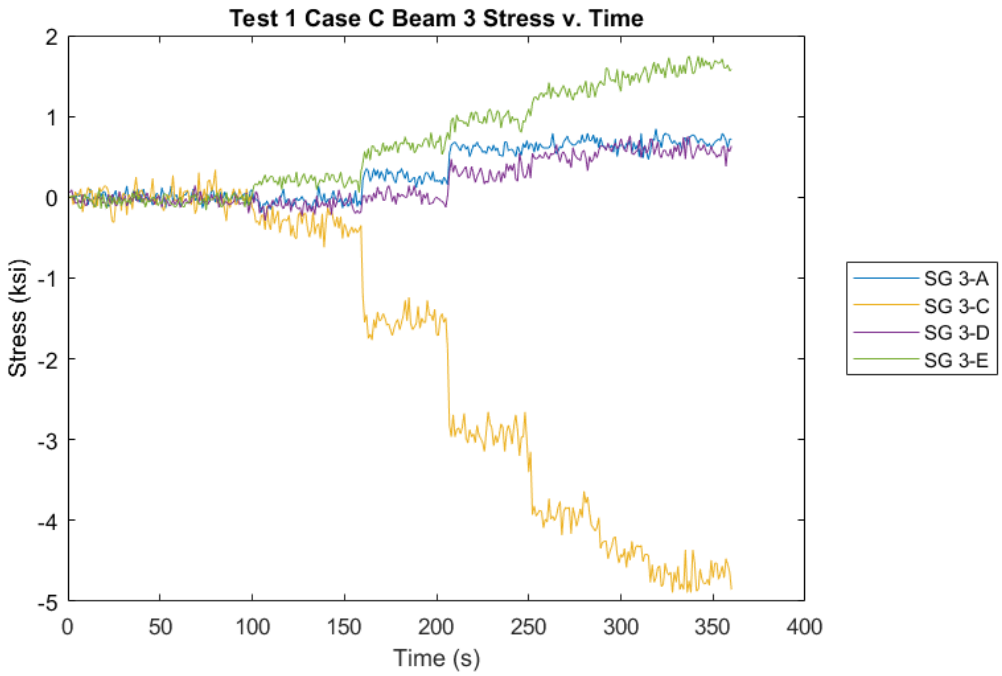

Figure 5.12: Test 1 Case C Beam 3 Stress v. Time

Figure 5.13, Figure 5.14, and Figure 5.15 show the stress time histories for all three beams for Test 2, the concrete pour. The wet concrete was released from the bucket in portions over Beam 2, which is likely why the increases in stress are more clearly defined. Beams 1 and 3 experienced load whenever the wet concrete was spread over to them, which was more random. Once the concrete was spread and leveled, the stresses in each figure leveled off. The stresses on Beam 2 were uniform across the top and bottom flange, while Beams 1 and 3 have stresses at all different magnitudes since they are experiencing an eccentric load.

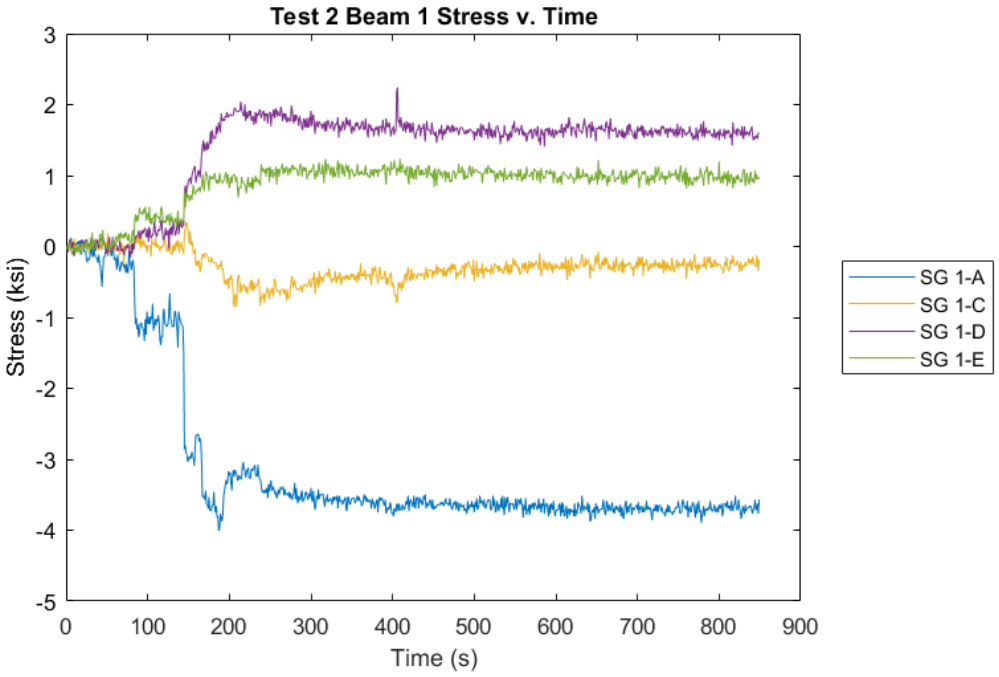

Figure 5.13: Test 2 Beam 1 Stress v. Time

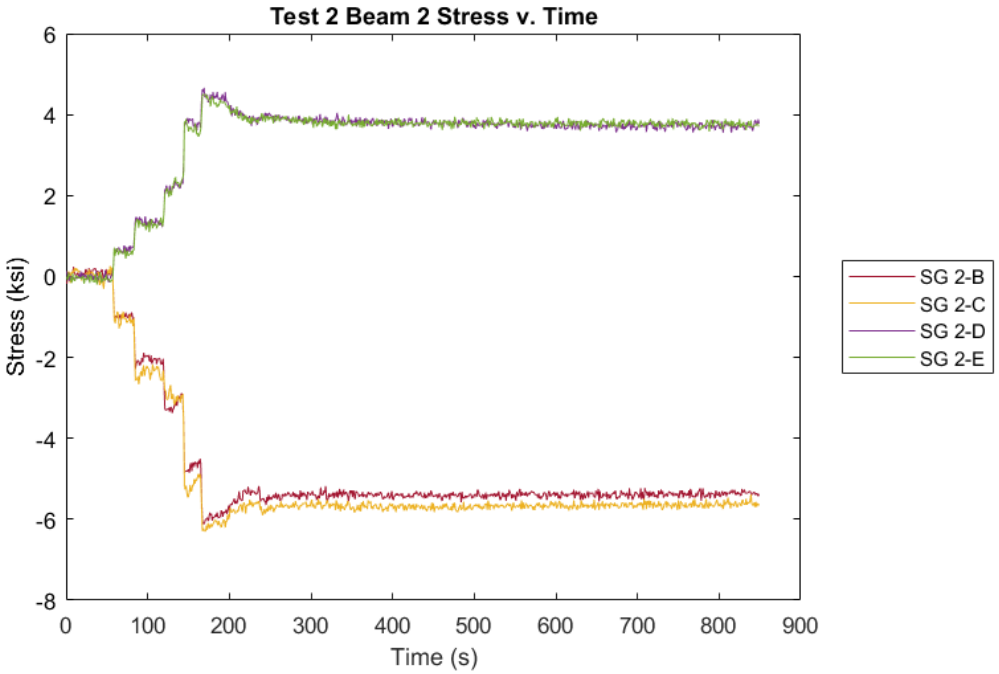

Figure 5.14: Test 2 Beam 2 Stress v. Time

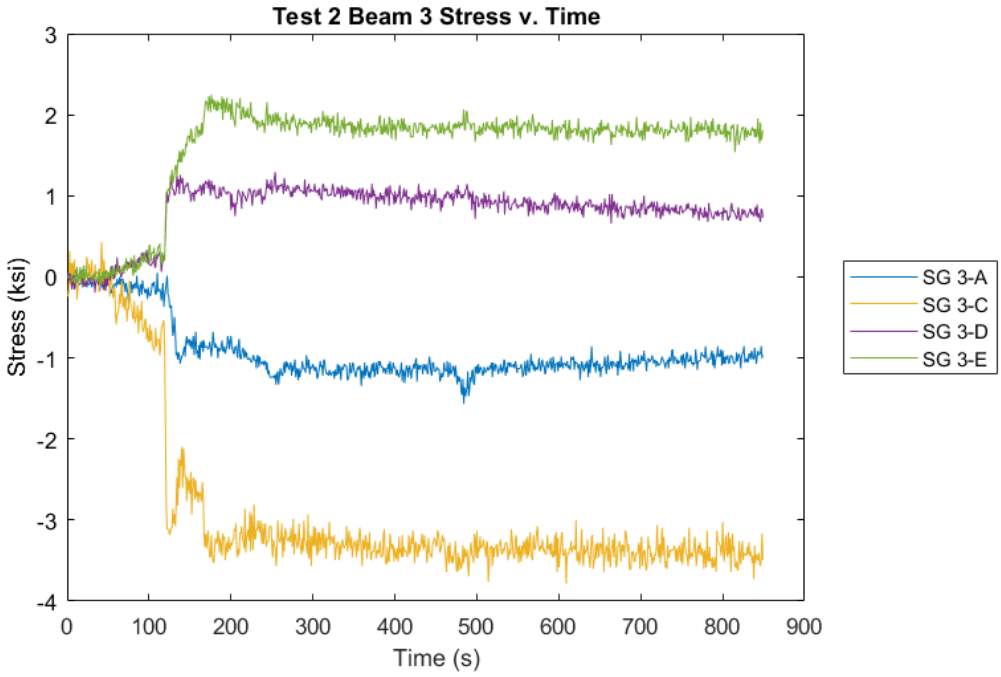

Figure 5.15: Test 2 Beam 3 Stress v. Time

Figure 5.16 through Figure 5.21 show the stress and microstrain time histories for all three beams for Test 3. The data was collected for Test 3 in two stages: service loading and failure loading. The service loading included the tests for 35 psf and 85 psf while the failure loading loaded the system to failure (where the 100 psf and 200 psf data was pulled from).

Figure 5.16, Figure 5.17, and Figure 5.18 show the stress time histories for each beam during the service loading. These figures are different when compared to the time histories of the previous tests. All the figures have the same shape rather than Beam 2 being different. This is because, with the concrete deck, the outer beams do not rotate and therefore have uniform stress profiles across their top and bottom flanges, just like Beam 2.

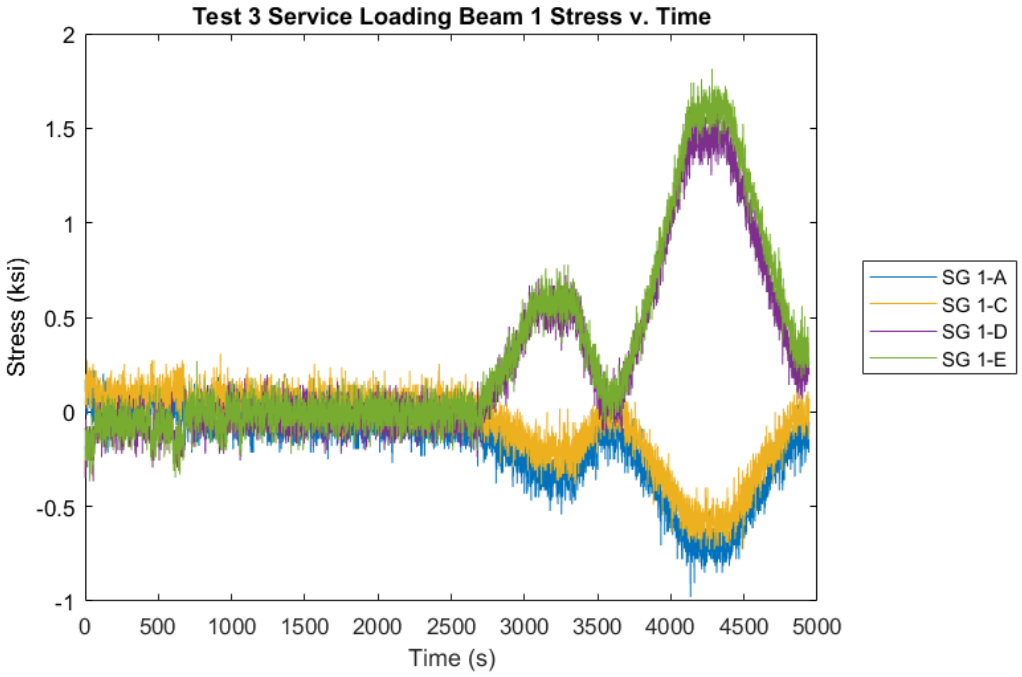

Figure 5.16: Test 3 Service Loading Beam 1 Stress v. Time

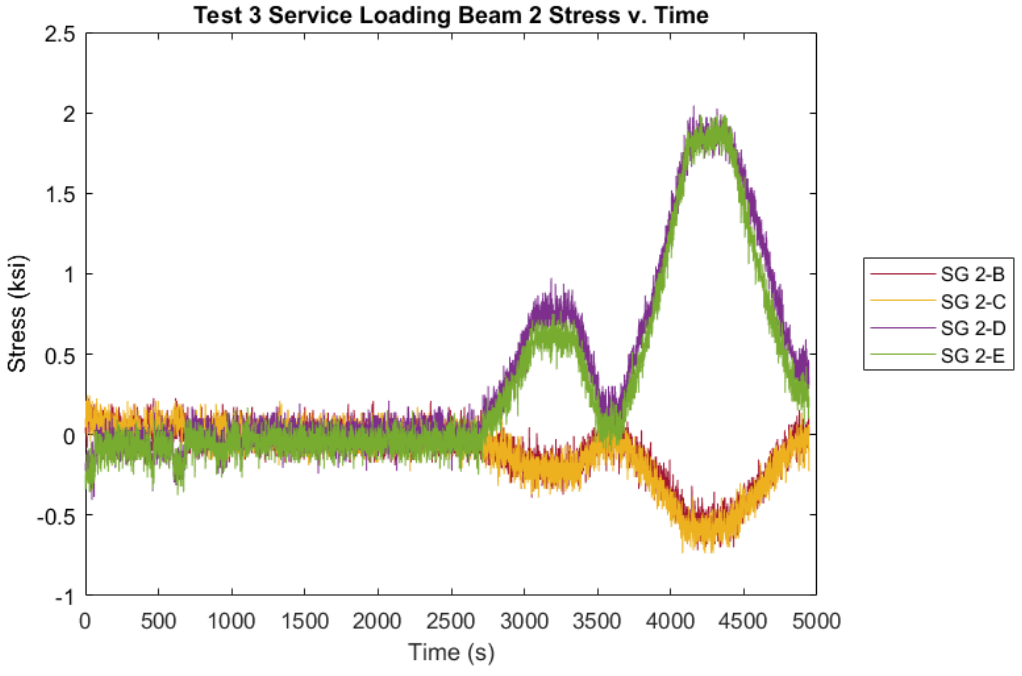

Figure 5.17: Test 3 Service Loading Beam 2 Stress v. Time

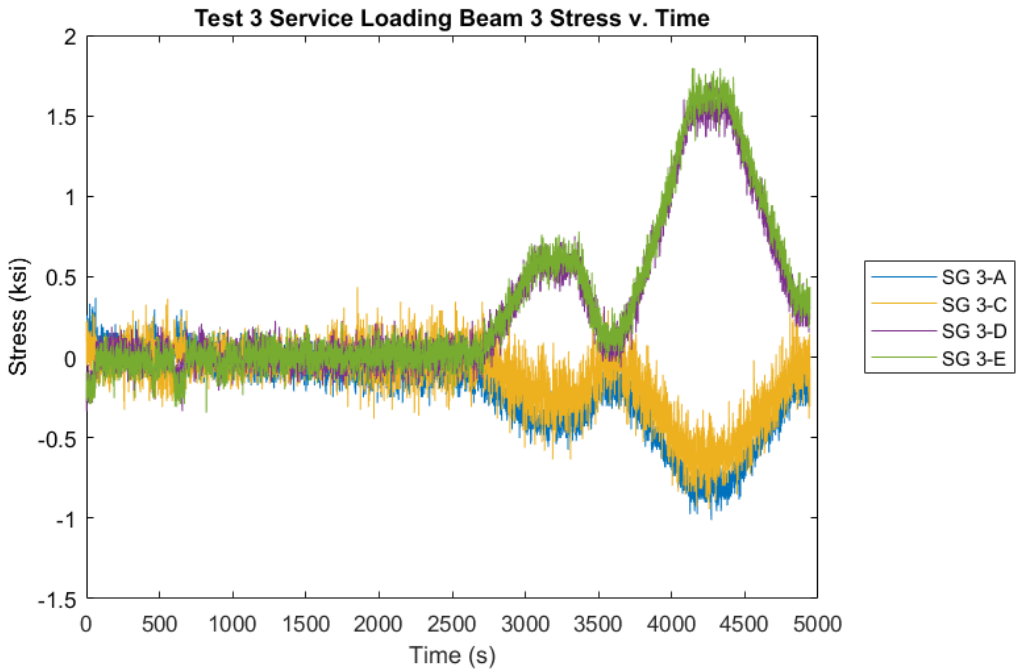

Figure 5.18: Test 3 Service Loading Beam 3 Stress v. Time

Figure 5.19, Figure 5.20, and Figure 5.21 show the microstrain time histories for each beam for failure loading. Microstrain is used for these figures instead of stress because the system experiences nonlinear behavior during this stage of testing. Therefore, Equation 1 is not valid, and stresses cannot be linearly calculated. For all three beams, the microstrains increase in magnitude gradually until failure. After failure, Beams 1 and 3 experience a small, sharp increase promptly followed by a sharp decrease. The microstrains are then constant until the load is removed, and they return toward zero. However, for Beam 2, the microstrains continue increasing after failure because the bond broke between the steel and the concrete, and the loading was more than the non-composite capacity of the beam. 35 microstrain is approximately equal to 1.0 ksi, meaning the assumed yield stress of 50 ksi is about 1750 microstrain. Figure

5.20 shows the strain increasing rapidly past 1750 microstrain for the top flange. This means that after the bond broke, the top flange yielded and experienced plastic behavior. This all matches with the evidence of the failure mode, which is further explained in Section 5.3.3.

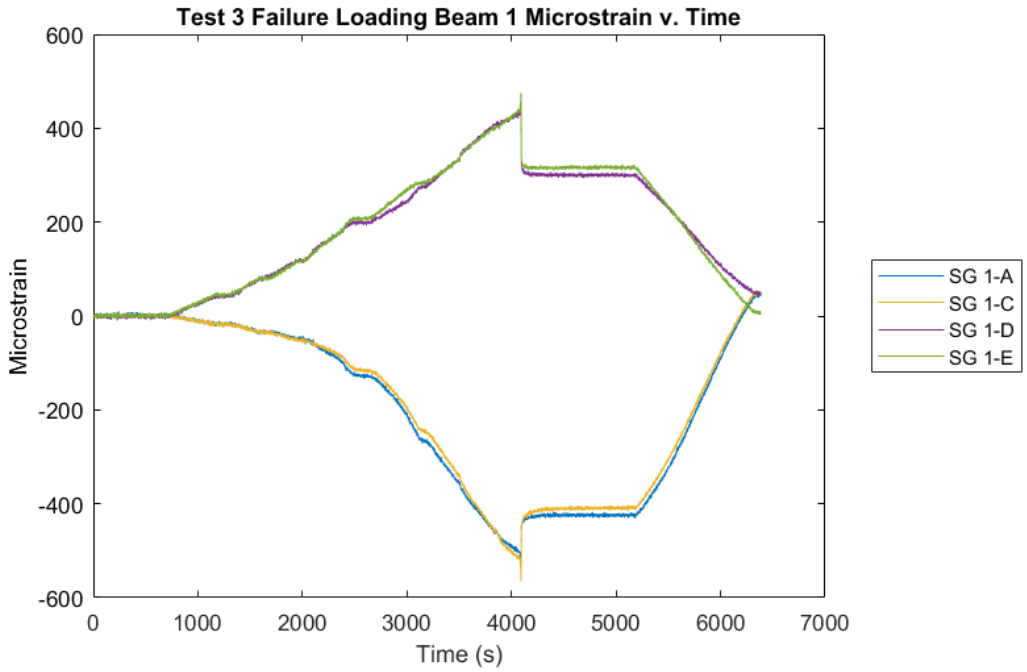

Figure 5.19: Test 3 Failure Loading Beam 1 Microstrain v. Time

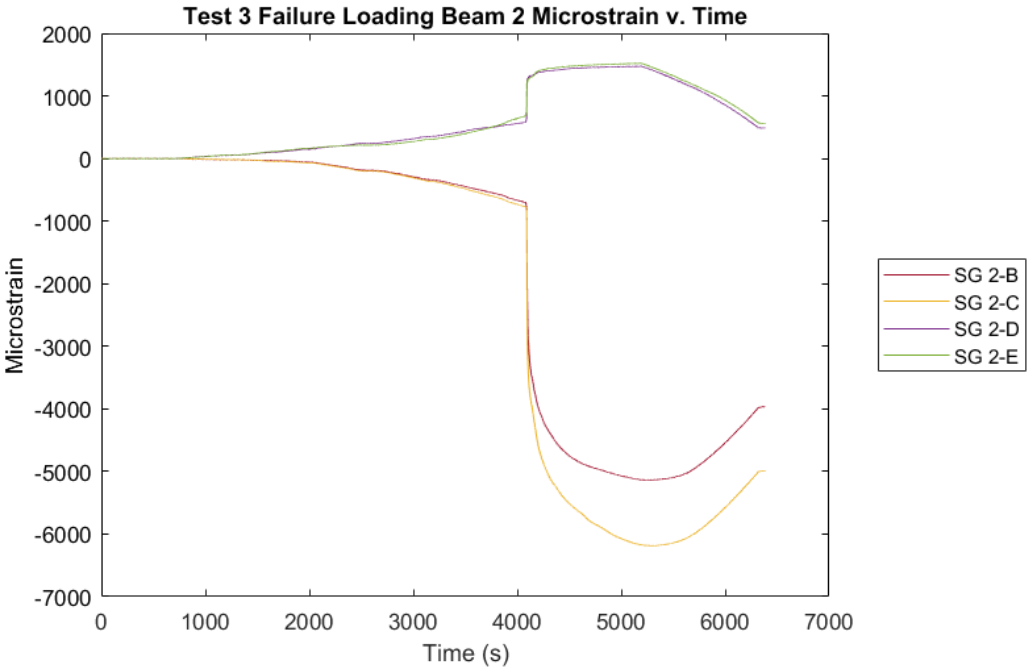

Figure 5.20: Test 3 Failure Loading Beam 2 Microstrain v. Time

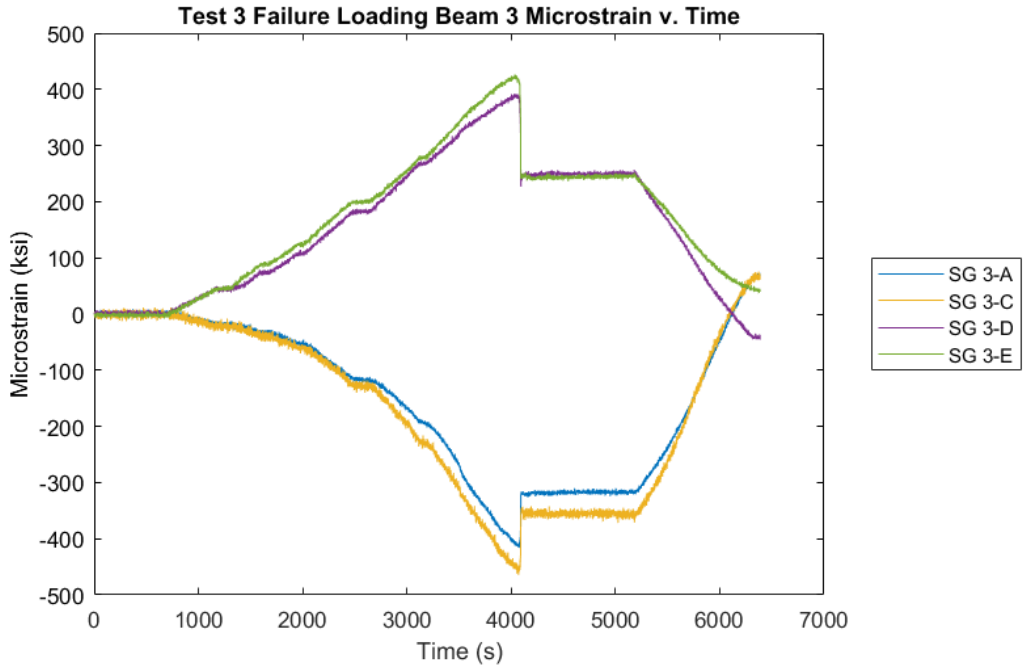

Figure 5.21: Test 3 Failure Loading Beam 3 Microstrain v. Time

The quality of the stress data can be seen in these time histories because they look as expected with the loads that were put on the system for each test. This can be even more clearly seen in Figure 5.22, which shows the strain v. time and load v. time graphs superimposed over each other for Beam 2 during Test 3. The stress changes correspond to the changes in load, which further reinforces the stress data quality.

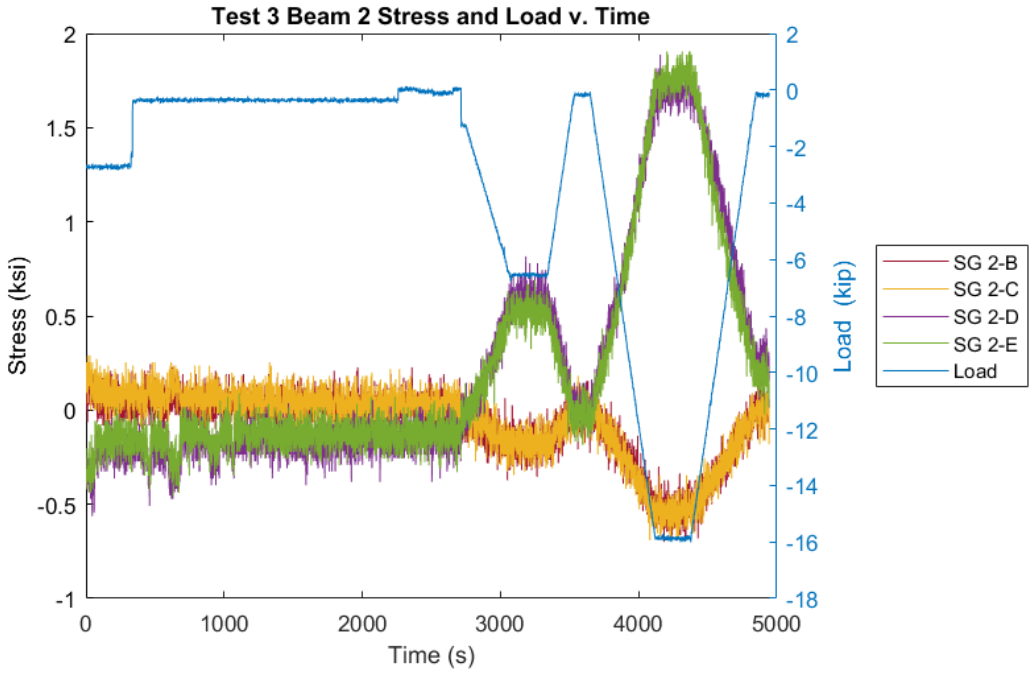

Figure 5.22: Test 3 Beam 2 Stress and Load v. Time

5.2.2. Deflection Data

The deflections collected during the experiment were measured in inches. Like the stresses, the deflections were taken as an average over which the data was steady (except for Test 3 Cases B and C) and zeroed at the beginning of each test so as to only capture the deflection due to the load in that test. However, capturing the deflection only for each test was made more complicated due to an issue with string pot recovery. As

shown in Figure 5.23, the vertical string pots did not recover during the tests as the load was taken off, meaning the deflection did not go back to zero. This occurred in both Test 1 and Test 3. However, the deflections can still be taken to be reasonably accurate for two reasons. The first is that, as shown in Section 5.4.2, the experimental deflections are reasonable when compared to theoretical calculations. These calculations use a flexural rigidity EI that is further validated in the comparison of the experimental versus theoretical stresses.

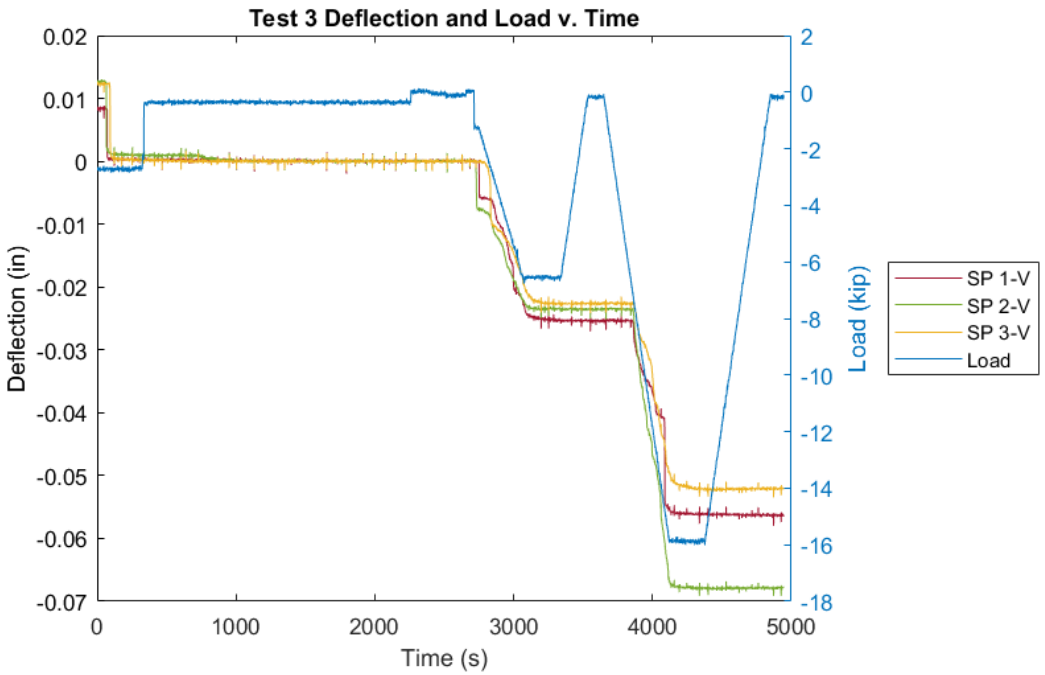

Figure 5.23: Test 3 Deflection and Load v. Time

The second reason is that the actuator stroke corresponds reasonably with the deflection data, as shown in Figure 5.24. It follows the deflection of SP 2-V closely since the actuator is directly above Beam 2. These two pieces of evidence support the decision to record the deflections as a summation over the test. Like the stress data, the

deflection data was zeroed at the beginning, but depending on a string pot's recovery, the deflection reported had to be adjusted. For example, if a string pot deflected 1 inch for Case A, but did not recover and then deflected 0 inches for Case B, the deflection for Case B would be reported as 1 inch.

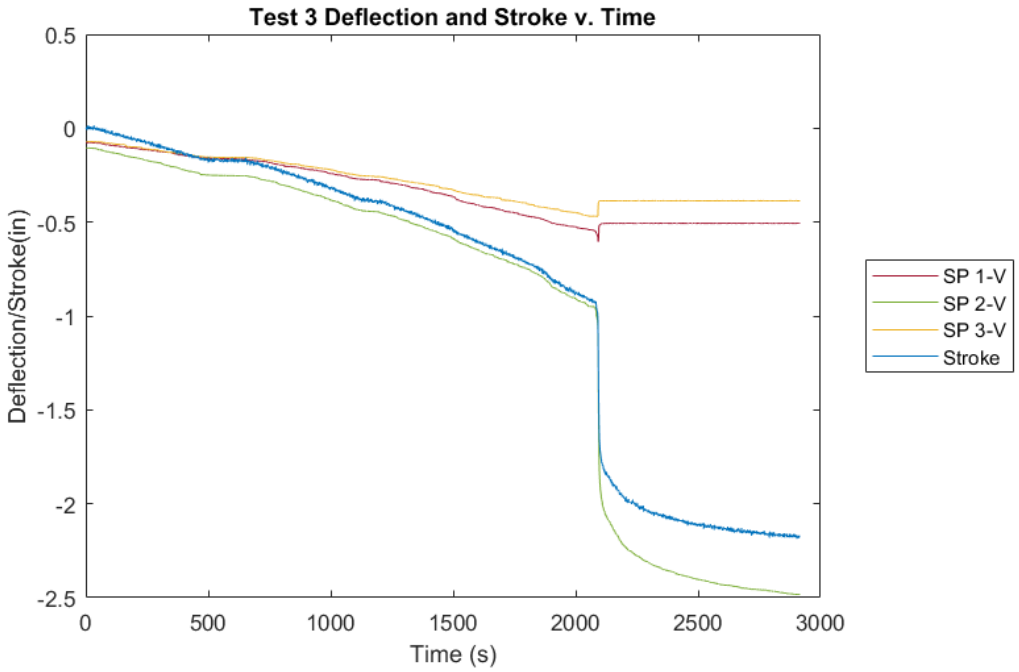

Figure 5.24: Test 3 Deflection and Stroke v. Time

Figure 5.25, Figure 5.26, and Figure 5.27 show the deflection over time for Cases A, B, and C of Test 1, respectively. The lack of recovery in the string pots was accounted for in these time histories, which is why Figure 5.26 and Figure 5.27 have deflections not starting at 0 inches. Figure 5.25 and Figure 5.27 show a larger deflection for Beam 2 than that of Beams 1 and 3. Figure 5.26 shows similar deflections for Beams 1 and 2 since they are loaded similarly for Case B.

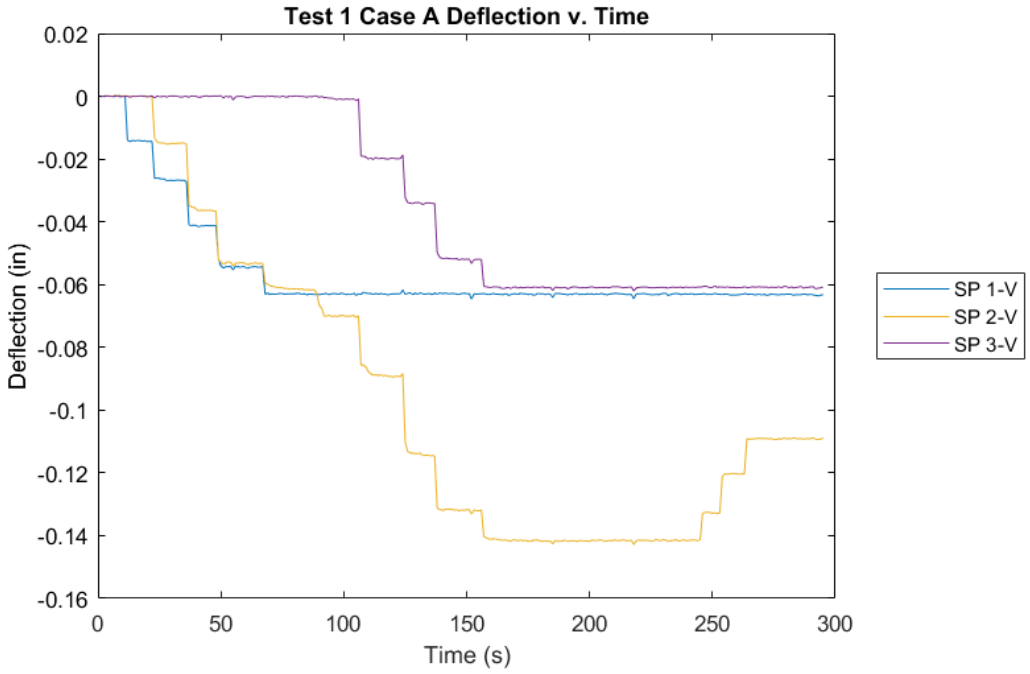

Figure 5.25: Test 1 Case A Deflection v. Time

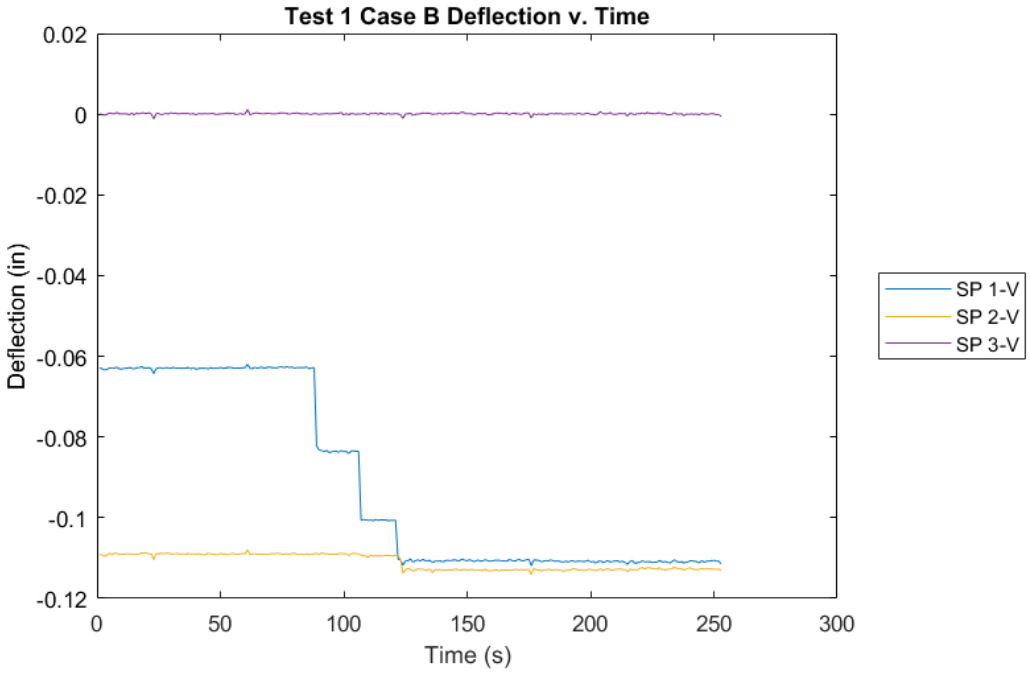

Figure 5.26: Test 1 Case B Deflection v. Time

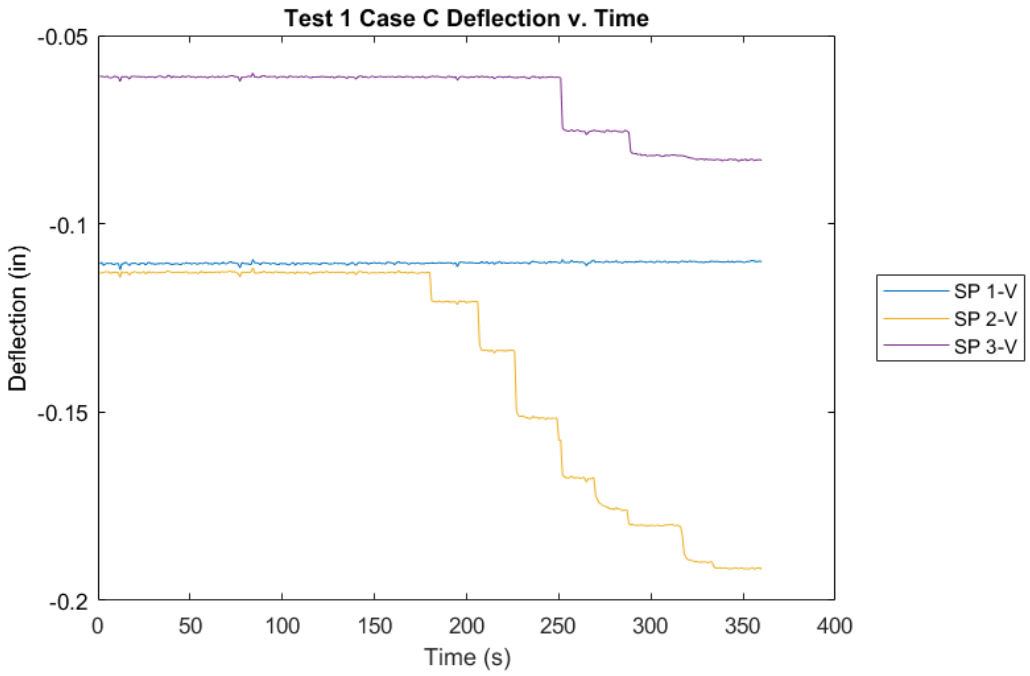

Figure 5.27: Test 1 Case C Deflection v. Time

Figure 5.28 shows the deflection over time for Test 2, which is the only test where load was not removed during data collection, and thus, string pot recovery did not need to be taken into account. This means that the deflections should be accurate; however, the magnitudes of SP 1-V and SP 3-V are much smaller than that of SP 2-V. Generally, Beam 2 should have about double the deflection that Beams 1 and 3 have.

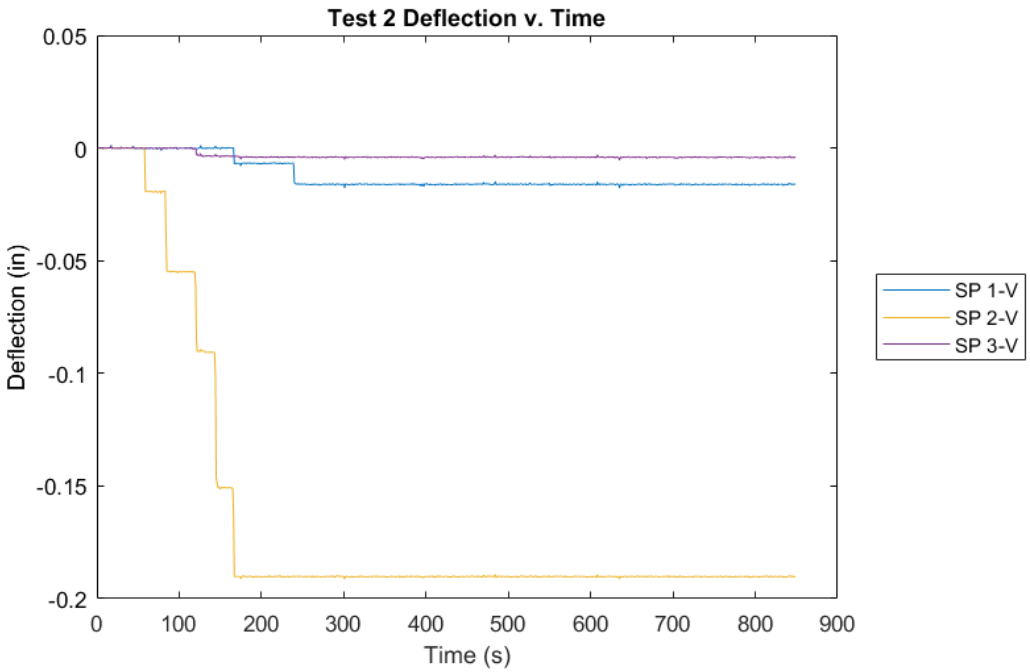

Figure 5.28: Test 2 Deflection v. Time

The deflection v. time graphs for Test 3 are shown in Figure 5.29 and Figure 5.30. The deflections for the service loading look accurate, with SP 2-V recording a larger deflection than SP 1-V or SP 3-V by the end. For the failure loading, the deflections again look accurate, with SP 2-V measuring larger deflections before failure and then experiencing a large increase in deflection since Beam 2 failed. Since Beam 2 experienced plastic deformation, its deflection does not recover as well as that of Beams 1 and 3.

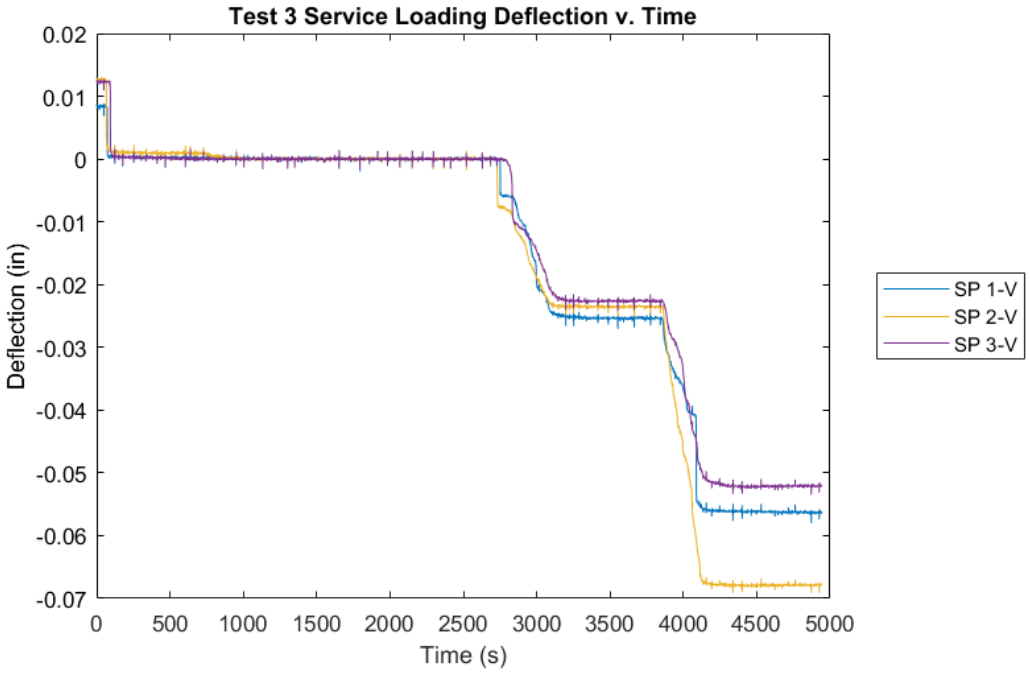

Figure 5.29: Test 3 Service Loading Deflection v. Time

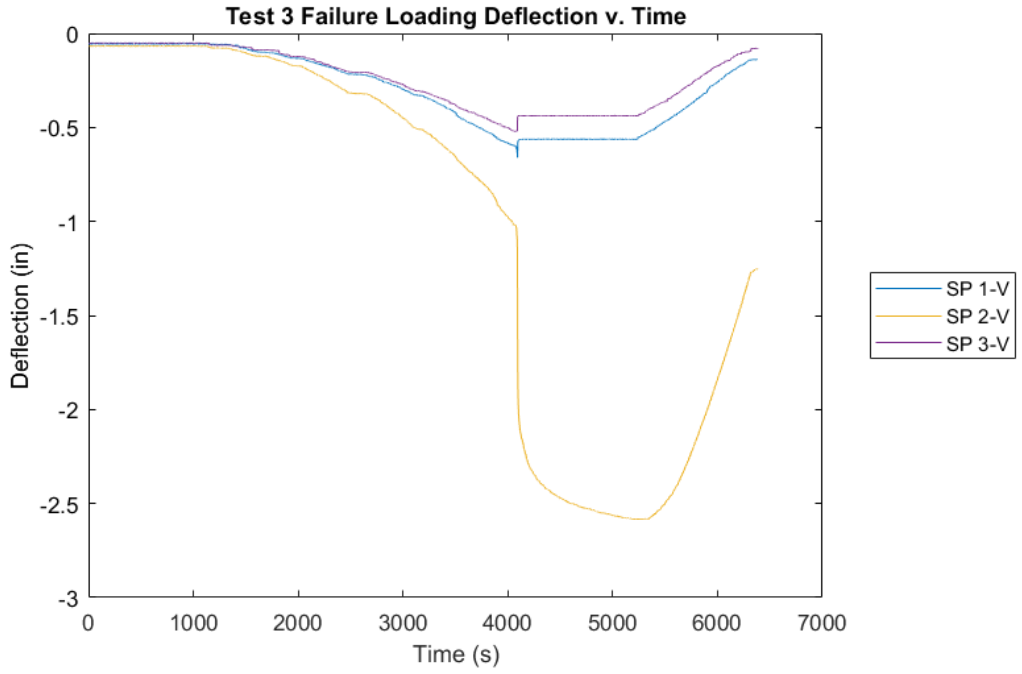

Figure 5.30: Test 3 Failure Loading Deflection v. Time

The rotation of the beam in degrees was determined from the lateral deflections using Equation 2, where Δ_{top} is the lateral deflection measured by the string pot attached to the top of the flange, Δ_{bottom} is the same, but for the bottom flange, d is the depth of the steel beam, and h_{angle} is the height off the beam of the string tied to steel angle, as seen in Figure 4.14. The factor at the end of the equation converts the rotation from radians to degrees. The values of d and h_{angle} are 12.1 inches and 2.1 inches, respectively.

$$Rotation = tan\left(\frac{\Delta_{top}-\Delta_{bottom}}{d+(2h_{angle})}\right)\left(\frac{180}{\pi}\right) \quad (2)$$

5.2.3. Actuator Data

The actuator provides the load and stroke it is using throughout the test, with the load measured in kips and the stroke measured in inches. It is important to note that, unlike the stress and deflection data, the load and stroke recorded during the tests are absolute, which means the data does not have to be zeroed before taking values.

Figure 5.31 and Figure 5.32 show the load time histories for the service loading and failure loading, respectively. Both are accurate reflections of the tests. Figure 5.31 shows steady increases to the desired load and decreases back to approximately zero load, representing the two service loads recorded during the test. Figure 5.32 shows steady increases in load to the stopping points outlined in Section 4.6, until failure at about 94.0 kips. This is corresponded with a slight jump in the graph, followed by a constant load since the load control method stopped the actuator from applying more load.

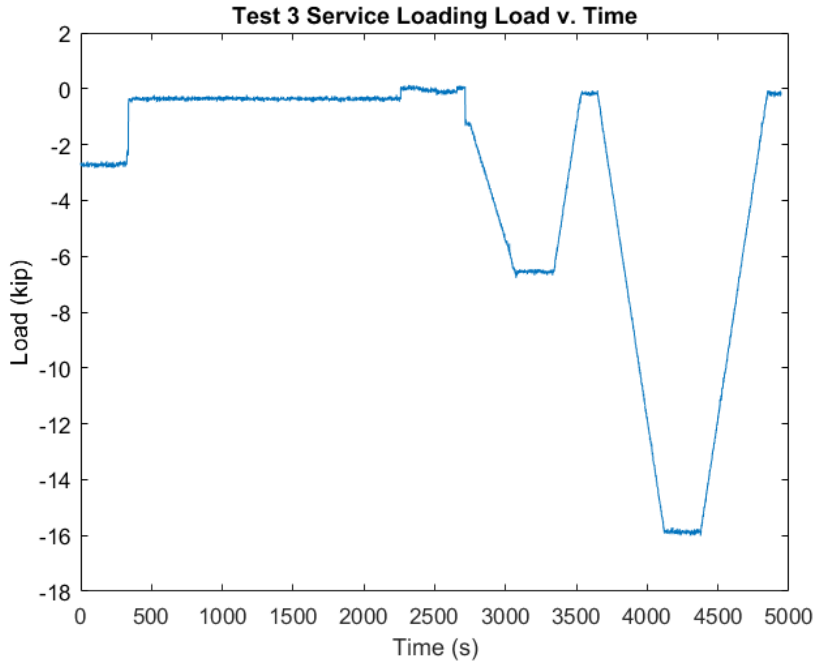

Figure 5.31: Test 3 Service Loading Load v. Time

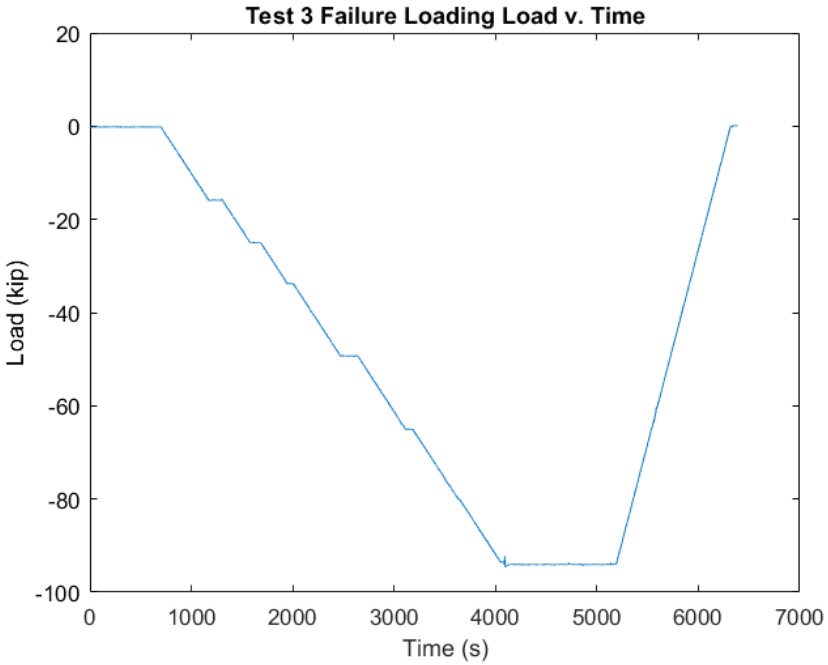

Figure 5.32: Test 3 Failure Loading Load v. Time

As shown before in Figure 5.22 and Figure 5.24, the load and stroke data correspond well with the stresses and deflections measured. Figure 5.33 shows that the load and stroke data also correspond well with each other, further reinforcing the quality of the data collection.

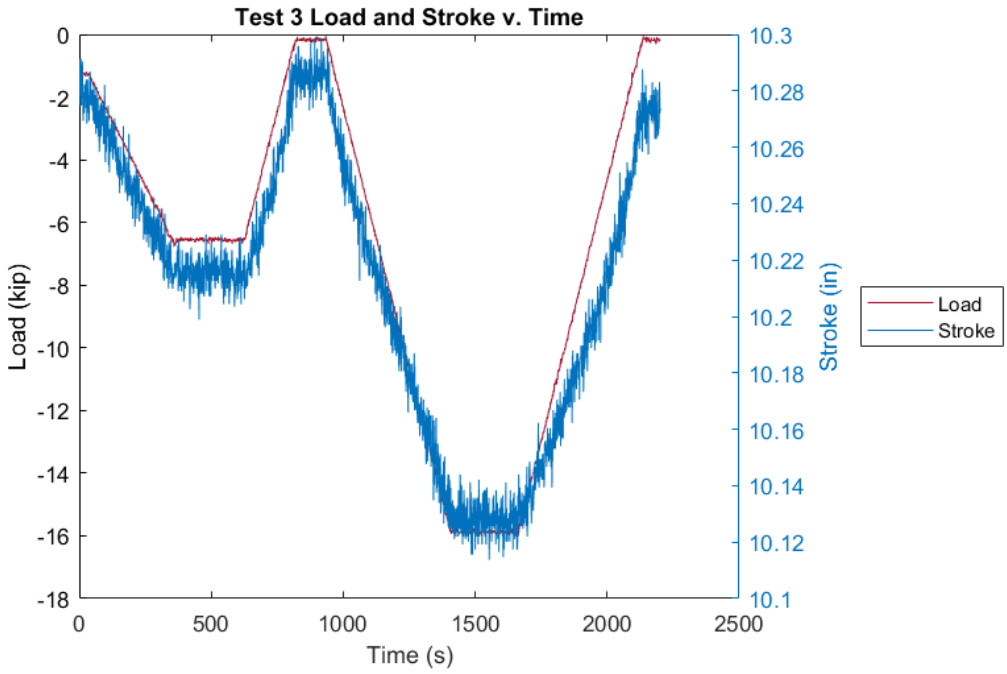

Figure 5.33: Test 3 Load and Stroke v. Time

5.3. Test Data and Initial Conclusions

This section provides experimental data visualization and data interpretation for the three tests, including the stresses, deflections, and rotations. All of the data in these sections was taken as an average over where the data was steady. Tests 1, 2, and 3 are covered by Sections 5.3.1, 5.3.2 and 5.3.3, respectively. Comparison of the experimental data with theoretical calculation is provided in Section 5.4.

5.3.1. Test 1: Panel Placement

The stresses, deflections, and rotations for all three cases of Test 1 are laid out in this section. The data given in this section for each case is when all of the panels were on the system. For Cases A and C, this is all ten panels, and for Case B, this is all five panels in the bay between Beams 1 and 2, as previously shown in Figure 4.16.

Figure 5.34 and Figure 5.35 visualize the stresses, deflections, and rotation experienced by the beams for Case A. The stresses for Beam 2 should be uniform across the flanges since the beam has the same load on either side. This is true for the top flange; the stresses along the bottom flange, however, are more imbalanced. Beams 1 and 3 have stresses of larger magnitude on the outside of the beam due to the torsion they are experiencing, and these stresses are fairly symmetrical. The deflection for Beam 2 is a little more than double those for Beams 1 and 3 because it is taking approximately double the load. The rotation is 1.50 degrees.

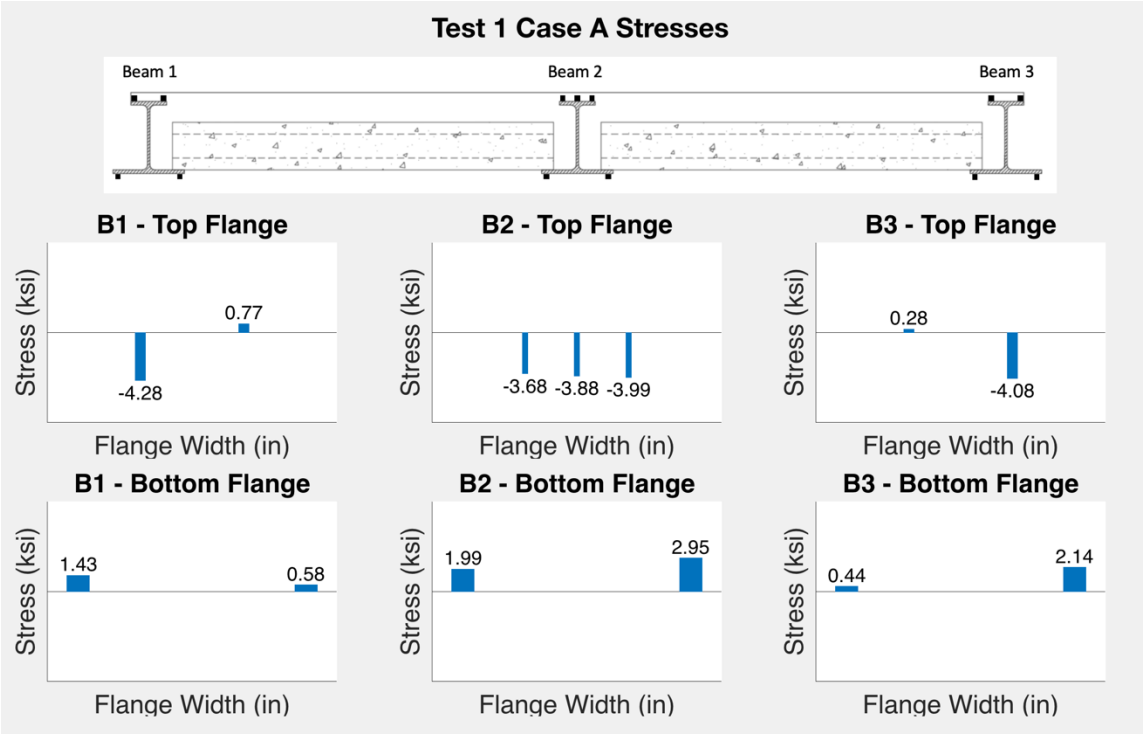

Figure 5.34: Test 1 Case A Stresses

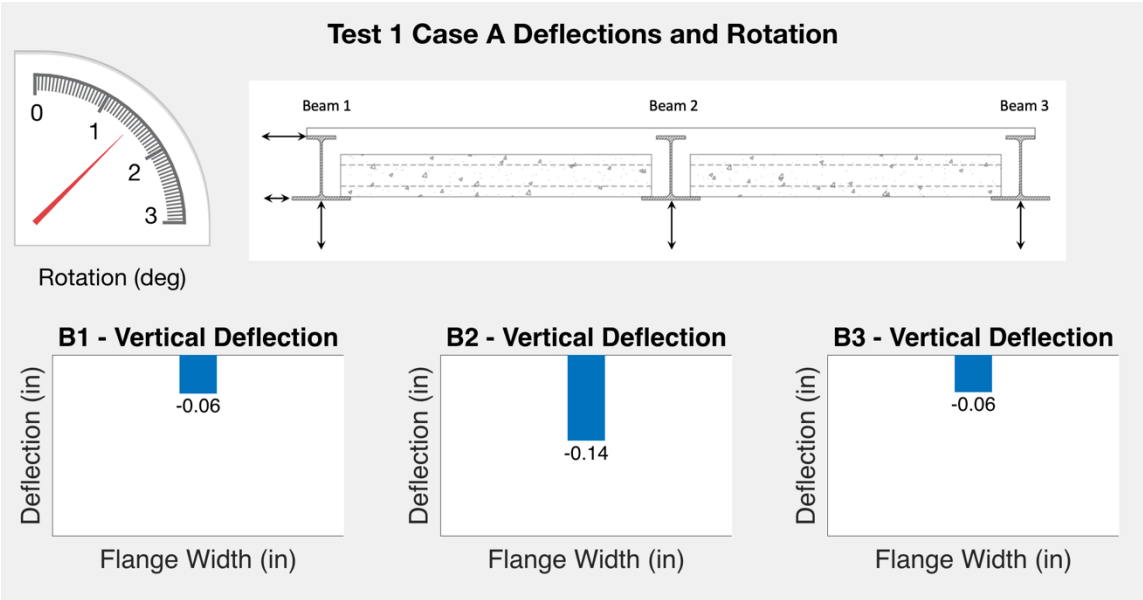

Figure 5.35: Test 1 Case A Deflections and Rotation

Figure 5.36 and Figure 5.37 show the stresses, deflections, and rotation for the beams during Case B. Case B only had panels in the bay between Beams 1 and 2, so Beam 3 did not experience any significant stress or any deflection. Unlike Case A, Beam 2 is now experiencing torsion, so the stresses on the outside of the beam are larger in magnitude than those on the inside. Beam 1 had a shear tab connection for Case B rather than the fixed connection it had for Cases A and C. This connection resulted in slightly higher stresses, deflection, and rotation, but ultimately, the pinned connection performed adequately. The deflections for Beams 1 and 2 are similar since both beams are taking the same load.

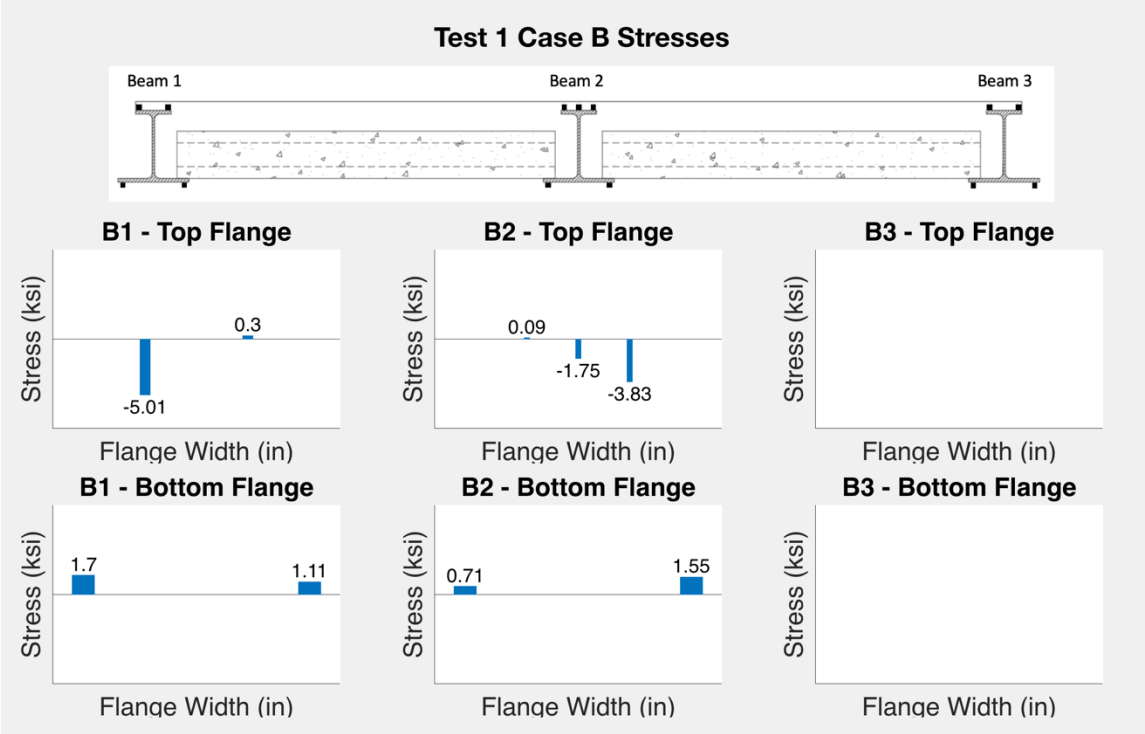

Figure 5.36: Test 1 Case B Stresses

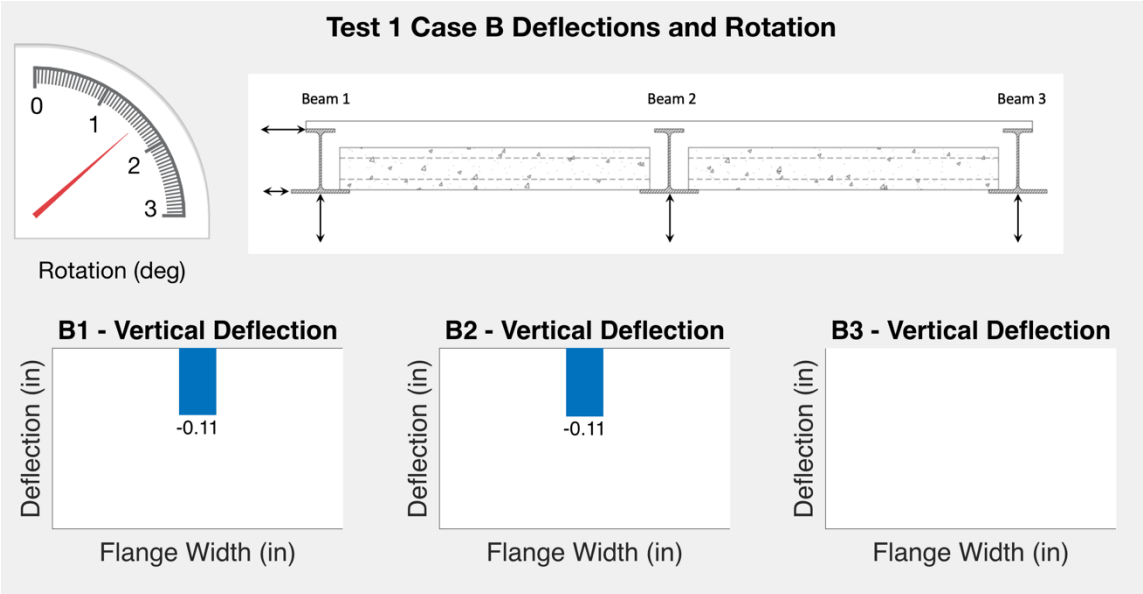

Figure 5.37: Test 1 Case B Deflections and Rotation

Figure 5.38 and Figure 5.39 show the stresses, deflections, and rotation for the beams during Case C. Cases A and C were conducted to see the effect of the order of panel placement on the results. The test values should be similar since they are both for all 10 panels on the system. The stresses and rotation are close, but the deflections for Case C are higher than those for Case A. The reason for this is unclear, but the deflections are still of reasonable magnitude. Ultimately, this data in combination with no issues during construction, shows that either order of panel placement is suitable.

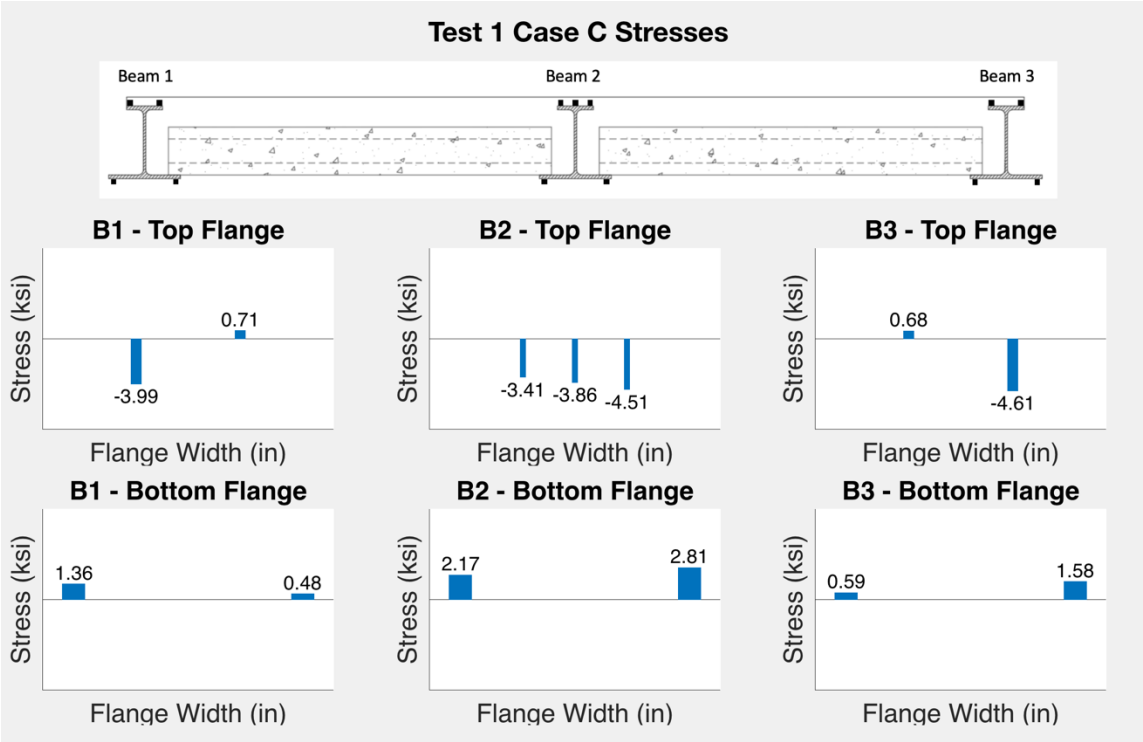

Figure 5.38: Test 1 Case C Stresses

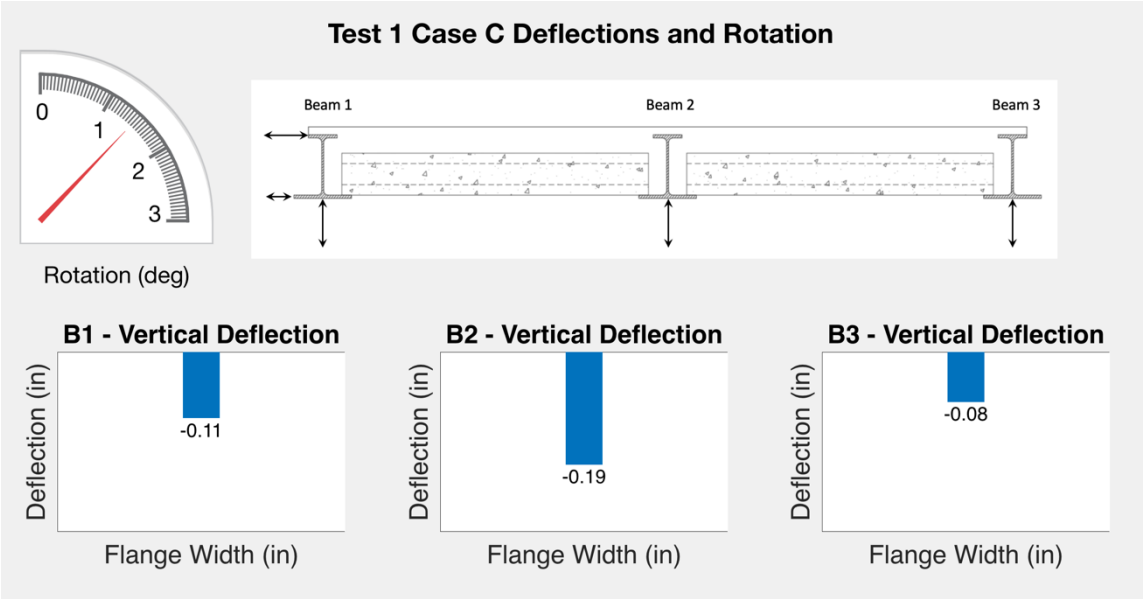

Figure 5.39: Test 1 Case C Deflections and Rotation

The test values for all three Test 1 cases are summarized in Table 5.1.

Table 5.1: Test 1 Experimental Values

			Case A	Case B	Case C
Beam 1	**Stress (ksi)**	**A**	-4.28	-5.01	-3.99
		C	0.77	0.30	0.71
		D	1.43	1.70	1.36
		E	0.58	1.11	0.48
	Deflection (in)		0.06	0.11	0.11
	Rotation (deg)		1.50	1.62	1.45
Beam 2	**Stress (ksi)**	**A**	-3.68	0.09	-3.41
		B	-3.88	-1.75	-3.86
		C	-3.99	-3.83	-4.51
		D	1.99	0.71	2.17
		E	2.95	1.55	2.81
	Deflection (in)		0.14	0.11	0.19
Beam 3	**Stress (ksi)**	**A**	0.28	-	0.68
		C	-4.08	-	-4.61
		D	0.44	-	0.59
		E	2.14	-	1.58
	Deflection (in)		0.06	-	0.08

The other information collected during Test 1 included the subjective evaluation of constructability. The erection of the steel and precast panels went smoothly without any major issues. The full evaluation can be found later in Section 6.1.

5.3.2. Test 2: Concrete Pour

The stresses, deflections, and rotations for Test 2 are laid out in this section. The data given in this section for each case is when all of the wet concrete was on the system. Data was collected throughout the concrete pour, but these values are from when the system was stable and taking the full weight of the wet concrete.

Figure 5.40 and Figure 5.41 show the stresses, deflections, and rotation for Test 2. As noted earlier in Section 5.2.1, SG 2-A is not shown because it failed during Test 2. Like Test 1 Cases A and C, the Beam 2 stresses are uniform, and the Beam 1 and 3 stresses are larger in magnitude on the outside of the beam due to the torsion they are experiencing.

When compared to Test 1, the Beam 2 stresses are larger in magnitude, while the Beam 1 and 3 stresses are similar in magnitude. The Beam 2 deflection is also much larger than the Beam 1 and 3 deflections, while for Test 1, the deflections were closer in magnitude. This could be because the wet concrete is more focused on the center beam, but the values of the Beam 1 and 3 deflections should be more comparable with that of Beam 2. The rotation is 0.65 degrees just for the Test 2 loads, but when added to the Test 1 rotation, the true rotation of Test 2 is 2.10 degrees.

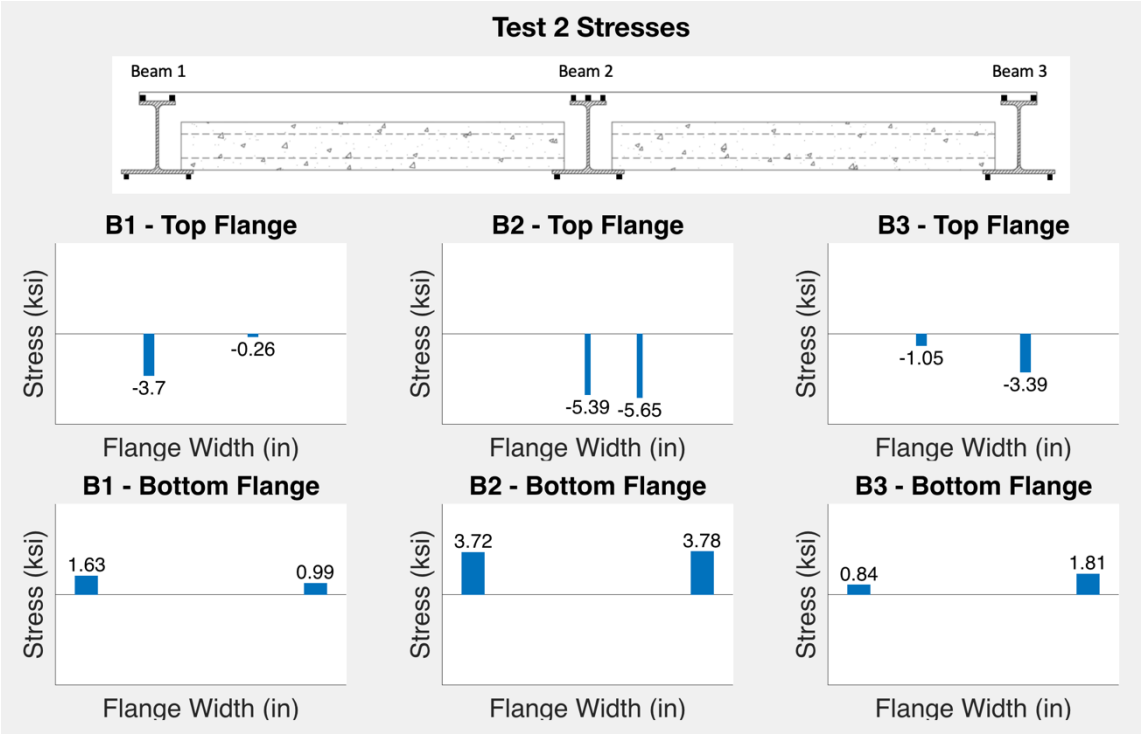

Figure 5.40: Test 2 Stresses

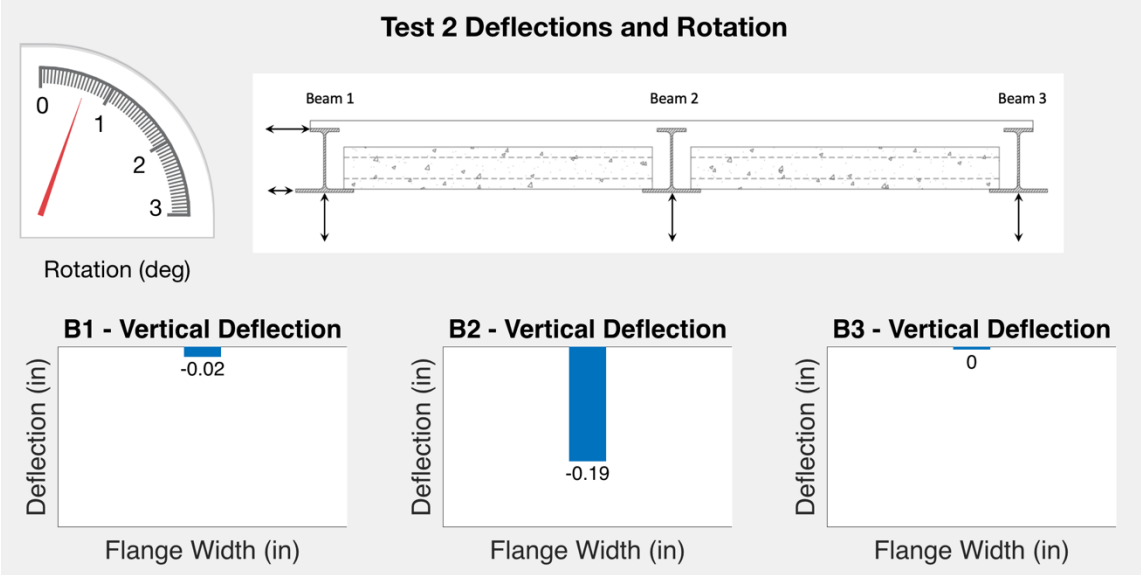

Figure 5.41: Test 2 Deflections and Rotation

The test values for Test 2 are summarized in Table 5.2.

Table 5.2: Test 2 Experimental Values

Beam 1	**Stress (ksi)**	**A**	-3.70
		C	-0.26
		D	1.63
		E	0.99
	Deflection (in)		0.02
	Rotation (deg)		0.65
Beam 2	**Stress (ksi)**	**A**	
		B	-5.39
		C	-5.65
		D	3.72
		E	3.78
	Deflection (in)		0.19
Beam 3	**Stress (ksi)**	**A**	-1.05
		C	-3.39
		D	0.84
		E	1.81
	Deflection (in)		0.00

As with Test 1, subjective observations were made about the concrete pour with A-shapes. The main concern was being able to fully fill the voids by the web of the A-

shape with wet concrete. This proved to not be an issue with 8-inch precast panels and a 12-inch deep section. However, if the A-shape is not as deep, the panels will either need to be shallower, or chamfers will need to be added to the top edges of the panels. Again, the full constructability evaluation can be found later in Section 6.1.

5.3.3. Test 3: Actuator Loading

The stresses, deflections, and rotations for all four cases of Test 3 are laid out in this section. As discussed in Section 5.1.1, the data for Case A, the 85 psf equivalent, was taken during the service loading test, which means the system was held steady at that load. The data for Cases B and C, the 100 and 200 psf equivalents, were taken during the ultimate loading test. As discussed in Sections 5.2.1 and 5.2.2, the data for Case A was taken as an average over when the data, or the load, was held steady. For Cases B and C, the load and data values were steadily increasing, so an average was taken over ±0.5 kips from the desired actuator load.

The concrete deck present for Test 3 causes a few differences in the results when compared to Tests 1 and 2. The first is that Beams 1 and 3 are laterally braced by the concrete deck, so they do not significantly rotate in Test 3. This results in uniform stress across the flanges for all the beams, not just Beam 2. The second difference is that the stresses on the top flange are smaller in magnitude than those on the bottom flange for Cases A, B, and C of Test 3. For Tests 1 and 2, the stresses on the top flange were larger. This is because for Test 3, while the system experiences composite behavior, the strain distribution is linear from the top of the concrete deck to the bottom of the steel. This means that the maximum compressive stress is on the top of the concrete deck, not the

top of the steel, and the stress on the top of the steel will be smaller in magnitude. This is further explained in Section 5.5.4.

Figure 5.42 and Figure 5.43 show the stresses, deflections, and rotation for Test 3 Case A (85 psf equivalent). The stresses on the top flange of Beam 2 are smaller than the stresses on the top flange of Beam 1 or 3, even though it should be taking more load. It is possible this is because the top flange of Beam 2 is completely encased in the concrete deck while the top flanges of Beams 1 and 3 are only partially encased.

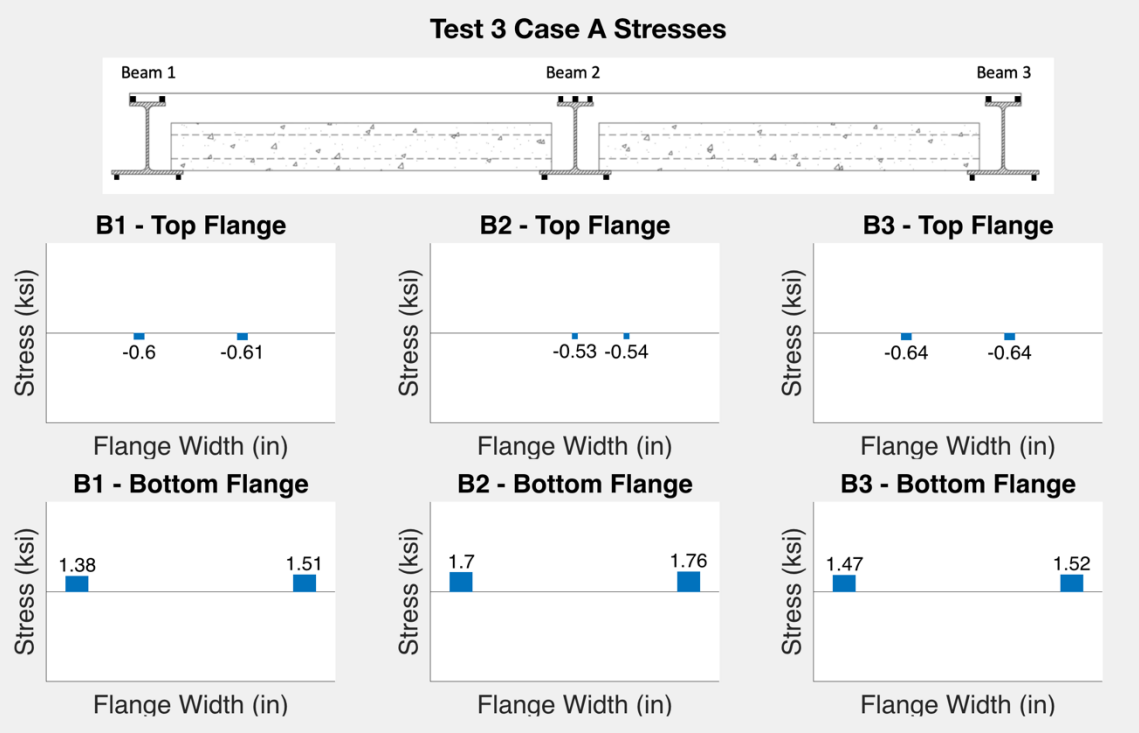

Figure 5.42: Test 3 Case A Stresses

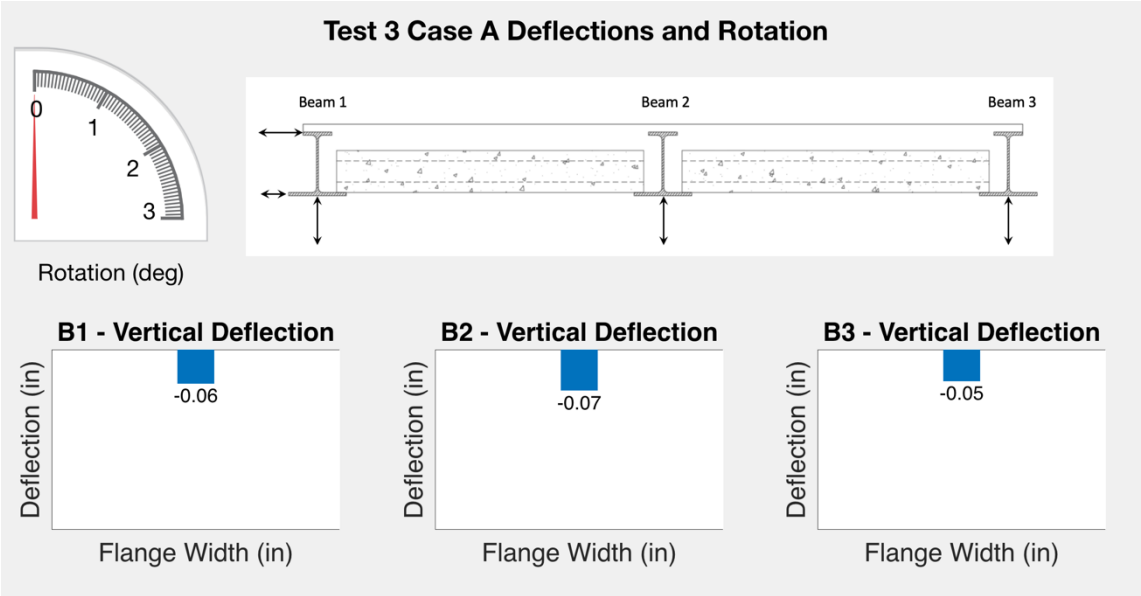

Figure 5.43: Test 3 Case A Deflections and Rotation

Figure 5.44 and Figure 5.45 show the stresses, deflections, and rotation for Test 3 Case B. The top flange stresses for Beam 2 are now approximately equal to those for Beams 1 and 3. Case B was the 100 psf equivalent, which is the design service live load. The general serviceability requirement for live load deflections is that the deflections must be less than L/360. The Beam 2 deflection of 0.09 inches is approximately equal to L/3000.

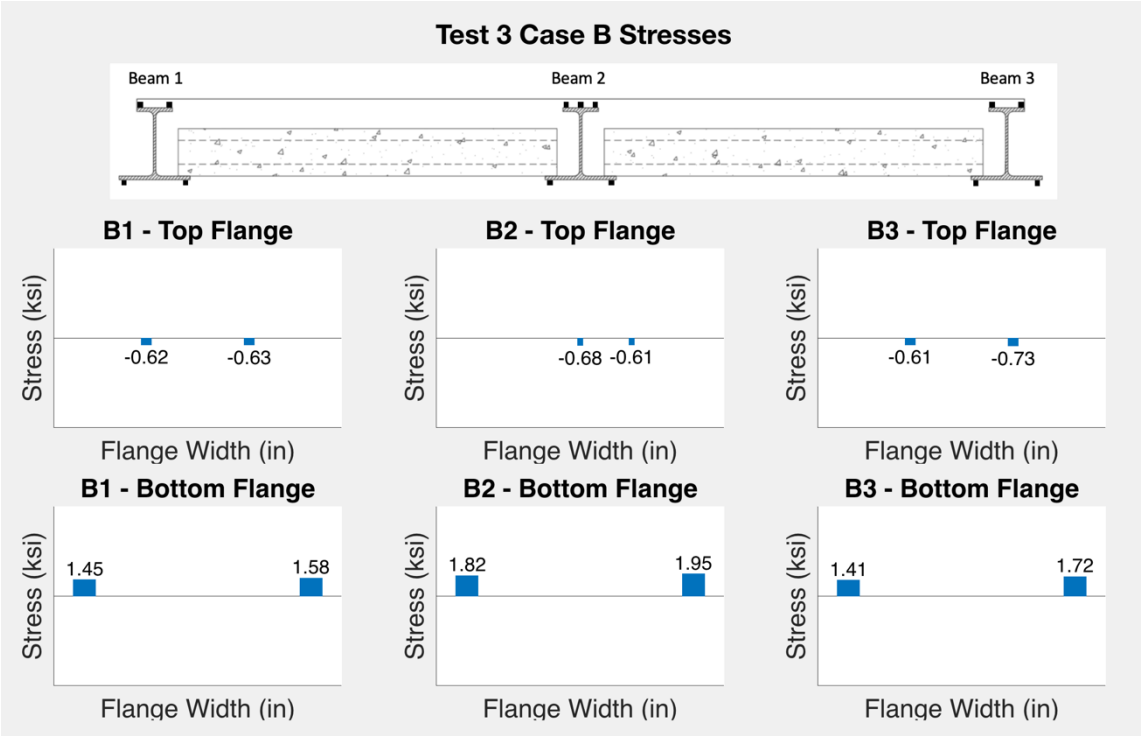

Figure 5.44: Test 3 Case B Stresses

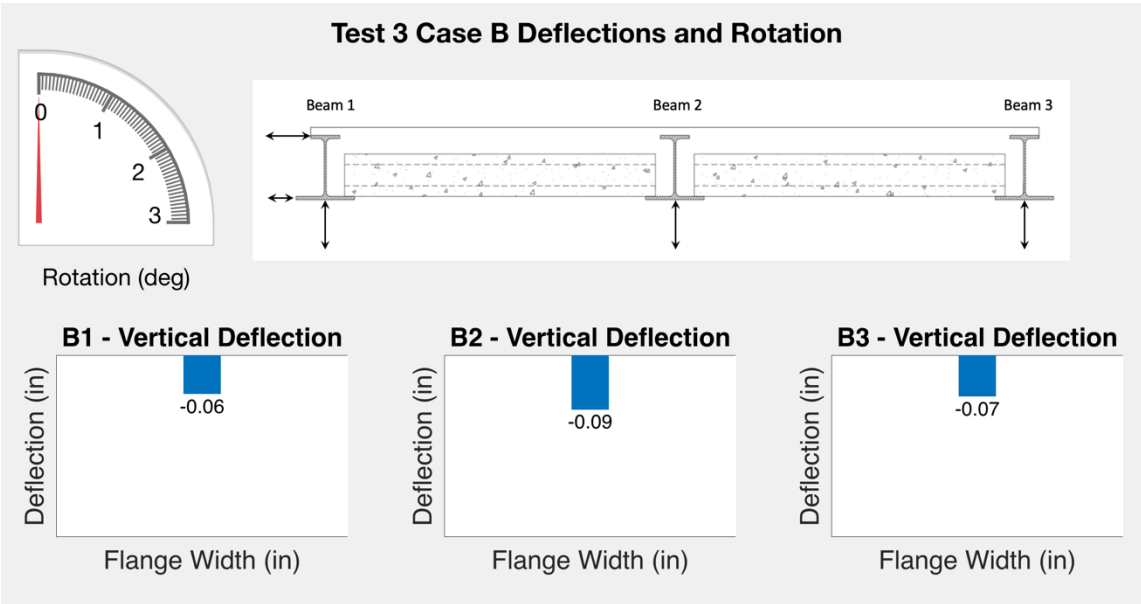

Figure 5.45: Test 3 Case B Deflections and Rotation

Figure 5.46 and Figure 5.47 show the stresses, deflections, and rotation for Test 3 Case C (200 psf equivalent). It is interesting to note here that the stresses for Beam 2 are higher than those for Beams 1 or 3, but this was not the case for Cases A and B. The load from the actuator is concentrated on Beam 2, and it is possible that Beam 2 took on more of the load as it increased. The deflection for Beam 2, 0.20 inches, is approximately equal to L/1300.

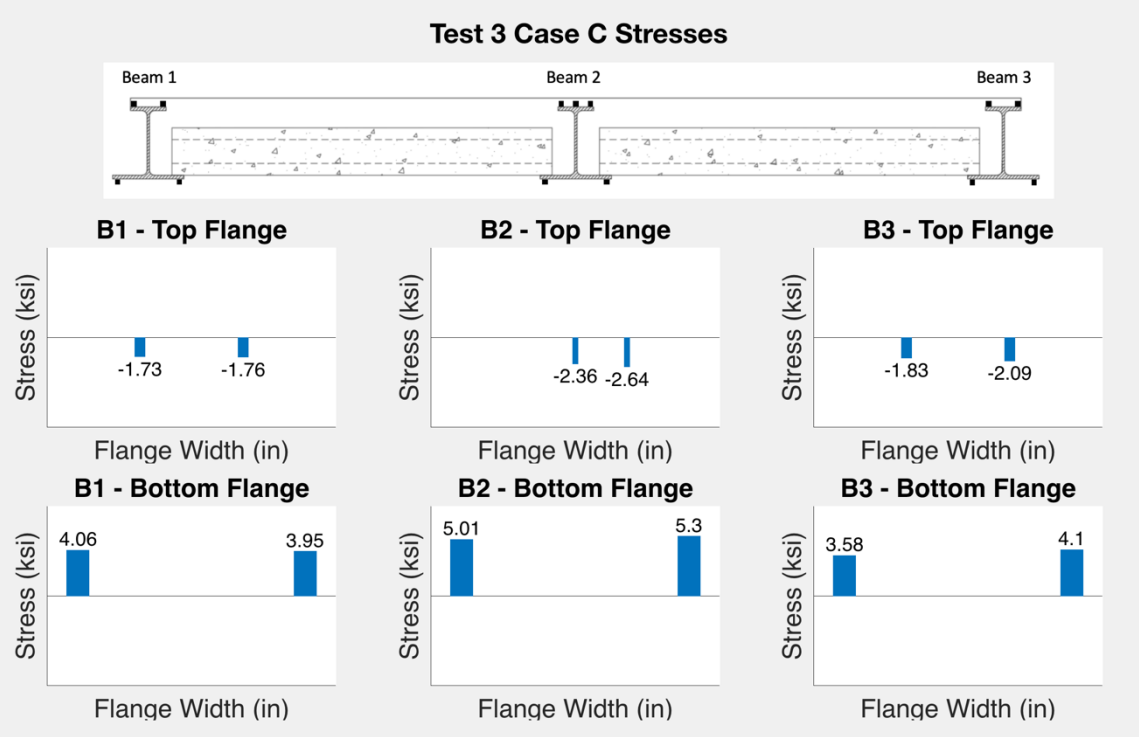

Figure 5.46: Test 3 Case C Stresses

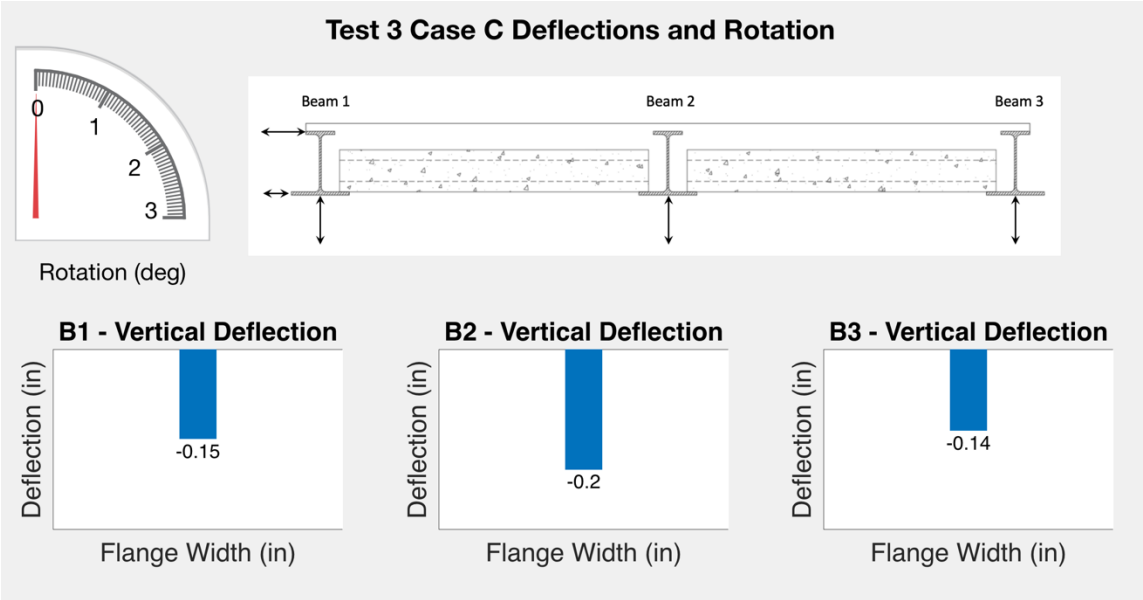

Figure 5.47: Test 3 Case C Deflections and Rotation

Test 3 Case D is the failure case for the system. The system failed at 94.0 kips, which was evidenced by a loud noise and the entire system rapidly bending before the actuator was stopped. The center beam experienced permanent deformation, as evidenced in Figure 5.48 by its steeper decline compared to the other two beams. The concrete slab separated from the steel beams, shown in Figure 5.48, Figure 5.49, and Figure 5.50. The precast panels and the concrete deck experienced cracking as well, shown in Figure 5.51 and Figure 5.52, respectively. The cracks in the concrete deck were concentrated around the midspan of the center beam (where it was loaded) and spread out from there.

Figure 5.48: Center beam deformation and steel-concrete separation (Photo by Matthew Yarnold)

Figure 5.49: Concrete deck separation from steel beam (Photo by Matthew Yarnold)

Figure 5.50: Concrete deck cracking and separation from steel beam (Photo by Sheyenne Davis)

Figure 5.51: Precast panel cracking (Photo by Sheyenne Davis)

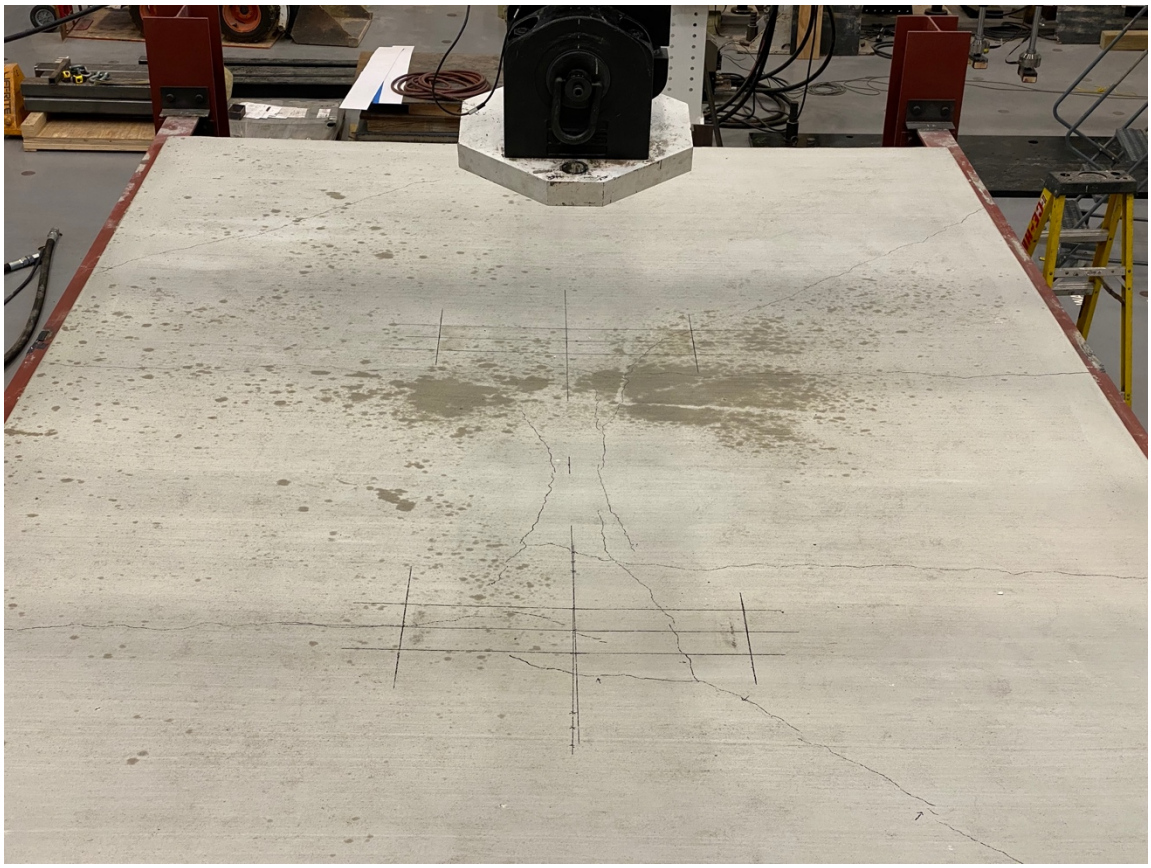

Figure 5.52: Concrete deck cracking (Photo by Sheyenne Davis)

From the permanent center beam deformation and separation of the concrete deck from the steel beams, it can be inferred that the system experienced composite behavior up until failure, upon which the bond between the steel and concrete broke, leaving the non-composite beams. Without the composite strength, the system quickly deformed. This inference is further supported by the calculations in Appendix A. If about half the load went to the center beam, the actuator load associated with yielding of the steel beam was 74 kips. At 94.0 kips, the steel beam quickly experienced plastic

deformation. The failure mode and level of composite behavior are further discussed in Section 5.5.4.

Figure 5.53 and Figure 5.54 show the stresses, deflections, and rotation for Test 3 Case D, or right before failure at 94.0 kips. All the values are much higher than all the cases, even that of Case C. This is encouraging because it means that the response due to double the service load (Case C) does not come close to failure, and the floor system has more than adequate strength. It is also worth noting that, unlike the earlier Test 3 cases, the stresses on the top flange are larger in magnitude than the stresses on the bottom flange. This shows that there was already slip between the steel and concrete, and the system was only partially composite before the failure made it non-composite. This is further discussed in Section 5.5.4. The deflection for Beam 2, 1.03 inches, is approximately equal to L/270. The failure of 94.0 kips is approximately equal to an area load of 500 psf, which is five times the design service load of 100 psf.

The test values for all four Test 3 cases are summarized in Table 5.3. The live load deflection equivalents are summarized in Table 5.4. The failure parameters are summarized in Table 5.5.

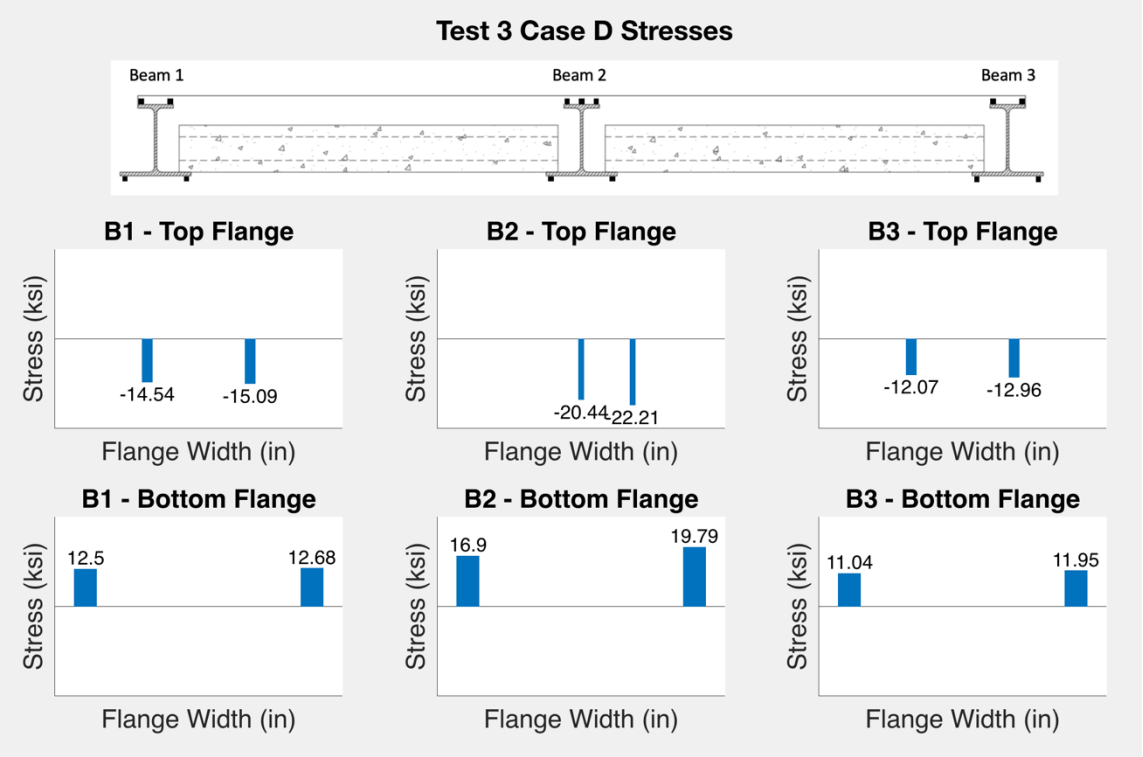

Figure 5.53: Test 3 Case D Stresses

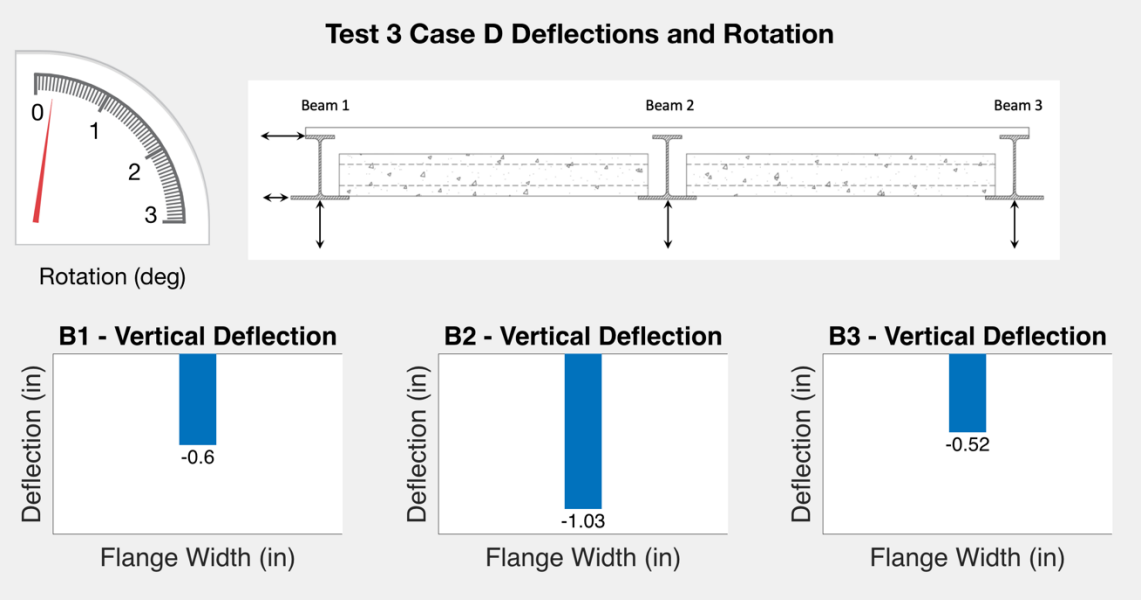

Figure 5.54: Test 3 Case D Deflections and Rotation

Table 5.3: Test 3 Experimental Values

			Case A	Case B	Case C	Case D
Beam 1	**Stress (ksi)**	**A**	-0.60	-0.62	-1.73	-14.54
		C	-0.61	-0.63	-1.76	-15.09
		D	1.38	1.45	4.06	12.50
		E	1.51	1.58	3.95	12.68
	Deflection (in)		0.06	0.06	0.15	0.60
	Rotation (deg)		0.00	0.00	0.01	0.26
Beam 2	**Stress (ksi)**	**A**				
		B	-0.53	-0.68	-2.36	-20.44
		C	-0.54	-0.61	-2.64	-22.21
		D	1.70	1.82	5.01	16.90
		E	1.76	1.95	5.30	19.79
	Deflection (in)		0.07	0.09	0.20	1.03
Beam 3	**Stress (ksi)**	**A**	-0.64	-0.61	-1.83	-12.07
		C	-0.64	-0.73	-2.09	-12.96
		D	1.47	1.41	3.58	11.04
		E	1.52	1.72	4.10	11.95
	Deflection (in)		0.05	0.07	0.14	0.52

Table 5.4: Live Load Deflection Equivalents

Case	Deflection Equivalent
Case B (100 psf)	L/3000
Case C (200 psf)	L/1300
Case D (Failure)	L/270

Table 5.5: Failure Parameters

Parameter	Value
Actuator Load	94.0 kips
Area Load Equivalent	500 psf
Failure Mode	Bond breaking

5.4. Theoretical vs. Experimental Values

In order to evaluate the performance of the system, its behavior must be understood beyond the raw data. A good beginning point for this is to compare the theoretical response to the experimental response and determine how close the behavior was to what was expected.

5.4.1. Theoretical Calculations

Calculations were done to determine the stress, deflection, and rotation values the beams would theoretically undergo for each test. Each test had a calculation for the center beam, which was loaded concentrically, as well as an edge beam, which was loaded eccentrically. The calculations for Tests 1 and 2 were done for a non-composite steel A-shape with lateral bracing at the ends. The calculations for Test 3 were done for a

composite steel A-shape with a concrete deck that was continuously braced. A full sample calculation for each test can be found in Appendix B.

Table 5.6 shows the values of major parameters in the calculations for each test. E is the modulus of elasticity, measured in ksi. E_s and E_c are the moduli for the steel and concrete, respectively. G is the shear modulus, measured in ksi. The values in the table are for structural steel and stay constant. Grade 50 steel was used, as reflected by the yield strength, F_y. I_x is the moment of inertia of the section, which is measured in in^4, and whose calculation can be seen as a part of Appendix B. E and I_x together describe the flexural rigidity of the beam, EI. For the non-composite system, E is E_s, and for the composite system, E is accounted for by using the modular ratio, n, which is the ratio of E_s to E_c. I_x of the composite system also depends on this modular ratio. The eccentricity of the load on the edge beams, e, is measured in inches from the center of the section to the concentrated load (assumed as the center of bearing). Test 3 does not include an eccentricity because it was torsionally braced by the concrete encasement. This was later supported by the experimental results where negligible rotation was experienced prior to the ultimate load.

Table 5.6: Calculation Values

		Test 1	Test 2	Test 3
E_s (ksi)	-	29000		
E_c (ksi)	-	-		4187
G (ksi)	-	11200		
F_y (ksi)	-	50		
I_x (in^4)	Center Beam	373.3		1223.0
	Edge Beam			918.9
e (in)	-	5.0	3.0	-
Load	-	64 psf	150 pcf	85 psf
				100 psf
				200 psf

Along with these parameters, there were a few significant uncertainties associated with the calculations for the theoretical response. This required some assumptions to be made, several of which are explained below.

1. Boundary Conditions: In theory, the beams are assumed to have either pinned or fixed boundary conditions at their ends (for bending and torsion), but in reality, the connections will fall somewhere between these conditions. This assumption affects the equations used to determine both the bending and torsional stresses. These equations also assume the loading, which was a distributed load for Tests 1 and 2 and two point

loads for Test 3, shown in Figure 5.55. Both loading types are assumed to be loaded at the center of bearing. Since the boundary condition is a binary assumption, calculations were done for both pinned and fixed connections.

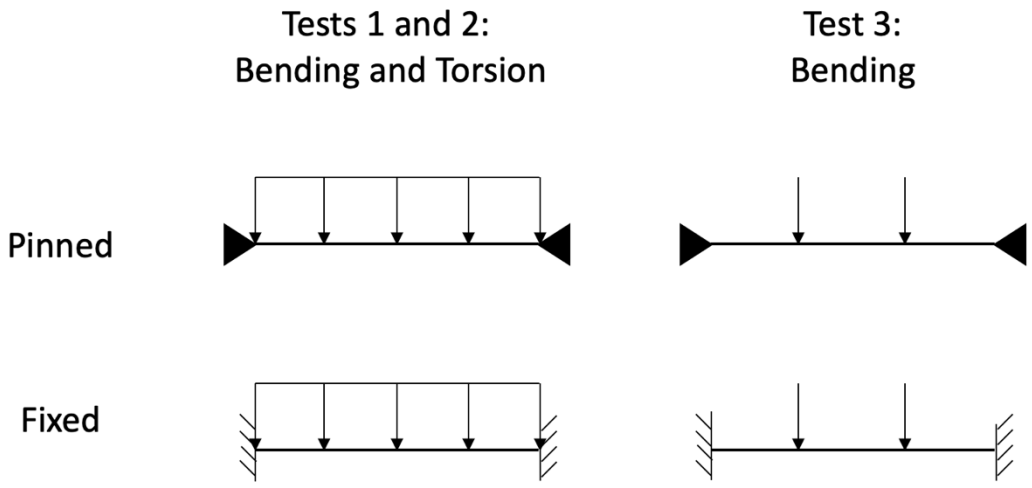

Figure 5.55: Loading and Boundary Condition Cases

2. Load Distribution: The load distribution between the beams during Test 3 is complicated due to the setup, which includes different connection types. Beams are normally assumed to take load based on tributary widths, meaning for this setup, the load distribution would be assumed to be 25%-50%-25% for Beams 1, 2, and 3, respectively. This is generally correct for non-composite systems, as used in Tests 1 and 2. For Test 3 however, since there is a concrete deck and the actuator is loading right

over Beam 2, the load may distribute differently. For these calculations, the load distribution was assumed to be 25%-50%-25% for every test.

3. Composite Section Flexural Rigidity: The flexural rigidity of the system for Tests 1 and 2 is well known, as the steel modulus of elasticity, E_s, stays constant at 29,000 ksi for structural steel, and I_x is easily calculated. For Test 3, the calculation of the composite flexural rigidity takes the concrete deck into account. The biggest unknowns in the calculation of this composite flexural rigidity are the effective width of the composite section, which determines how the stresses develop in the concrete, and E_c, the modulus of elasticity of the concrete deck. For these calculations, the effective width was assumed to be the tributary width, which is three feet for the edge beams and six feet for the center beam. E_c was calculated from the f'c value (concrete compressive strength) obtained from testing concrete cylinders.

In addition to these assumptions, there is one more known parameter that had to be taken into account. The outer strain gauges are set half an inch inside the flanges, as shown earlier in Figure 4.9. The equations for the torsional stresses calculate the maximum, which is at the edge of the flange. Therefore, these values were adjusted properly for the half-inch difference.

5.4.2. Overall Comparison

For the initial comparison of theoretical to experimental values, the results were bounded between the calculations for pinned and fixed boundary conditions (bending

and torsion). In the following tables, the experimental stresses, deflections, and rotations are shown alongside those from the theoretical calculations for both the pinned and fixed conditions. If the experimental result bounds between the pinned and fixed theoretical value, its cell is green. If it does not bound, its cell is red.

Table 5.7 shows the value comparison for all the cases for Test 1. As before in Section 5.3.1, the experimental stresses for each case are from when all the panels are on the system. This means that for Beams 1 and 3, all the cases have the same theoretical stresses, just mirrored. For Beam 2, Cases A and C have the same theoretical values, but since Case B only loads one side of Beam 2, it has the same theoretical values as Beams 1 and 3. The experimental stresses and deflection of Beam 3 for Case B are zero or near-zero, so they are not included in this table. As can be seen in the table, only one of the stresses did not bound at 1.11 ksi, and it is very close to the theoretical value for the pinned condition, 1.05 ksi (only 5% over). All of the deflections and rotations are bound.

Table 5.7: Test 1 Comparison

			Theoretical		Experimental		
			Pinned	Fixed	Case A	Case B	Case C
Beam 1	Stress (ksi)	A	-6.06	-3.37	-4.28	-5.01	-3.99
		C	0.05	1.37	0.77	0.30	0.71
		D	2.73	1.28	1.43	1.70	1.36
		E	1.05	-0.02	0.58	1.11	0.48
	Deflection (in)		0.11	0.02	0.06	0.11	0.11
	Rotation (deg)		1.98	0.98	1.50	1.62	1.45
Beam 2	Stress (ksi)	A	-6.01	-2.01	-3.68	-	-3.41
			0.05	1.37	-	0.09	-
		B	-6.01	-2.01	-3.88	-	-3.86
			-3.03	-1.01	-	-1.75	-
		C	-6.01	-2.01	-3.99	-	-4.51
			-6.06	-3.37	-	-3.83	-
		D	3.78	1.26	1.99	-	2.17
			1.05	-0.02	-	0.71	-
		E	3.78	1.26	2.95	-	2.81
			2.73	1.28	-	1.55	-
	Deflection (in)		0.22	0.04	0.14	-	0.19
			0.11	0.02	-	0.11	-

Table 5.7 Continued

			Theoretical		Experimental		
			Pinned	**Fixed**	**Case A**	**Case B**	**Case C**
Beam 3	**Stress (ksi)**	**A**	0.05	1.37	0.28	-	0.68
		C	-6.06	-3.37	-4.08	-	-4.61
		D	1.05	-0.02	0.44	-	0.59
		E	2.73	1.28	2.14	-	1.58
	Deflection (in)		0.11	0.02	0.06	-	0.08

Table 5.8 shows the value comparison for Test 2. All of the stresses and most of the deflections are bound, but one of the deflections and the rotation are not bound. However, both of the deflections for the edge beams and the rotation are very close to the theoretical values for the fixed condition.

Table 5.9, Table 5.10, and Table 5.11 show the value comparisons for Test 3. For Cases A and B, shown in Table 5.9 and Table 5.10, all of the stresses and deflections are bound. For Case C, shown in Table 5.11, two of the stresses and one of the deflections do not bound, but they are close to the theoretical values for the pinned condition. A table for Case D is not included because it is a more complicated case discussed further in Section 5.5.4.

Table 5.8: Test 2 Comparison

			Theoretical		Experimental
			Pinned	Fixed	
Beam 1	Stress (ksi)	A	-5.46	-2.73	-3.71
		C	-1.32	0.47	-0.26
		D	2.70	1.15	1.63
		E	1.56	0.27	0.99
	Deflection (in)		0.12	0.02	0.02
	Rotation (deg)		1.34	0.66	0.65
Beam 2	Stress (ksi)	A			
		B	-6.78	-2.26	-5.39
		C	-6.78	-2.26	-5.65
		D	4.26	1.39	3.72
		E	4.26	1.39	3.78
	Deflection (in)		0.25	0.05	0.19
Beam 3	Stress (ksi)	A	-1.32	0.47	-1.05
		C	-5.46	-2.73	-3.39
		D	1.56	0.27	0.84
		E	2.70	1.15	1.81
	Deflection (in)		0.12	0.02	0.00

Table 5.9: Test 3 Case A Comparison

			Theoretical		Experimental
			Pinned	Fixed	
Beam 1	Stress (ksi)	A	-0.82	-0.30	-0.60
		C	-0.82	-0.30	-0.61
		D	1.81	0.67	1.38
		E	1.81	0.67	1.51
	Deflection (in)		0.06	0.01	0.06
Beam 2	Stress (ksi)	A			
		B	-1.00	-0.37	-0.53
		C	-1.00	-0.37	-0.54
		D	2.96	1.09	1.70
		E	2.96	1.09	1.76
	Deflection (in)		0.09	0.02	0.07
Beam 3	Stress (ksi)	A	-0.82	-0.30	-0.64
		C	-0.82	-0.30	-0.64
		D	1.81	0.67	1.47
		E	1.81	0.67	1.52
	Deflection (in)		0.06	0.01	0.05

Table 5.10: Test 3 Case B Comparison

			Theoretical		Experimental
			Pinned	Fixed	
Beam 1	Stress (ksi)	A	-0.97	-0.36	-0.62
		C	-0.97	-0.36	-0.63
		D	2.14	0.79	1.45
		E	2.14	0.79	1.58
	Deflection (in)		0.07	0.01	0.06
Beam 2	Stress (ksi)	A			
		B	-1.18	-0.44	-0.68
		C	-1.18	-0.44	-0.61
		D	3.49	1.29	1.82
		E	3.49	1.29	1.95
	Deflection (in)		0.10	0.02	0.09
Beam 3	Stress (ksi)	A	-0.97	-0.36	-0.61
		C	-0.97	-0.36	-0.73
		D	2.14	0.79	1.41
		E	2.14	0.79	1.72
	Deflection (in)		0.07	0.01	0.07

Table 5.11: Test 3 Case C Comparison

			Theoretical		Experimental
			Pinned	Fixed	
Beam 1	Stress (ksi)	A	-1.94	-0.72	-1.73
		C	-1.94	-0.72	-1.76
		D	4.27	1.58	4.06
		E	4.27	1.58	3.95
	Deflection (in)		0.14	0.03	0.15
Beam 2	Stress (ksi)	A			
		B	-2.36	-0.87	-2.36
		C	-2.36	-0.87	-2.64
		D	6.98	2.57	5.01
		E	6.98	2.57	5.30
	Deflection (in)		0.21	0.04	0.20
Beam 3	Stress (ksi)	A	-1.94	-0.72	-1.83
		C	-1.94	-0.72	-2.09
		D	4.27	1.58	3.58
		E	4.27	1.58	4.10
	Deflection (in)		0.14	0.03	0.14

Overall, more than 90% of the values bounded. The experimental values did not show a clear pattern of leaning toward one boundary condition versus the other. This

illustrates the complexity of the floor system behavior. The boundary conditions are further investigated in Section 5.4.3. With the stresses and deflections mostly bounding, it was likely that the distribution factor and flexural rigidity values were not an issue but were still further investigated in Sections 5.5.1 and 5.5.2.

5.4.3. Bending and Torsion Comparison

In order to further investigate the bending and torsional restraint and the boundary conditions, the bending and torsional stresses are investigated separately in this section. The following tables compare theoretical and experimental stresses but separate the bending and torsional components. Table 5.12 shows the comparison for Test 1 Case A, Table 5.13 shows Test 1 Case B, Table 5.14 shows Test 1 Case C, and Table 5.15 shows Test 2. These tables only show stresses for Beams 1 and 3 because Beam 2 did not experience significant torsion. Test 3 is not included because the beams did not experience significant rotation, meaning there were no significant torsional stresses. The percent fixed column represents where the experimental stress falls between the pinned and fixed theoretical stress. If the percent fixed is 0%, the column is fully pinned, and if the percent fixed is 100%, the column is fully fixed.

The experimental bending stresses were found by averaging the stress values for the two strain gauges on each flange. The bending stress is distributed uniformly across a beam's flanges while the torsional stress is distributed linearly, with the maximum magnitudes at the flange ends and the center having zero torsional stress. Therefore, the stress at the center of the flange is equal to the bending stress. The experimental

torsional stresses were then found by subtracting the bending stress from the total stress recorded at each strain gauge.

Table 5.12: Test 1 Case A Bending and Torsion Stress Comparison (ksi)

		Bending				Torsion			
		Theoretical		Exp.	% Fix	Theoretical		Exp.	% Fix
		Pin.	Fix.			Pin.	Fix.		
Beam 1	A	-3.01	-1.00	-1.75	62%	-3.06	-2.37	-2.52	78%
	C	-3.01	-1.00	-1.75	62%	3.06	2.37	2.52	78%
	D	1.89	0.63	1.00	70%	0.84	0.65	0.43	219%
	E	1.89	0.63	1.00	70%	-0.84	-0.65	-0.43	219%
Beam 3	A	-3.01	-1.00	-1.90	55%	3.06	2.37	2.18	127%
	C	-3.01	-1.00	-1.90	55%	-3.06	-2.37	-2.18	127%
	D	1.89	0.63	1.29	48%	-0.84	-0.65	-0.85	-6%
	E	1.89	0.63	1.29	48%	0.84	0.65	0.85	-6%

Table 5.13: Test 1 Case B Bending and Torsion Stress Comparison (ksi)

		Bending				Torsion			
		Theoretical		Exp.	% Fix	Theoretical		Exp.	% Fix
		Pin.	Fix.			Pin.	Fix.		
Beam 1	A	-3.01	-1.00	-2.36	32%	-3.06	-2.37	-2.65	59%
	C	-3.01	-1.00	-2.36	32%	3.06	2.37	2.65	59%
	D	1.89	0.63	1.40	39%	0.84	0.65	0.30	288%
	E	1.89	0.63	1.40	39%	-0.84	-0.65	-0.30	288%
Beam 2	A	-3.01	-1.00	-1.75	63%	3.06	2.37	1.84	177%
	C	-3.01	-1.00	-1.75	63%	-3.06	-2.37	-2.09	141%
	D	1.89	0.63	1.13	60%	-0.84	-0.65	-0.42	221%
	E	1.89	0.63	1.13	60%	0.84	0.65	0.42	221%

Table 5.14: Test 1 Case C Bending and Torsion Stress Comparison (ksi)

		Bending				Torsion			
		Theoretical		Exp.	% Fix	Theoretical		Exp.	% Fix
		Pin.	Fix.			Pin.	Fix.		
Beam 1	A	-3.01	-1.00	-1.64	68%	-3.06	-2.37	-2.35	102%
	C	-3.01	-1.00	-1.64	68%	3.06	2.37	2.35	102%
	D	1.89	0.63	0.92	77%	0.84	0.65	0.44	212%
	E	1.89	0.63	0.92	77%	-0.84	-0.65	-0.44	212%
Beam 3	A	-3.01	-1.00	-1.97	52%	3.06	2.37	2.64	60%
	C	-3.01	-1.00	-1.97	52%	-3.06	-2.37	-2.64	60%
	D	1.89	0.63	1.08	64%	-0.84	-0.65	-0.50	182%
	E	1.89	0.63	1.08	64%	0.84	0.65	0.50	182%

Table 5.15: Test 2 Bending and Torsion Stress Comparison (ksi)

		Bending				Torsion			
		Theoretical		Exp.	% Fix	Theoretical		Exp.	% Fix
		Pin.	Fix.			Pin.	Fix.		
Beam 1	A	-3.39	-1.13	-1.98	62%	-2.07	-1.60	-1.72	74%
	C	-3.39	-1.13	-1.98	62%	2.07	1.60	1.72	74%
	D	2.13	0.71	1.31	58%	0.57	0.44	0.32	194%
	E	2.13	0.71	1.31	58%	-0.57	-0.44	-0.32	194%
Beam 3	A	-3.39	-1.13	-2.22	52%	2.07	1.60	1.17	192%
	C	-3.39	-1.13	-2.22	52%	-2.07	-1.60	-1.17	192%
	D	2.13	0.71	1.32	57%	-0.57	-0.44	-0.49	65%
	E	2.13	0.71	1.32	57%	0.57	0.44	0.49	65%

Overall, all of the bending stresses bounded while only some of the torsional stresses did. For Test 1 Cases A and C and Test 2, the bending stresses ranged from 48% - 77% fixed, while the bending stresses for Test 1 Case B ranged from 32% - 39% fixed. This occurred because Beam 1 had shear tab connections for Case B while top and bottom angles were added for the other cases.

The large number of torsional stresses not bound could be due to the eccentricity of the load and the width of the top flange of the beam not being fully accurate in the calculations. The eccentricities listed in Table 5.6 are based on the center of where the

load is bearing, but it is possible the actual eccentricity varies. As previously mentioned in Section 4.3, the width of the top flange of the beam was intended to be 6.0 inches, but ranged from 5.75 to 6.0 inches on the beams used in the experiment. When the eccentricity is lowered by ½-inch and 5.75 inches is used for the top flange width, about 80% of the torsional stresses are bound or close to bound.

5.5. Other Defining Parameters

The performance of the system can be further understood through determining its defining parameters. The load distribution is further investigated in Section 5.5.1. Section 5.5.2 summarizes the flexural rigidity of the system. Section 5.5.3 discusses the critical limit state of the system, while Section 5.5.4 explores the level of composite behavior the system experienced.

5.5.1. Distribution Factors

The distribution factors describe how the load is distributed to each beam in the system, which is important for the design. As discussed previously in Section 5.4.1, the distribution factors for Test 3 were assumed to be 25%-50%-25% for Beam 1, 2, and 3, respectively. They can be more precisely calculated by comparing the experimental values for the three beams to each other.

The distribution factors can be calculated using one of three parameters: the bending stress of the top flange, the bending stress of the bottom flange, or the deflection. For each of these parameters, its experimental value was used to calculate what distributed load would be necessary to induce that stress or deflection using Equations 3 and 4, respectively. The distributed loads were calculated for each beam,

and the load for each beam as a fraction of the sum of distributed loads was calculated to be the distribution factor using Equation 5.

$$w = \frac{8S_x\sigma}{L^2} \tag{3}$$

$$w = \frac{384EI\Delta}{L^4} \tag{4}$$

$$DF = \frac{w_i}{\sum_1^3 w_i} \tag{5}$$

Table 5.16 shows the calculated distribution factors for Test 3. σ_{top} refers to the top stress, σ_{bottom} refers to the bottom stress, and Δ refers to the deflection. The average distribution factors reveal that the load was distributed approximately 28%-44%-28%, for Beam 1, 2 and 3, respectively. These values are not much different from the initially assumed 25%-50%-25%. The load was applied directly over Beam 2, but the stiffness of the composite system shed more than half of the load to the edge beams. Note that when the calculated distribution factors are used for the theoretical calculations described in Section 5.4.1, the same number of stresses are bound. Therefore, for the purposes of 2D analysis and calculations for this system, it can be assumed that the load distributes 25%-50%-25%. However, the 28%-44%-28% load distribution factors are used for a more precise calculation in Appendix E, which is discussed later in Section 5.5.4.

Table 5.16: Distribution Factors for Test 3

	Case A			Case B			Case C			Avg.
	σ_{top}	σ_{bot}	Δ	σ_{top}	σ_{bot}	Δ	σ_{top}	σ_{bot}	Δ	
Beam 1	0.29	0.29	0.28	0.26	0.28	0.25	0.23	0.28	0.27	**0.28**
Beam 2	0.41	0.42	0.46	0.46	0.43	0.47	0.51	0.45	0.48	**0.44**
Beam 3	0.30	0.30	0.26	0.28	0.29	0.27	0.26	0.27	0.25	**0.28**

5.5.2. System Flexural Rigidity Values

The flexural rigidity of the system, EI, is an important characteristic as it determines how well the system resists bending. The flexural rigidity of the steel beams for Tests 1 and 2 is well-known, but the flexural rigidity of the composite system for Test 3 was more uncertain, especially because of the effective width and modulus of concrete, as discussed in Section 5.4.1. Section 5.4.2 showed that most of the deflections bounded for Test 3, meaning the flexural rigidity values were reasonably accurate. However, the flexural rigidity values can be further refined by calculating the flexural rigidities from the experimental deflections and performing a sensitivity study on the effective width.

It should be noted that the flexural rigidity of the composite section with the center beam is going to differ from that of the edge beam. In a normal floor system, there will be more interior beams that will make up the majority of the floor, so the flexural rigidity of the system will be mostly defined by the flexural rigidity of the center beam. Therefore, only the flexural rigidity of the center beam is considered.

Table 5.17 shows the flexural rigidity values calculated from the experimental deflections using Equation 6 for the pinned condition and Equation 7 for the fixed condition. These equations were based on the deflection equations for beams under two symmetric and equal point loads. P is the magnitude of one of the point loads, L is the length of the beam, a is the distance from the point load to the end of the beam, b is the length of the beam minus a, and Δ is the experimental deflection. A full sample calculation can be found in Appendix C.

$$EI_{pinned} = \frac{Pa}{24\Delta}(3L^2 - 4a^2) \tag{6}$$

$$EI_{fixed} = \frac{\frac{Pa^3}{6} + \left(\frac{-Pa^2b}{L^2} + \frac{-Pb^2a}{L^2}\right)\left(\frac{a^2}{2}\right)}{\Delta} \tag{7}$$

Table 5.17 also shows the theoretical flexural rigidity, which is E times I, using the values in Table 5.6. As can be seen, the pinned calculation gives values much closer to the theoretical values and is more likely to be correct. This is interesting because the outer beams had stiffer connections with the additional top and bottom angles, but during Test 3, the load was concentrated on the center beam with shear tab connections. Table 5.18 is similar to Table 5.17, but it shows only the pinned connection flexural rigidities and calculates an average for the beam.

Table 5.17: Test 3 Flexural Rigidity Values (kip-in^2 * 10^7)

	Theoretical	Experimental					
		Case A		Case B		Case C	
		Pinned	Fixed	Pinned	Fixed	Pinned	Fixed
Beam 2	3.55	4.05	0.80	3.60	0.71	3.21	0.64

Table 5.18: Test 3 Flexural Rigidity Values – Pinned Equation (kip-in^2 * 10^7)

	Theoretical	Experimental			
		Case A	Case B	Case C	Average
Beam 2	3.55	4.05	3.60	3.21	3.62

A sensitivity study was performed to see how the flexural rigidity values vary as the effective width changes. As discussed in Section 5.4.1, both the effective width and the modulus of concrete are parameters that can affect the flexural rigidity. Effective width was chosen as the varied parameter because its assumed value was less certain than that of the modulus of concrete, which was calculated based on the compressive strength. The sensitivity study recorded how I_x and subsequently EI changed as the effective width was changed. The values for the effective width were chosen to be 0 to 144 inches for the center beam, which are all of the physically possible values for the effective width.

Figure 5.56 shows the relationship between the effective width and the flexural rigidity, along with the theoretical and experimental average values from Table 5.18. It is worth noting that the flexural rigidities in Table 5.17 calculated using the fixed

connection equation are too small to appear on the graph, meaning they are not possible to achieve. The experimental effective width shown on the graph is 78 inches while the theoretical effective width used in the Test 3 calculation in Appendix B was 72 inches for the center beam. This indicates that while the theoretical value was fairly accurate, the center beam had a larger stress distribution than its tributary width. It is important to note that the experimental effective width being larger than the theoretical could have been due to the relatively close beam spacing. With a larger beam spacing, the effective width could be less than the tributary width.

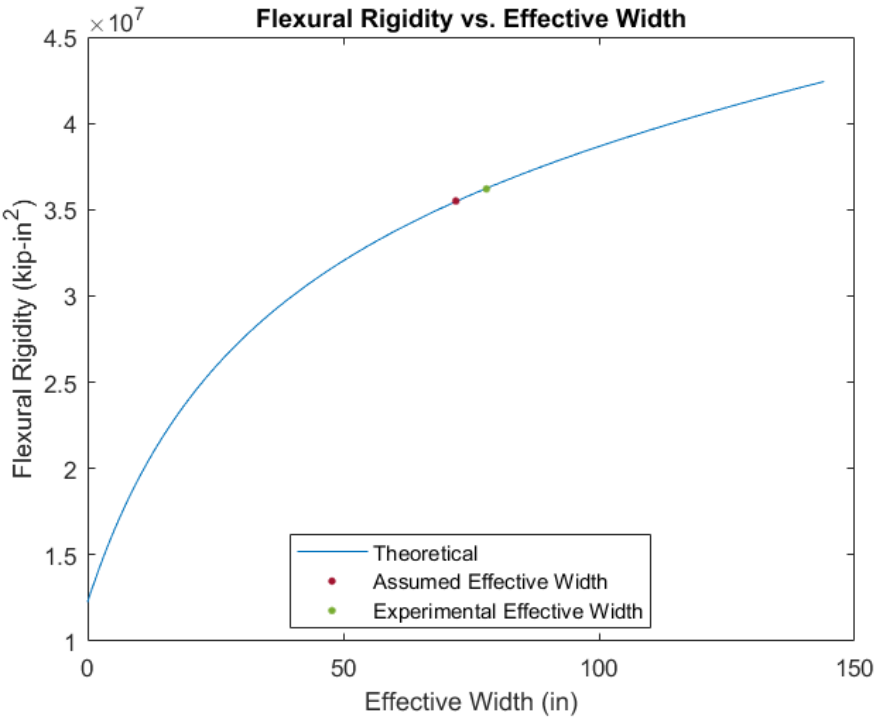

Figure 5.56: Flexural Rigidity v. Effective Width

Based on all of this information, the flexural rigidity of the system can be taken to the calculated value for the center beam, $3.62 * 10^7$ kip-in^2.

5.5.3. Critical Limit State

During design, the critical limit state is the one whose demand over capacity ratio is the largest and controls the design of the system. The limit states of concern for this system were yielding due to normal stress, lateral-torsional buckling (LTB), the live load deflections, and the rotation of the edge beams. Not every limit state applied to all the tests for this experiment. LTB and rotation were not concerns for Test 3 because the system had a cured concrete deck that laterally braced the steel beams and prevented their rotation. The live load deflection limit state only applied to Test 3 because its capacity is specifically for the deflection only under live load.

Table 5.19 shows the ratios for each limit state for the tests of interest. Since Tests 1 and 2 had the same limit states but more load was experienced during Test 2, only that one is shown. Test 3 Case B, or the 100 psf equivalent case, is the only one shown for Test 3 since it is the service level design load. The calculation for the capacity of each limit state can be found in Appendix D. The exception to this is the rotation capacity, for which 4.0 degrees was chosen based on visual inspection.

The numbers tabulated are the ratio of the experimental value to the capacity, which means that the value of 0.53, for example, means that during Test 2, the experimental rotation reached 53% of its capacity of 4.0 degrees. The experimental values used in this ratio were additive, meaning that they include the values from the previous tests to capture the true stress, deflection, or rotation the system is experiencing. The exception to this is the live load deflection because, once again, its capacity is specifically for the deflection only under live load.

Table 5.19: Limit State Ratios

		Test 2			Test 3: 100 psf		
Limit State	**Capacity**	**B1**	**B2**	**B3**	**B1**	**B2**	**B3**
Yielding (ksi)	45.0	0.17	0.23	0.18	0.18	0.24	0.19
LTB (ksi)	22.6	0.34	0.45	0.35	-	-	-
Live Load Deflection (in)	0.76	-	-	-	0.08	0.12	0.09
Rotation (deg)	4.0	0.53	-	-	-	-	-

The critical limit states for this experiment were LTB of Beam 2 and the rotation of the edge beams during Test 2. This was expected because when compared to more conventional steel-concrete floor systems, the smaller top flange of the A-shape left more concern for LTB, while the eccentric loading on the bottom flange affected the rotation. This makes Test 2, the concrete pour, the critical design stage for this floor system.

5.5.4. Level of Composite Behavior

The level of composite behavior of the system determines how well it will perform. Composite action is developed from the friction and cohesion between the concrete slab and steel since no mechanical connection is provided in the system. When there is full composite behavior, there is complete horizontal shear transfer between the concrete and steel, and there is no slip. This means that the system acts as one, and the strains are linear from the top of the slab to the bottom of the steel beam. When there is no composite behavior, there is no interaction between the concrete and steel, and there is slip. The strains for the concrete and steel will differ where they meet. There is also

partial composite behavior, which falls in the middle. The strain distributions of all three stages are shown in Figure 5.57.

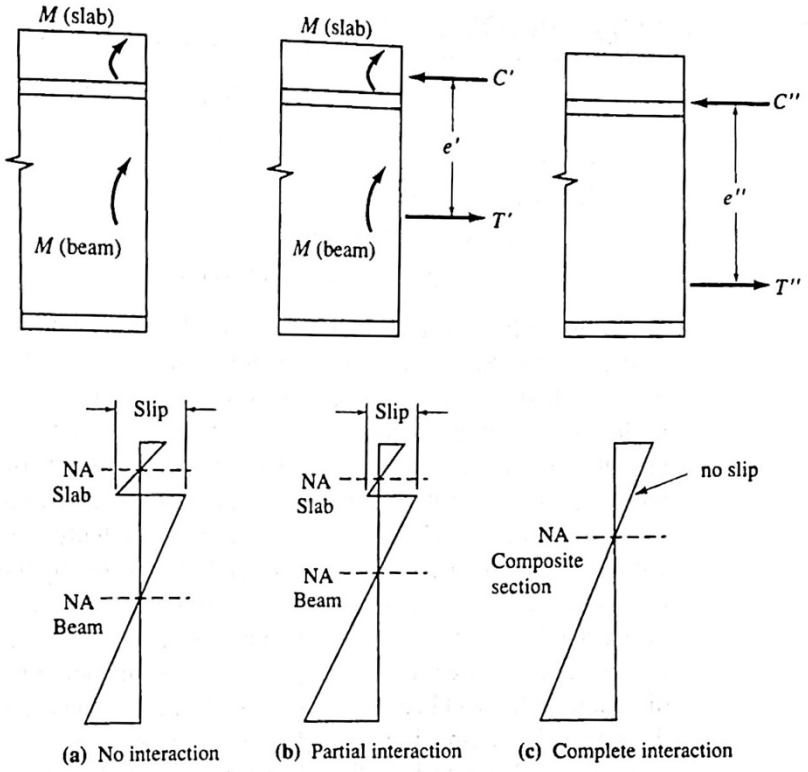

Figure 5.57: Strain distributions for different levels of composite behavior [24]

The level of composite behavior is unknown for this system because normally, shear connectors are used in composite systems to ensure sufficient horizontal shear transfer develops between the steel and the concrete for a fully composite connection. However, for this system, no shear connectors were used, and the interaction was developed purely with the bond between the steel and the concrete.

As stated in Section 5.3.3, the failure mode of the system was the bond breaking between the steel and concrete. This was evidence of the system transitioning to

complete non-composite behavior. Before that, however, the system had transitioned from composite to partially composite behavior. This can first be seen in Figure 5.53, where the stresses on the top flange just before failure are larger than those on the bottom flange. Because of where the neutral axis of the composite section falls, the stresses on the top flange of the steel section should be small in magnitude if there is full composite behavior, as seen for Case A, B, and C in Figure 5.42, Figure 5.44, and Figure 5.46. It can also be seen, in the time histories of the failure loading in Figure 5.19, Figure 5.20, and Figure 5.21, that the stresses on the top flange did not drastically change until after the failure of the system. This means the large stresses on the top flange taken right before failure were approached gradually, indicating the bond between the steel and concrete experienced slip slowly until the bond broke entirely. This all indicates that it is likely the system experienced linear composite behavior until somewhere between Test 3 Case C and Case D, where it then shifted to partially composite behavior.

The level of composite behavior can be quantified by comparing the moment in the composite beam during failure to the capacity of the composite system. The capacity of the composite system is 322 kip-ft, and the failure occurred at 175 kip-ft. The calculations for both of these values can be found in Appendix E. The failure occurred at 54% of the capacity. This reveals two things. The first is that more strength could be utilized from the system if more bond was developed between the steel and the concrete through the use of shear connectors or other mechanical means. The second is that even with only 54% of the potential capacity used, the system failed at five times the service load, which is plenty of capacity for conventional residential floor systems.

6. CONCLUSIONS

The following conclusions were made based on the results discussed in Section 5. Section 6.1 details how the constructability was evaluated, which accomplishes Research Objective 1. Sections 6.2 and 6.3 cover the performance of the system during construction and service loading, which achieves Research Objectives 2 and 3, respectively. Section 6.4 covers what occurred in the system during failure, which accomplishes Research Objective 4, and Section 6.5 summarizes the conclusions of this research study as a whole.

6.1. Evaluation of Constructability

As stated in Section 1, part of the advantage of using A-shapes in this specific floor system type is that it is easier and faster to construct than similar systems using standard shapes. The constructability of the system was evaluated on a subjective basis for the fabrication, steel erection, panel placement, and deck casting.

When compared to similar floor systems using built-up AIBs, as discussed in Section 3.1.3, the fabrication for the hot-rolled A-shapes was simpler. There was no welding involved, and normally the beams would not have to be flame-cut to the right length. The only fabrication work that was done was punching holes in the beam ends for the beam-to-column connection. Once hot-rolling A-shapes become standardized in the United States, the fabrication will be a fairly simple process: hot-roll the beams and punch the holes in the ends.

The steel was erected without any major issues. The slotted holes in the angles allowed for the framing to come together easily, as it gave the bolts more leeway. Steel erection using A-shapes is essentially the same as with standard W-shapes.

The placement of the panels went well. The panels had plenty of clearance dropping between the top flanges of the beams, and the seat width on the beam's bottom flange was sufficient. There was an issue with some panels cracking, but that was due to improper panel design, not the method of construction.

The biggest issue with the casting of the concrete deck was assuring that the concrete filled the voids around the beam webs. This was able to be done rather easily since 8-inch panels were used for the 12.1-inch deep section. However, a chamfer may be necessary on the panels if the difference between the depths of the panels and the steel section is smaller, which would likely be the case if a shallower steel section was used.

Overall, the construction of the system went relatively easily, and it was accomplished more quickly than if it had been constructed with built-up AIBs. The use of A-shapes helps fulfill AISC's "need for speed" initiative, justifying the development of standardized A-shapes.

6.2. Construction Performance

The performance of the A-shapes during construction is important because it is the stage where the steel beams do not have the additional lateral restraint from the concrete deck. Stability during construction was one of the concerns with this floor

system, particularly with the rotation of the beams as they are loaded unevenly on their bottom flanges.

The controlling limit states were LTB of the center beam and the rotation of the edge beams during Test 2, making the concrete pour the critical construction stage. The stresses in the center beam reached 45% of the LTB capacity, and the rotation of Beam 1 reached 53% of the rotation limit. These are both at reasonable levels and show that both the center and edge beams were stable during construction.

However, the rotation of Beam 1 was mitigated with the top and bottom angles that made it a fixed connection. The total rotation of the beam due to both Test 1 and 2 was 2.1 degrees. When these angles were unbolted to make a pinned connection for Test 1 Case B, the rotation increased from 1.50 degrees to 1.62 degrees, which is notable, but not troubling. If the connection had been pinned for Test 2, the rotation would have likely increased slightly from 0.65 degrees, making the total rotation with a pinned connection still well under the 4.0 degree limit. Therefore, it is probable that a pinned connection could have been used for this test.

Section 4.1.1 states that normally larger sections are used for the outer beams in a floor system. The relatively small demand to capacity ratios suggest that the same A-shapes could be used as the outer beams instead. It is important to note the experiment did not have all the same conditions that a real construction site may have, including construction live load and an uneven concrete pour. Conversely, as mentioned in Section 4.3, the top flanges of the A-shapes were less than six inches and had more imperfections than true hot-rolled shapes. In order to be conservative, it may still be

better to use a larger section for the edge beams in a real system, but the use of the same A-shape could be considered.

Sections 5.4.2 and 5.4.3 showed that the connections are partially restrained and fall between theoretical pinned and fixed connections. In Section 5.4.3, all of the bending stresses were bound while the torsional stresses required adjusting the eccentricity and top flange width for most of them to bound. However, for the original conditions, most of the torsional stresses that did not bound fell closer to the fixed value, which was smaller in magnitude. Therefore, for the purposes of design, it is conservative to assume a pinned connection for the beams.

6.3. Service Level Performance

The system performed well at the service level. For the equivalent design service load, 100 psf, the deflections were equal to L/3000, which is well below the limit of L/360. The small stresses in the top flange of the beam evidenced linear composite behavior, and the flexural rigidity of the center beam, and the system itself, was around $3.62 * 10^7$ kip-in^2. All of these factors reveal that the system is strong and able to handle the loads it is designed for. Because of the substantial strength this system has, future systems may be able to use 8 or 9-inch deep sections for a similar span range. This would make the system even shallower, which makes it even better for use in residential buildings.

6.4. System Failure

The system failed at 94.0 kips, which is approximately equivalent to 500 psf, or five times the design service load. The failure mode was the bond breaking between

Beam 2 and the concrete deck, reaching non-composite behavior after slowly transitioning from full composite to partial composite behavior.

The failure load of 94.0 kips translated to a moment of 175 kip-ft, and the ultimate capacity of the composite beam is 322 kip-ft, meaning the system reached 54% of its composite capacity. This composite capacity was derived from the bond between the steel and concrete. Shear connectors could be used to reach a higher capacity. However, one of the main advantages of this floor system is that it is easy and fast to assemble, and adding shear connectors (or other means of mechanical connection) would take away from that. In future systems with longer spans, larger spacing, or shallower sections, strength may be more of an issue and could warrant more of a need for shear connectors. However, for the configuration of this setup, the system failed at five times the design service load, and more strength is not needed.

6.5. Overall Conclusions

The overarching goal of this research was to investigate a shallow-depth steel-concrete floor system utilizing A-shapes, with a focus on their use in residential buildings. This was done by addressing the knowledge gaps, which included the constructability of the system, the stability of the system during construction, how well the system would perform under live load, and the level of composite behavior.

After this investigation, it can be concluded that this steel-concrete floor system made of A-shapes, precast panels, and a concrete deck is a viable option for a shallow-depth floor system. It is easy and fast to construct, and it provides an adequate level of strength and composite behavior for the loads of a residential building. This floor system

can help AISC fulfill its “need for speed” initiative, and its shallow depth can allow for steel floor systems to become more common in multi-story residential buildings. All of this justifies further research and development of standardized hot-rolled A-shapes in the United States.

REFERENCES

[1] AISC, *Steel Construction Manual*, 15th ed. Chicago: American Institute of Steel Construction, 2017.

[2] MTC. "Why Does the Steel Floor Decking Become Increasingly Popular?" Shanghai MTC Industrial Co., LTD. (accessed October 4, 2021).

[3] AISC. "Need for Speed." AISC. https://www.aisc.org/why-steel/innovative-systems/need-for-speed/ - 111788 (accessed.

[4] M. T. Yarnold and E. Stoddard, "Future Hot-Rolled Asymmetric Steel I-Beams," *Journal of Structural Engineering,* vol. 146, no. 9, p. 06020008, 2020, doi: 10.1061/(asce)st.1943-541x.0002768.

[5] T. A. Helwig, K. H. Frank, and J. A. Yura, "Lateral-Torsional Buckling of Singly Symmetric I-Beams," *Journal of Structural Engineering,* vol. 123, no. 9, pp. 1172-1179, 1997, doi: doi:10.1061/(ASCE)0733-9445(1997)123:9(1172).

[6] J. Rackham, S. Hicks, and G. M. Newman, *Design of asymmetric slimflor beams with precast concrete slabs*. 2006.

[7] B. Steel. "Sections Product Range." https://britishsteel.co.uk/what-we-do/construction-steel/sections-product-range/ (accessed September 15, 2021).

[8] G. A. Alpsten, "Thermal Residual Stresses in Hot-Rolled Steel Members," Fritz Engineering Laboratory Report No. 337.3., 1968.

[9] S. Quayyum and T. Hassan, "Initial Residual Stresses in Hot-Rolled Wide-Flange Shapes: A Computational Technique and Influence on Structural Performances," *Journal of Structural Engineering,* vol. 143, no. 5, p. 04017013, 2017, doi: 10.1061/(asce)st.1943-541x.0001739.

[10] Nucor Representatives, "Interview with Nucor," M. Yarnold and E. Stoddard, Eds., ed, 2020.

[11] Steel Dynamics Representatives, "Interview with Steel Dynamics, Inc.," M. Yarnold and E. Stoddard, Eds., ed, 2020.

[12] G. Representatives, "Interview with Gerdau," M. Yarnold, E. Stoddard, and S. Davis, Eds., ed, 2021.

[13] *The GIRDER-SLAB® System Design Guide v3.3*. (2016). Girder-Slab Technologies, LLC.

[14] *Slim-Floor: An innovative concept for floors*. ArcelorMittal.

[15] "COMSLAB®." Bailey Metal Products Ltd. http://www.bmp-group.com/products/comslab (accessed September 17, 2021).

[16] A. J. Nadaskay and C. D. Buckner, "Direct Model Test of Stub Girder Floor System," *Journal of Structural Engineering,* vol. 111, no. 7, pp. 1504-1516, 1985, doi: doi:10.1061/(ASCE)0733-9445(1985)111:7(1504).

[17] M. Ahmad, E. Y. L. Chien, and M. U. Hosain, "Modified Stub-Girder Floor System: Full-Scale Tests," *Journal of Structural Engineering,* vol. 118, no. 11, pp. 3222-3236, 1992, doi: doi:10.1061/(ASCE)0733-9445(1992)118:11(3222).

[18] C. P. Pantelides, B. A. Burkhart, L. D. Reaveley, and D. Platt, "Short-Span and Full-Scale Experiments of a Prefabricated Composite Floor-Building System," *Journal of Performance of Constructed Facilities,* vol. 30, no. 2, p. 04015018, 2016, doi: doi:10.1061/(ASCE)CF.1943-5509.0000758.

[19] E. J. Barbero, S.-H. Fu, and I. Raftoyiannis, "Ultimate Bending Strength of Composite Beams," *Journal of Materials in Civil Engineering,* vol. 3, no. 4, pp. 292-306, 1991.

[20] Y. K. Ju, S.-C. Chun, and S.-D. Kim, "Flexural Test of a Composite Beam Using Asymmetric Steel Section with Web Openings," *Journal of Structural Engineering,* vol. 135, no. 4, pp. 448-458, 2009, doi: doi:10.1061/(ASCE)0733-9445(2009)135:4(448).

[21] T. Sheehan, X. Dai, and D. Lam, "Flexural behaviour of asymmetric composite beam with low degree of shear connection," *Journal of Constructional Steel Research,* vol. 141, pp. 251-261, 2018, doi: 10.1016/j.jcsr.2017.11.018.

[22] O. Hechler, M. Braun, R. Obiala, U. Kuhlmann, F. Eggert, and G. Hauf, "CoSFB—Composite Slim-Floor Beam: Experimental Test Campaign and Evaluation," 2016: American Society of Civil Engineers, doi: 10.1061/9780784479735.013. [Online]. Available: https://dx.doi.org/10.1061/9780784479735.013

[23] E. A. Stoddard, "Behavior of Hot Rolled Asymmetric Steel I-Beams: Concept to Construction," Doctor of Philosophy in Civil Engineering, Zachry Department of Civil and Environmental Engineering, Texas A&M University, 2022.

[24] C. G. Salmon, J. E. Johnson, and F. A. Malhas, *Steel Structures: Design and Behavior*, 5th ed. Upper Saddle River, New Jersey: Pearson Education Inc., 2009.

APPENDIX A

YIELD, PLASTIC, AND FULLY COMPOSITE MOMENT CAPACITY CALCULATIONS

The following calculations find the yield and plastic moment capacity of the A-shape, along with capacity of the system if it were fully composite. There are two sets of capacities: one assuming all the load goes to the center beam and one assuming half the load goes to the center beam.

Yield, Plastic, and Fully Composite Moment Capacity

The yield, plastic, and fully composite moment capacity are calculated, first assuming all the load goes to the center beam, then assuming half the load goes to the center beam.

Steel Beam Properties:

$d := 12.1\ in$ full depth

$b_t := 6\ in$ width of top flange

$b_b := 12\ in$ width of bottom flange

$t_t := 0.605\ in$ thickness of top flange

$t_b := 0.605\ in$ thickness of bottom flange

$t_w := 0.390\ in$ thickness of web

$h := d - t_t - t_b = 10.89\ in$ height of web only

$h_0 := h + (0.5\ t_t) + (0.5\ t_b) = 11.495\ in$ center of top flange to center of bottom flange

$A_t := t_t \cdot b_t = 3.63\ in^2$ area of top flange

$A_b := t_b \cdot b_b = 7.26\ in^2$ area of bottom flange

$A_w := t_w \cdot h = 4.247\ in^2$ area of web

$A_s := A_t + A_b + A_w = 15.137\ in^2$ total approximate area

$f_y := 50\ ksi$

$E := 29000\ ksi$

$G := 11200\ ksi$

$C_b := 1.0$

$\gamma_s := 0.490\ \frac{kip}{ft^3}$

$L := 22.906\ ft$ span length - column bolt to column bolt

$s := 6\ ft$ spacing between beams

$e := 5\ in$ eccentricity of concrete panel distributed load

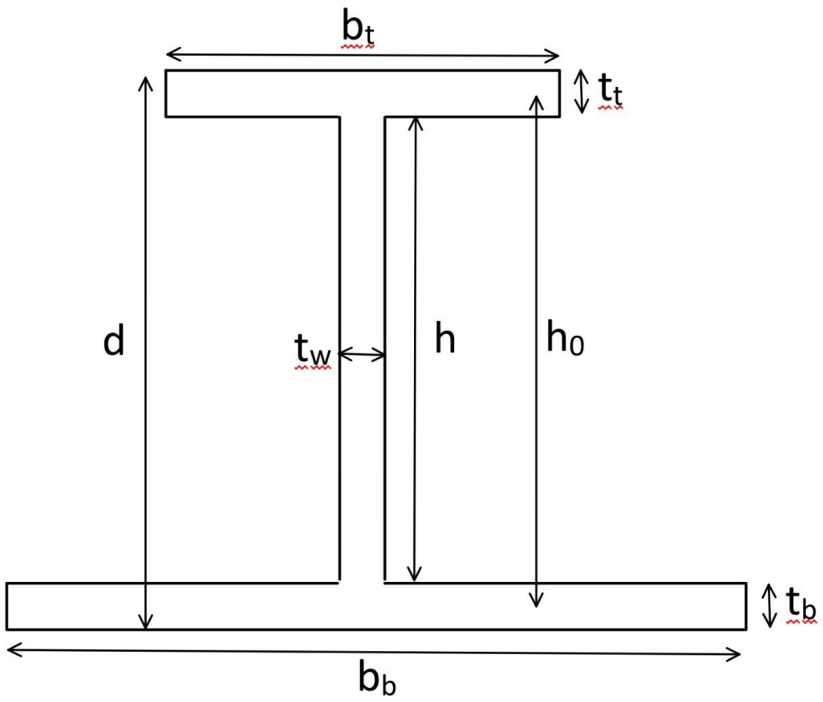

Steel Beam Section Properties:

$$y_t := d - \frac{t_t}{2} = 11.798\ in$$

$$y_b := \frac{t_b}{2} = 0.303\ in$$

distances to centroids of each part of the section, measured from the bottom

$$y_w := t_b + \frac{h}{2} = 6.05\ in$$

$$y_{bar.bot} := \frac{(A_t \cdot y_t) + (A_b \cdot y_b) + (A_w \cdot y_w)}{A_t + A_b + A_w} = 4.672\ in$$

distance from bottom of the section to the ENA

$$y_{bar.top} := d - y_{bar.bot} = 7.428\ in$$

distance from the top of the section to the ENA

$$I_x := \left(\frac{1}{12}\ t_w \cdot h^3 + A_w \cdot \left(y_w - y_{bar.bot}\right)^2\right) \hookleftarrow = 373.286\ in^4$$
$$+ \left(\frac{1}{12}\ b_b \cdot {t_b}^3 + (A_b) \cdot \left(y_b - y_{bar.bot}\right)^2\right) \hookleftarrow$$
$$+ \left(\frac{1}{12}\ b_t \cdot {t_t}^3 + (A_t) \cdot \left(y_t - y_{bar.bot}\right)^2\right)$$

$$I_y := \frac{1}{12} \cdot t_b \cdot {b_b}^3 + \frac{1}{12} \cdot t_t \cdot {b_t}^3 + \frac{1}{12} \cdot h \cdot {t_w}^3 = 98.064\ in^4$$

$$J := \frac{1}{3} \cdot b_b \cdot {t_b}^3 + \frac{1}{3} \cdot b_t \cdot {t_t}^3 + \frac{1}{3} \cdot h_0 \cdot {t_w}^3 = 1.6\ in^4$$

Find Sx for the bottom and top

$$S_{xtop} := \frac{I_x}{y_{bar.top}} = 50.252\ in^3$$

$$S_{xbot} := \frac{I_x}{y_{bar.bot}} = 79.904\ in^3$$

Find Zx

$$A_{half} := \frac{A_s}{2} = 7.569\ in^2$$

$$y_p := \frac{A_{half} - A_b}{t_w} + t_b = 1.396\ in$$

PNA location from the bottom of the section

PNA is located in the web:

$$UPWA := \left(d - t_t - y_p\right) \cdot t_w = 3.939\ in^2$$

upper plastic web area
aka web area in compression

$$LPWA := A_w - UPWA = 0.309\ in^2$$

lower plastic web area
aka web area in tension

Calculate areas/centroids of compression and tension based on PNA location:

$$AC := A_t + UPWA = 7.569\ in^2$$

compression area

$$AT := A_b + LPWA = 7.569\ in^2$$

tension area

$$yC := \frac{\left(UPWA \cdot \frac{d - t_t - y_p}{2}\right) + \left(A_t \cdot \left(d - \frac{t_t}{2} - y_p\right)\right)}{AC} = 7.616\ in$$

distance to centroid of compression area

$$yT := \frac{\left(LPWA \cdot \frac{y_p - t_b}{2}\right) + \left(A_b \cdot \left(y_p - \frac{t_b}{2}\right)\right)}{AT} = 1.065\ in$$

distance to centroid of tension area

$$Z_x := \left(AC \cdot yC\right) + \left(AT \cdot yT\right) = 65.706\ in^3$$

Concrete Section Properties:

$D_d := 8\ in$

$D_s := 5\ in$

$D_c := D_d + D_s - t_b - h = 1.505\ in$ depth of concrete slab on top of steel

$f'c := 5395\ psi$

$B_e := 6\ ft$

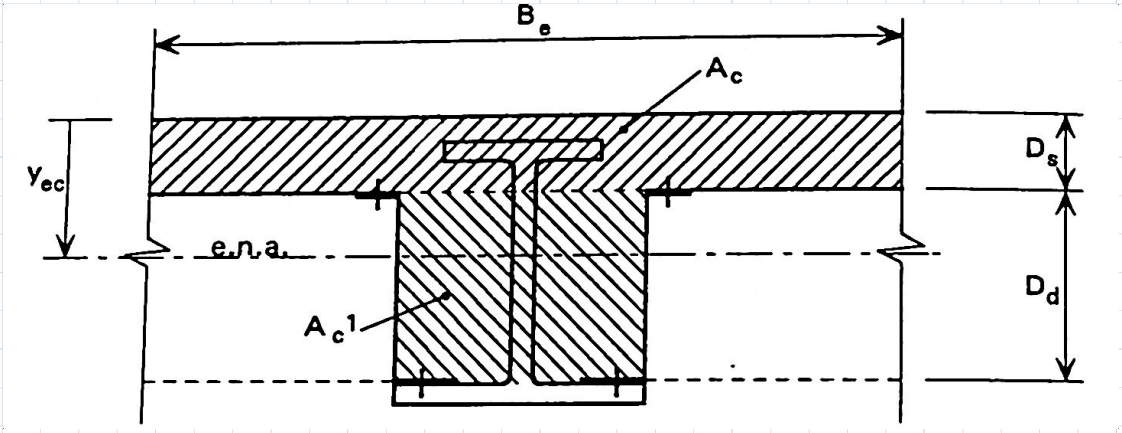

Yield and Plastic Moment Capacity

$S_x := min\left(S_{xtop}, S_{xbot}\right) = 50.252\ in^3$

$M_y := f_y \cdot S_x = 209\ kip \cdot ft$ yield moment capacity

$M_p := f_y \cdot Z_x = 274\ kip \cdot ft$ plastic moment capacity

Composite Capacity

Check if plastic neutral axis (PNA) lies in concrete slab above the steel, hence no steel is in compression

$a := \frac{A_s \cdot f_y}{0.85 \cdot f'c \cdot B_e} = 2.292\ in$ > $D_c = 1.505\ in$

PNA will lie within steel section

Check if PNA is in concrete slab and steel top flange.
Guess where the PNA is and iterate until C and T match

$y_{PNA} := 1.793\ in$ from top of concrete slab

$C_c := 0.85 \cdot f'c \cdot \left(\begin{matrix}\left(B_e \cdot D_c\right) \\ + \left(\left(B_e - b_t\right) \cdot \left(y_{PNA} - D_c\right)\right)\end{matrix}\right) = 584.078\ kip$ force of concrete in compression

$C_s := f_y \cdot \left(b_t \cdot \left(y_{PNA} - D_c\right)\right) = 86.4\ kip$ force of steel in compression

$C := C_c + C_s = 670.478\ kip$ total compressive force

$T := A_s \cdot f_y - C_s = 670.455\ kip$ force of steel in tension

Calculate moment arms and moment capacity

$T_{centroid} := \frac{d + D_c - y_{PNA}}{2} + y_{PNA} = 7.699\ in$

$C_{c.centroid} := \frac{\left(B_e \cdot D_c \cdot \frac{D_c}{2}\right) + \left(B_e - b_t\right) \cdot \left(y_{PNA} - D_c\right) \cdot \left(\frac{y_{PNA} - D_c}{2} + D_c\right)}{B_e \cdot D_c + \left(B_e - b_t\right) \cdot \left(y_{PNA} - D_c\right)} = 0.886\ in$

$C_{s.centroid} := \frac{y_{PNA} - D_c}{2} + D_c = 1.649\ in$

$d_c := T_{centroid} - C_{c.centroid} = 6.813\ in$

$d_s := T_{centroid} - C_{s.centroid} = 6.05\ in$

$M_c := C_c \cdot d_c + C_s \cdot d_s = 375\ kip \cdot ft$

Calculate Equivalent Actuator Load

My, Mp, and Mc are the moment capacities under all loads. In order to find the capacity under live load only, the moment due to dead loads must be subtracted out.

$w_C := 64\ psf \cdot 6\ ft = 384\ plf$

$w_{CIP} := 150\ pcf \cdot 415.3\ in^2 = 432.6\ plf$

$M_D := \frac{w_C \cdot L^2}{8} + \frac{w_{CIP} \cdot L^2}{8} = 53.6\ kip \cdot ft$

$M_{y.live} := M_y - M_D = 156\ kip \cdot ft$

$M_{p.live} := M_p - M_D = 220\ kip \cdot ft$

$M_{c.live} := M_c - M_D = 322\ kip \cdot ft$

Assume all the load is going to the center beam:

$a := \frac{(L - 6\ ft)}{2} = 8.453\ ft$

$yield\_actuator\_load := \frac{2 \cdot M_{y.live}}{a} = 36.9\ kip$

$plastic\_actuator\_load := \frac{2 \cdot M_{p.live}}{a} = 52.1\ kip$

$fully\_composite\_actuator\_load := \frac{2 \cdot M_{c.live}}{a} = 76.1\ kip$

Assume half the load goes to the center beam:

$yield\_actuator\_load := \frac{2 \cdot M_{y.live}}{0.5\ a} = 73.7\ kip$

$plastic\_actuator\_load := \frac{2 \cdot M_{p.live}}{0.5\ a} = 104.2\ kip$

$fully\_composite\_actuator\_load := \frac{2 \cdot M_{c.live}}{0.5\ a} = 152.2\ kip$

APPENDIX B

THEORETICAL STRESS SAMPLE CALCULATIONS

The following are sample calculations used to find the stresses on the A-shape for Tests 1, 2, and 3. There are six calculations in this appendix:

1. Test 1 Edge Beam: Pinned Condition
2. Test 1 Edge Beam: Fixed Condition
3. Test 2 Edge Beam: Pinned Condition
4. Test 2 Edge Beam: Fixed Condition
5. Test 3 Case B: Pinned Condition
6. Test 3 Case B: Fixed Condition

A Shape Construction Check: Test 1

Check **edge beam** under **one-sided concrete panel load**
- **Torsionally pinned:** Design Guide 9 Case 4 - distributed torsion
- **Flexurally pinned**
- Lb = L

Limit States:
- Yielding under normal stress
- LTB
- Rotation out of plane
- Vertical deflection

Assumptions:

- Cb = 1.0
- top flange smaller than bottom flange
- top flange in compression, bottom flange in tension
- unstiffened shear design
- end conditions are flexurally and torsionally pinned (restrained from warping)
- Grade 50 steel
- E = 29,000 ksi
- G = 11,200 ksi
- Unit weight of steel is 490 pcf
- **Only considering concrete panel load, no other loads**

Steel Beam Properties:

$d := 12.1\ in$	full depth
$b_t := 6\ in$	width of top flange
$b_b := 12\ in$	width of bottom flange
$t_t := 0.605\ in$	thickness of top flange
$t_b := 0.605\ in$	thickness of bottom flange
$t_w := 0.390\ in$	thickness of web
$h := d - t_t - t_b = 10.89\ in$	height of web only
$h_0 := h + (0.5\ t_t) + (0.5\ t_b) = 11.495\ in$	center of top flange to center of bottom flange

$A_t := t_t \cdot b_t = 3.63\ in^2$	area of top flange
$A_b := t_b \cdot b_b = 7.26\ in^2$	area of bottom flange
$A_w := t_w \cdot h = 4.247\ in^2$	area of web
$A := A_t + A_b + A_w = 15.137\ in^2$	total approximate area

$f_y := 50\ ksi$
$E := 29000\ ksi$
$G := 11200\ ksi$
$C_b := 1.0$
$\gamma_s := 0.490\ \frac{kip}{ft^3}$

$L := 22.906\ ft$	span length - column bolt to column bolt
$s := 6\ ft$	spacing between beams
$e := 5\ in$	eccentricity of concrete panel distributed load

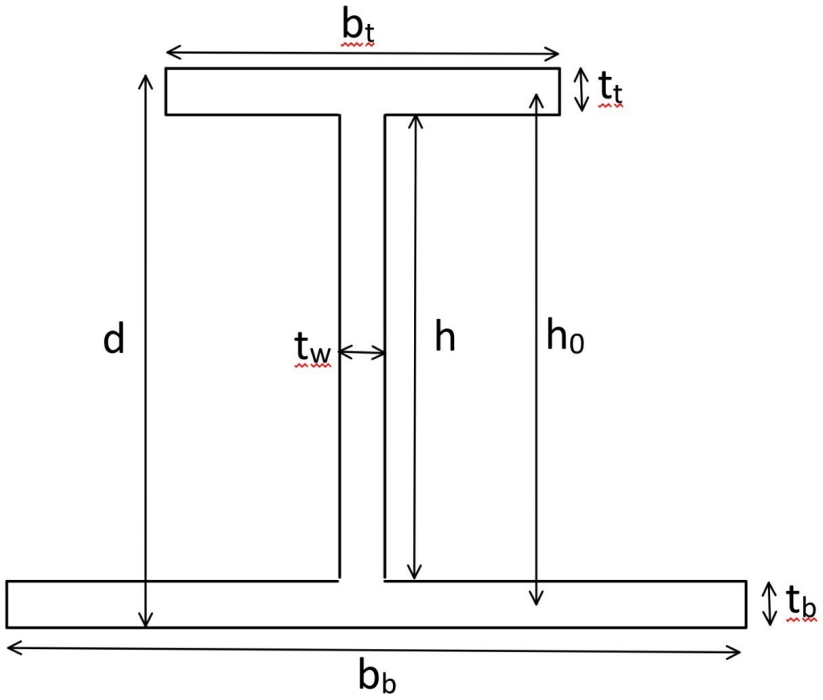

Steel Beam Section Properties:

$$y_t := d - \frac{t_t}{2} = 11.798\ in$$

$$y_b := \frac{t_b}{2} = 0.303\ in$$

distances to centroids of each part of the section, measured from the bottom

$$y_w := t_b + \frac{h}{2} = 6.05\ in$$

$$y_{bar.bot} := \frac{(A_t \cdot y_t) + (A_b \cdot y_b) + (A_w \cdot y_w)}{A_t + A_b + A_w} = 4.672\ in$$

distance from bottom of the section to the ENA

$$y_{bar.top} := d - y_{bar.bot} = 7.428\ in$$

distance from the top of the section to the ENA

$$I_x := \left(\frac{1}{12}\ t_w \cdot h^3 + A_w \cdot \left(y_w - y_{bar.bot}\right)^2\right) \hookleftarrow = 373.286\ in^4$$
$$+ \left(\frac{1}{12}\ b_b \cdot {t_b}^3 + (A_b) \cdot \left(y_b - y_{bar.bot}\right)^2\right) \hookleftarrow$$
$$+ \left(\frac{1}{12}\ b_t \cdot {t_t}^3 + (A_t) \cdot \left(y_t - y_{bar.bot}\right)^2\right)$$

$$I_y := \frac{1}{12} \cdot t_b \cdot {b_b}^3 + \frac{1}{12} \cdot t_t \cdot {b_t}^3 + \frac{1}{12} \cdot h \cdot {t_w}^3 = 98.064\ in^4$$

$$J := \frac{1}{3} \cdot b_b \cdot {t_b}^3 + \frac{1}{3} \cdot b_t \cdot {t_t}^3 + \frac{1}{3} \cdot h_0 \cdot {t_w}^3 = 1.6\ in^4$$

Find Sx for the bottom and top

$$S_{xtop} := \frac{I_x}{y_{bar.top}} = 50.252\ in^3$$

$$S_{xbot} := \frac{I_x}{y_{bar.bot}} = 79.904\ in^3$$

Torsional Properties:

From AISC Design Guide 9:

$$d' := d - \frac{t_t + t_b}{2} = 11.495\ in$$

$$\alpha := \frac{1}{1 + \left(\frac{b_t}{b_b}\right)^3 \cdot \left(\frac{t_t}{t_b}\right)} = 0.889$$

$$C_w := \frac{(d')^2 \cdot {b_t}^3 \cdot t_t \cdot \alpha}{12} = 1279.067\ in^6$$

$$\alpha := \frac{{b_b}^3 \cdot t_b}{{b_t}^3 \cdot t_t + {b_b}^3 \cdot t_b} \cdot h_0 = 10.218\ in$$

$$W_{no.top} := \frac{\alpha \cdot b_t}{2} = 30.653\ in^2 \qquad W_{no.bot} := \frac{h_0 - \alpha}{2} \cdot b_b = 7.663\ in^2$$

$$S_{wt} := \frac{W_{no.top} \cdot b_t \cdot t_t}{4} = 27.818\ in^4 \qquad S_{wb} := \frac{W_{no.bot} \cdot b_b \cdot t_b}{4} = 13.909\ in^4$$

$$Q_{ft} := \left(\left(\frac{b_t}{2} - t_w\right) \cdot t_t\right) \cdot \left(y_{bar.top} - \frac{t_t}{2}\right) = 11.252\ in^3$$

$$Q_{fb} := \left(\left(\frac{b_b}{2} - t_w\right) \cdot t_b\right) \cdot \left(y_{bar.bot} - \frac{t_b}{2}\right) = 14.829\ in^3$$

$$A_{w2} := \left(y_{bar.top} - t_t\right) \cdot t_w = 2.661\ in^2$$

$$Q_w := \left(A_t + A_{w2}\right) \cdot \frac{\left(A_t \cdot \left(y_{bar.top} - \frac{t_t}{2}\right) + A_{w2} \cdot \frac{y_{bar.top} - t_t}{2}\right)}{A_t + A_{w2}} = 34.945\ in^3$$

Loads:

From Gate Precast:

$w_C := 64\ psf \cdot (0.5 \cdot s) = 0.192\ \frac{kip}{ft}$ concrete panel distributed load

Demands:

$M_u := \frac{w_C \cdot L^2}{8} = 12.592\ kip \cdot ft$

$t_u := w_C \cdot e = 0.08\ \frac{kip \cdot in}{in}$

Bending Stresses:

From AISC Design Guide 9 Section 4.5:

$\sigma_{bx.compressive} := \frac{-M_u}{S_{xtop}} = -3.007\ ksi$ $\sigma_{bx.tensile} := \frac{M_u}{S_{xbot}} = 1.891\ ksi$

Torsional Stresses:

From AISC Design Guide 9:

$a := \sqrt{\frac{E \cdot C_w}{G \cdot J}} = 46.136\ in$

Appendix B - Case 4 (Distributed Torsional Moment with Pinned Ends)

$\alpha := 0.5$

$x := \frac{L}{a} = 5.958$

Midspan (z/L = 0.5)

$z := 0.5 \cdot L$

$$\theta''_m := \frac{d^2}{dz^2}\left(\frac{t_u \cdot a^2}{G \cdot J}\left(\frac{L^2}{2 \cdot a^2} \cdot \left(\frac{z}{L} - \frac{z^2}{L^2}\right) + \cosh\left(\frac{z}{a}\right) - \tanh\left(\frac{L}{2 \cdot a}\right) \cdot \sinh\left(\frac{z}{a}\right) - 1.0\right)\right) = -4.13 \cdot 10^{-6}\ \frac{rad}{in^2}$$

$$\theta'''_m := \frac{d^3}{dz^3}\left(\frac{t_u \cdot a^2}{G \cdot J}\left(\frac{L^2}{2 \cdot a^2} \cdot \left(\frac{z}{L} - \frac{z^2}{L^2}\right) + \cosh\left(\frac{z}{a}\right) - \tanh\left(\frac{L}{2 \cdot a}\right) \cdot \sinh\left(\frac{z}{a}\right) - 1.0\right)\right) = -8.93 \cdot 10^{-21}\ \frac{rad}{in^3}$$

Supports (z/L = 0.0)

$z := 0.0 \cdot L$

$$\theta'_s := \frac{d}{dz}\left(\frac{t_u \cdot a^2}{G \cdot J}\left(\frac{L^2}{2 \cdot a^2} \cdot \left(\frac{z}{L} - \frac{z^2}{L^2}\right) + \cosh\left(\frac{z}{a}\right) - \tanh\left(\frac{L}{2 \cdot a}\right) \cdot \sinh\left(\frac{z}{a}\right) - 1.0\right)\right) = \left(4.20 \cdot 10^{-4}\right)\ \frac{rad}{in}$$

$$\theta'''_s := \frac{d^3}{dz^3}\left(\frac{t_u \cdot a^2}{G \cdot J}\left(\frac{L^2}{2 \cdot a^2} \cdot \left(\frac{z}{L} - \frac{z^2}{L^2}\right) + \cosh\left(\frac{z}{a}\right) - \tanh\left(\frac{L}{2 \cdot a}\right) \cdot \sinh\left(\frac{z}{a}\right) - 1.0\right)\right) = -9.90 \cdot 10^{-8}\ \frac{rad}{in^3}$$

Normal Stresses Due to Warping

From AISC Design Guide 9 Section 4.1.3: At midspan

$\sigma_{wm.top} := E \cdot W_{no.top} \cdot \theta''_m = -3.667\ ksi$ $\sigma_{wm.bot} := E \cdot W_{no.bot} \cdot \theta''_m = -0.917\ ksi$

Account for strain gauge placement:

$sg\_placement := 0.5\ in$ 0.5 inches from edge

$$\sigma_{wm.top} := \sigma_{wm.top} \cdot \frac{3\ in - sg\_placement}{3\ in} = -3.056\ ksi$$

$$\sigma_{wm.bot} := \sigma_{wm.bot} \cdot \frac{6\ in - sg\_placement}{6\ in} = -0.84\ ksi$$

Limit States - Service

Rotation out of Plane

$$t := w_C \cdot e = 0.08 \ \frac{kip \cdot in}{in}$$

$$\alpha := 0.5$$

$$z := 0.5 \cdot L$$

$$\theta_m := \frac{t \cdot a^2}{G \cdot J}\left(\frac{L^2}{2 \cdot a^2} \cdot \left(\frac{z}{L} - \frac{z^2}{L^2}\right) + \cosh\left(\frac{z}{a}\right) - \tanh\left(\frac{L}{2 \cdot a}\right) \cdot \sinh\left(\frac{z}{a}\right) - 1.0\right) = 1.981 \ deg$$

$\theta_m = 1.981 \ deg$ <= $\theta_{max} := 3.0 \ deg$

Vertical Deflection

$$w_n := w_C = 0.016 \ \frac{kip}{in}$$

$$\Delta_T := \frac{5 \cdot w_C \cdot L^4}{384 \cdot E \cdot I_x} = 0.110 \ in \quad <= \quad \Delta_{Limit} := \frac{L}{360} = 0.764 \ in$$

Stresses on Shape

$\sigma_{bx.compressive} + \sigma_{wm.top} = -6.063$ ***ksi***

$\sigma_{bx.compressive} - \sigma_{wm.top} = 0.049$ ***ksi***

$\sigma_{bx.compressive} = -3.007$ ***ksi***

$\sigma_{bx.tensile} = 1.891$ ***ksi***

$\sigma_{bx.tensile} - \sigma_{wm.bot} = 2.731$ ***ksi***

$\sigma_{bx.tensile} + \sigma_{wm.bot} = 1.051$ ***ksi***

A Shape Construction Check: Test 1

Check **edge beam** under **one-sided concrete panel load**
- **Torsionally fixed:** Design Guide 9 Case 7 - distributed torsion
- **Flexurally fixed**
- Lb = L

Limit States:
- Yielding under normal stress
- LTB
- Rotation out of plane
- Vertical deflection

Assumptions:

- Cb = 1.0
- top flange smaller than bottom flange
- top flange in compression, bottom flange in tension
- unstiffened shear design
- end conditions are flexurally and torsionally pinned (restrained from warping)
- Grade 50 steel
- E = 29,000 ksi
- G = 11,200 ksi
- Unit weight of steel is 490 pcf
- **Only considering concrete panel load, no other loads**

Steel Beam Properties:

$d := 12.1\ in$	full depth
$b_t := 6\ in$	width of top flange
$b_b := 12\ in$	width of bottom flange
$t_t := 0.605\ in$	thickness of top flange
$t_b := 0.605\ in$	thickness of bottom flange
$t_w := 0.390\ in$	thickness of web
$h := d - t_t - t_b = 10.89\ in$	height of web only
$h_0 := h + (0.5\ t_t) + (0.5\ t_b) = 11.495\ in$	center of top flange to center of bottom flange

$A_t := t_t \cdot b_t = 3.63\ in^2$	area of top flange
$A_b := t_b \cdot b_b = 7.26\ in^2$	area of bottom flange
$A_w := t_w \cdot h = 4.247\ in^2$	area of web
$A := A_t + A_b + A_w = 15.137\ in^2$	total approximate area

$f_y := 50\ ksi$
$E := 29000\ ksi$
$G := 11200\ ksi$
$C_b := 1.0$
$\gamma_s := 0.490\ \frac{kip}{ft^3}$

$L := 22.906\ ft$	span length - column bolt to column bolt
$s := 6\ ft$	spacing between beams
$e := 5\ in$	eccentricity of concrete panel distributed load

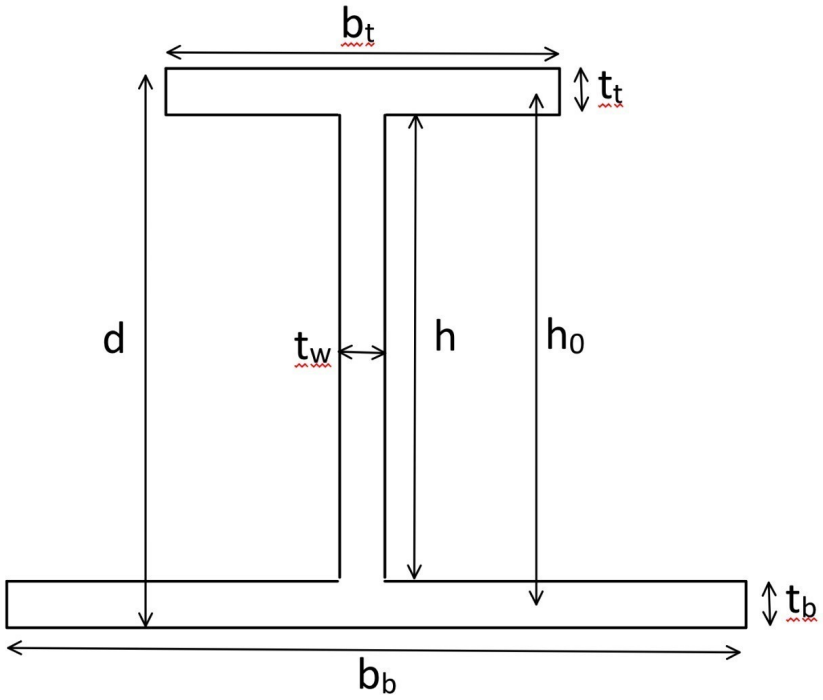

Steel Beam Section Properties:

$$y_t := d - \frac{t_t}{2} = 11.798\ in$$

$$y_b := \frac{t_b}{2} = 0.303\ in$$

distances to centroids of each part of the section, measured from the bottom

$$y_w := t_b + \frac{h}{2} = 6.05\ in$$

$$y_{bar.bot} := \frac{(A_t \cdot y_t) + (A_b \cdot y_b) + (A_w \cdot y_w)}{A_t + A_b + A_w} = 4.672\ in$$

distance from bottom of the section to the ENA

$$y_{bar.top} := d - y_{bar.bot} = 7.428\ in$$

distance from the top of the section to the ENA

$$I_x := \left(\frac{1}{12}\ t_w \cdot h^3 + A_w \cdot \left(y_w - y_{bar.bot}\right)^2\right) \hookleftarrow \quad = 373.286\ in^4$$
$$+ \left(\frac{1}{12}\ b_b \cdot {t_b}^3 + (A_b) \cdot \left(y_b - y_{bar.bot}\right)^2\right) \hookleftarrow$$
$$+ \left(\frac{1}{12}\ b_t \cdot {t_t}^3 + (A_t) \cdot \left(y_t - y_{bar.bot}\right)^2\right)$$

$$I_y := \frac{1}{12} \cdot t_b \cdot {b_b}^3 + \frac{1}{12} \cdot t_t \cdot {b_t}^3 + \frac{1}{12} \cdot h \cdot {t_w}^3 = 98.064\ in^4$$

$$J := \frac{1}{3} \cdot b_b \cdot {t_b}^3 + \frac{1}{3} \cdot b_t \cdot {t_t}^3 + \frac{1}{3} \cdot h_0 \cdot {t_w}^3 = 1.6\ in^4$$

Find Sx for the bottom and top

$$S_{xtop} := \frac{I_x}{y_{bar.top}} = 50.252\ in^3$$

$$S_{xbot} := \frac{I_x}{y_{bar.bot}} = 79.904\ in^3$$

Torsional Properties:

From AISC Design Guide 9:

$$d' := d - \frac{t_t + t_b}{2} = 11.495\ in$$

$$\alpha := \frac{1}{1 + \left(\frac{b_t}{b_b}\right)^3 \cdot \left(\frac{t_t}{t_b}\right)} = 0.889$$

$$C_w := \frac{(d')^2 \cdot {b_t}^3 \cdot t_t \cdot \alpha}{12} = 1279.067\ in^6$$

$$\alpha := \frac{{b_b}^3 \cdot t_b}{{b_t}^3 \cdot t_t + {b_b}^3 \cdot t_b} \cdot h_0 = 10.218\ in$$

$$W_{no.top} := \frac{\alpha \cdot b_t}{2} = 30.653\ in^2 \qquad W_{no.bot} := \frac{h_0 - \alpha}{2} \cdot b_b = 7.663\ in^2$$

$$S_{wt} := \frac{W_{no.top} \cdot b_t \cdot t_t}{4} = 27.818\ in^4 \qquad S_{wb} := \frac{W_{no.bot} \cdot b_b \cdot t_b}{4} = 13.909\ in^4$$

$$Q_{ft} := \left(\left(\frac{b_t}{2} - t_w\right) \cdot t_t\right) \cdot \left(y_{bar.top} - \frac{t_t}{2}\right) = 11.252\ in^3$$

$$Q_{fb} := \left(\left(\frac{b_b}{2} - t_w\right) \cdot t_b\right) \cdot \left(y_{bar.bot} - \frac{t_b}{2}\right) = 14.829\ in^3$$

$$A_{w2} := \left(y_{bar.top} - t_t\right) \cdot t_w = 2.661\ in^2$$

$$Q_w := \left(A_t + A_{w2}\right) \cdot \frac{\left(A_t \cdot \left(y_{bar.top} - \frac{t_t}{2}\right) + A_{w2} \cdot \frac{y_{bar.top} - t_t}{2}\right)}{A_t + A_{w2}} = 34.945\ in^3$$

Loads:

From Gate Precast:

$w_C := 64\ psf \cdot (0.5 \cdot s) = 0.192\ \frac{kip}{ft}$ concrete panel distributed load

Demands:

$M_u := \frac{w_C \cdot L^2}{24} = 4.197\ kip \cdot ft$

$t_u := w_C \cdot e = 0.08\ \frac{kip \cdot in}{in}$

Bending Stresses:

From AISC Design Guide 9 Section 4.5:

$\sigma_{bx.compressive} := \frac{-M_u}{S_{xtop}} = -1.002\ ksi$ $\sigma_{bx.tensile} := \frac{M_u}{S_{xbot}} = 0.63\ ksi$

Torsional Stresses:

From AISC Design Guide 9:

$a := \sqrt{\frac{E \cdot C_w}{G \cdot J}} = 46.136\ in$

Appendix B - Case 4 (Distributed Torsional Moment with Pinned Ends)

$\alpha := 0.5$

$x := \frac{L}{a} = 5.958$

Midspan (z/L = 0.5)

$z := 0.5 \cdot L$

$$\theta''_m := \frac{d^2}{dz^2}\left(\frac{t_u \cdot L \cdot a}{2\ G \cdot J}\left(\left(\frac{1+\cosh\left(\frac{L}{a}\right)}{\sinh\left(\frac{L}{a}\right)}\right)\cdot\left(\cosh\left(\frac{z}{a}\right)-1.0\right)+\frac{z}{a}\cdot\left(1-\frac{z}{L}\right)-\sinh\left(\frac{z}{a}\right)\right)\right) = -3.20\cdot 10^{-6}\ \frac{rad}{in^2}$$

$$\theta'''_m := \frac{d^3}{dz^3}\left(\frac{t_u \cdot L \cdot a}{2\ G \cdot J}\left(\left(\frac{1+\cosh\left(\frac{L}{a}\right)}{\sinh\left(\frac{L}{a}\right)}\right)\cdot\left(\cosh\left(\frac{z}{a}\right)-1.0\right)+\frac{z}{a}\cdot\left(1-\frac{z}{L}\right)-\sinh\left(\frac{z}{a}\right)\right)\right) = -1.08\cdot 10^{-19}\ \frac{rad}{in^3}$$

Supports (z/L = 0.0)

$z := 0.0 \cdot L$

$$\theta'_s := \frac{d}{dz}\left(\frac{t_u \cdot L \cdot a}{2\ G \cdot J}\left(\left(\frac{1+\cosh\left(\frac{L}{a}\right)}{\sinh\left(\frac{L}{a}\right)}\right)\cdot\left(\cosh\left(\frac{z}{a}\right)-1.0\right)+\frac{z}{a}\cdot\left(1-\frac{z}{L}\right)-\sinh\left(\frac{z}{a}\right)\right)\right) = \left(3.85\cdot 10^{-20}\right)\ \frac{rad}{in}$$

$$\theta'''_s := \frac{d^3}{dz^3}\left(\frac{t_u \cdot L \cdot a}{2\ G \cdot J}\left(\left(\frac{1+\cosh\left(\frac{L}{a}\right)}{\sinh\left(\frac{L}{a}\right)}\right)\cdot\left(\cosh\left(\frac{z}{a}\right)-1.0\right)+\frac{z}{a}\cdot\left(1-\frac{z}{L}\right)-\sinh\left(\frac{z}{a}\right)\right)\right) = -2.96\cdot 10^{-7}\ \frac{rad}{in^3}$$

Normal Stresses Due to Warping

From AISC Design Guide 9 Section 4.1.3: At midspan

$\sigma_{wm.top} := E \cdot W_{no.top} \cdot \theta''_m = -2.841\ ksi$ $\sigma_{wm.bot} := E \cdot W_{no.bot} \cdot \theta''_m = -0.71\ ksi$

Account for strain gauge placement:

$sg\_placement := 0.5\ in$ 0.5 inches from edge

$$\sigma_{wm.top} := \sigma_{wm.top} \cdot \frac{3\ in - sg\_placement}{3\ in} = -2.368\ ksi$$

$$\sigma_{wm.bot} := \sigma_{wm.bot} \cdot \frac{6\ in - sg\_placement}{6\ in} = -0.651\ ksi$$

Limit States - Service

Rotation out of Plane

$$t := w_C \cdot e = 0.08 \ \frac{kip \cdot in}{in}$$

$$\alpha := 0.5$$

$$z := 0.5 \cdot L$$

$$\theta_m := \frac{t \cdot L \cdot a}{2\ G \cdot J} \left(\left(\frac{1 + \cosh\left(\frac{L}{a}\right)}{\sinh\left(\frac{L}{a}\right)} \right) \cdot \left(\cosh\left(\frac{z}{a}\right) - 1.0 \right) + \frac{z}{a} \cdot \left(1 - \frac{z}{L} \right) - \sinh\left(\frac{z}{a}\right) \right) = 0.978 \ deg$$

$\theta_m = 0.978 \ deg$ <= $\theta_{max} := 3.0 \ deg$

Vertical Deflection

$$w_n := w_C = 0.016 \ \frac{kip}{in}$$

$$\Delta_T := \frac{w_C \cdot L^4}{384 \cdot E \cdot I_x} = 0.022 \ in \quad <= \quad \Delta_{Limit} := \frac{L}{360} = 0.764 \ in$$

Stresses on Shape

$\sigma_{bx.compressive} + \sigma_{wm.top} = -3.37$ ***ksi***

$\sigma_{bx.compressive} - \sigma_{wm.top} = 1.365$ ***ksi***

$\sigma_{bx.compressive} = -1.002$ ***ksi***

$\sigma_{bx.tensile} = 0.63$ ***ksi***

$\sigma_{bx.tensile} - \sigma_{wm.bot} = 1.282$ ***ksi***

$\sigma_{bx.tensile} + \sigma_{wm.bot} = -0.021$ ***ksi***

A Shape Construction Check: Test 2

Check **edge beam** under **one-sided wet concrete load**
- **Torsionally pinned:** Design Guide 9 Case 4 - distributed torsion
- **Flexurally pinned**
- Lb = L

Limit States:
- Yielding under normal stress
- LTB
- Rotation out of plane
- Vertical deflection

Assumptions:

- Cb = 1.0
- top flange smaller than bottom flange
- top flange in compression, bottom flange in tension
- unstiffened shear design
- end conditions are flexurally and torsionally pinned (restrained from warping)
- Grade 50 steel
- E = 29,000 ksi
- G = 11,200 ksi
- Unit weight of steel is 490 pcf
- **Only considering wet concrete load, no other loads**

Steel Beam Properties:

$d := 12.1\ in$	full depth
$b_t := 6\ in$	width of top flange
$b_b := 12\ in$	width of bottom flange
$t_t := 0.605\ in$	thickness of top flange
$t_b := 0.605\ in$	thickness of bottom flange
$t_w := 0.390\ in$	thickness of web
$h := d - t_t - t_b = 10.89\ in$	height of web only
$h_0 := h + (0.5\ t_t) + (0.5\ t_b) = 11.495\ in$	center of top flange to center of bottom flange

$A_t := t_t \cdot b_t = 3.63\ in^2$	area of top flange
$A_b := t_b \cdot b_b = 7.26\ in^2$	area of bottom flange
$A_w := t_w \cdot h = 4.247\ in^2$	area of web
$A := A_t + A_b + A_w = 15.137\ in^2$	total approximate area

$f_y := 50\ ksi$
$E := 29000\ ksi$
$G := 11200\ ksi$
$C_b := 1.0$
$\gamma_s := 0.490\ \frac{kip}{ft^3}$

$L := 22.906\ ft$	span length
$s := 6\ ft$	spacing between beams
$e := 3\ in$	eccentricity of concrete panel distributed load

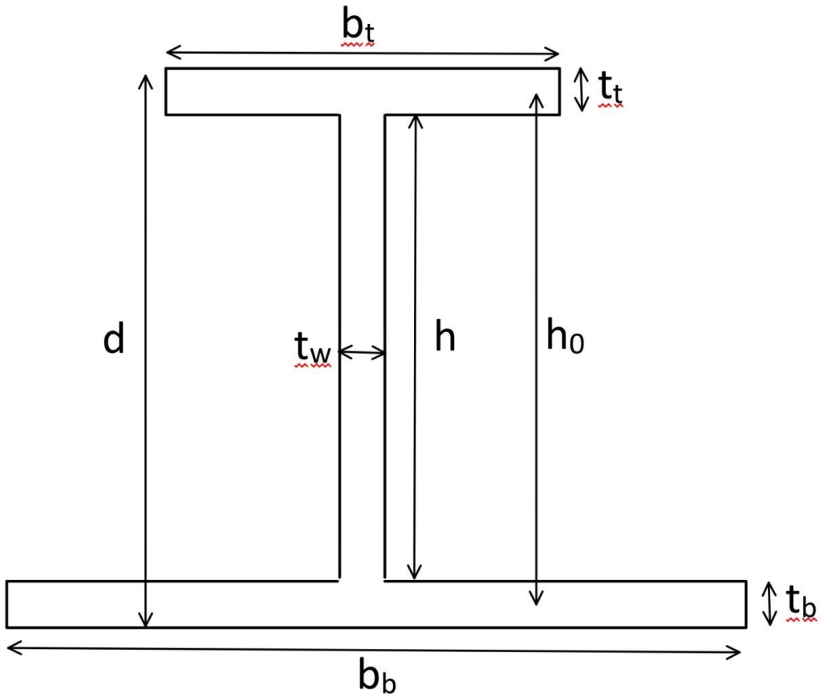

Steel Beam Section Properties:

From Eric's equations:

$$y_t := d - \frac{t_t}{2} = 11.798\ in$$

$$y_b := \frac{t_b}{2} = 0.303\ in$$

$$y_w := t_b + \frac{h}{2} = 6.05\ in$$

distances to centroids of each part of the section, measured from the bottom

$$y_{bar.bot} := \frac{(A_t \cdot y_t) + (A_b \cdot y_b) + (A_w \cdot y_w)}{A_t + A_b + A_w} = 4.672\ in$$

distance from bottom of the section to the ENA

$$y_{bar.top} := d - y_{bar.bot} = 7.428\ in$$

distance from the top of the section to the ENA

$$I_x := \left(\frac{1}{12}\ t_w \cdot h^3 + A_w \cdot \left(y_w - y_{bar.bot}\right)^2\right) \hookleftarrow \quad = 373.286\ in^4$$
$$+ \left(\frac{1}{12}\ b_b \cdot {t_b}^3 + (A_b) \cdot \left(y_b - y_{bar.bot}\right)^2\right) \hookleftarrow$$
$$+ \left(\frac{1}{12}\ b_t \cdot {t_t}^3 + (A_t) \cdot \left(y_t - y_{bar.bot}\right)^2\right)$$

$$I_y := \frac{1}{12} \cdot t_b \cdot {b_b}^3 + \frac{1}{12} \cdot t_t \cdot {b_t}^3 + \frac{1}{12} \cdot h \cdot {t_w}^3 = 98.064\ in^4$$

$$J := \frac{1}{3} \cdot b_b \cdot {t_b}^3 + \frac{1}{3} \cdot b_t \cdot {t_t}^3 + \frac{1}{3} \cdot h_0 \cdot {t_w}^3 = 1.6\ in^4$$

Find Sx for the bottom and top

$$S_{xtop} := \frac{I_x}{y_{bar.top}} = 50.252\ in^3$$

$$S_{xbot} := \frac{I_x}{y_{bar.bot}} = 79.904\ in^3$$

Torsional Properties:

$$d' := d - \frac{t_t + t_b}{2} = 11.495\ in$$

$$\alpha := \frac{1}{1 + \left(\frac{b_t}{b_b}\right)^3 \cdot \left(\frac{t_t}{t_b}\right)} = 0.889$$

$$C_w := \frac{(d')^2 \cdot {b_t}^3 \cdot t_t \cdot \alpha}{12} = 1279.067\ in^6$$

$$\alpha := \frac{{b_b}^3 \cdot t_b}{{b_t}^3 \cdot t_t + {b_b}^3 \cdot t_b} \cdot h_0 = 10.218\ in$$

$$W_{no.top} := \frac{\alpha \cdot b_t}{2} = 30.653\ in^2 \qquad W_{no.bot} := \frac{h_0 - \alpha}{2} \cdot b_b = 7.663\ in^2$$

$$S_{wt} := \frac{W_{no.top} \cdot b_t \cdot t_t}{4} = 27.818\ in^4 \qquad S_{wb} := \frac{W_{no.bot} \cdot b_b \cdot t_b}{4} = 13.909\ in^4$$

$$Q_{ft} := \left(\left(\frac{b_t}{2} - t_w\right) \cdot t_t\right) \cdot \left(y_{bar.top} - \frac{t_t}{2}\right) = 11.252\ in^3$$

$$Q_{fb} := \left(\left(\frac{b_b}{2} - t_w\right) \cdot t_b\right) \cdot \left(y_{bar.bot} - \frac{t_b}{2}\right) = 14.829\ in^3$$

$$A_{w2} := \left(y_{bar.top} - t_t\right) \cdot t_w = 2.661\ in^2$$

$$Q_w := \left(A_t + A_{w2}\right) \cdot \frac{\left(A_t \cdot \left(y_{bar.top} - \frac{t_t}{2}\right) + A_{w2} \cdot \frac{y_{bar.top} - t_t}{2}\right)}{A_t + A_{w2}} = 34.945\ in^3$$

Loads:

$A := 207.9\ in^2$

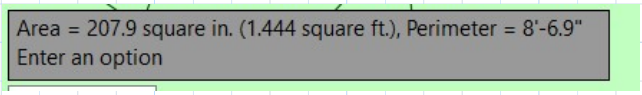

area of wet concrete wet beam is taking - calculated using AutoCAD

$w_{CIP} := 150\ pcf \cdot A = 216.563\ plf$ cast-in-place concrete load - only one side

Demands:

$M_u := \frac{w_{CIP} \cdot L^2}{8} = 14.203\ kip \cdot ft$

$t_u := w_{CIP} \cdot e = 0.054\ \frac{kip \cdot in}{in}$

Bending Stresses:

From AISC Design Guide 9 Section 4.5:

$\sigma_{bx.compressive} := \frac{-M_u}{S_{xtop}} = -3.392\ ksi$ $\sigma_{bx.tensile} := \frac{M_u}{S_{xbot}} = 2.133\ ksi$

Torsional Stresses:

From AISC Design Guide 9:

$a := \sqrt{\frac{E \cdot C_w}{G \cdot J}} = 46.136\ in$

Appendix B - Case 4 (Distributed Torsional Moment)

$\alpha := 0.5$

$x := \frac{L}{a} = 5.958$

Midspan (z/L = 0.5)

$z := 0.5 \cdot L$

$$\theta''_m := \frac{d^2}{dz^2}\left(\frac{t_u \cdot a^2}{G \cdot J}\left(\frac{L^2}{2 \cdot a^2} \cdot \left(\frac{z}{L} - \frac{z^2}{L^2}\right) + \cosh\left(\frac{z}{a}\right) - \tanh\left(\frac{L}{2 \cdot a}\right) \cdot \sinh\left(\frac{z}{a}\right) - 1.0\right)\right) = -2.79 \cdot 10^{-6}\ \frac{rad}{in^2}$$

$$\theta'''_m := \frac{d^3}{dz^3}\left(\frac{t_u \cdot a^2}{G \cdot J}\left(\frac{L^2}{2 \cdot a^2} \cdot \left(\frac{z}{L} - \frac{z^2}{L^2}\right) + \cosh\left(\frac{z}{a}\right) - \tanh\left(\frac{L}{2 \cdot a}\right) \cdot \sinh\left(\frac{z}{a}\right) - 1.0\right)\right) = -6.77 \cdot 10^{-21}\ \frac{rad}{in^3}$$

Supports (z/L = 0.0)

$z := 0.0 \cdot L$

$$\theta'_s := \frac{d}{dz}\left(\frac{t_u \cdot a^2}{G \cdot J}\left(\frac{L^2}{2 \cdot a^2} \cdot \left(\frac{z}{L} - \frac{z^2}{L^2}\right) + \cosh\left(\frac{z}{a}\right) - \tanh\left(\frac{L}{2 \cdot a}\right) \cdot \sinh\left(\frac{z}{a}\right) - 1.0\right)\right) = \left(2.84 \cdot 10^{-4}\right)\ \frac{rad}{in}$$

$$\theta'''_s := \frac{d^3}{dz^3}\left(\frac{t_u \cdot a^2}{G \cdot J}\left(\frac{L^2}{2 \cdot a^2} \cdot \left(\frac{z}{L} - \frac{z^2}{L^2}\right) + \cosh\left(\frac{z}{a}\right) - \tanh\left(\frac{L}{2 \cdot a}\right) \cdot \sinh\left(\frac{z}{a}\right) - 1.0\right)\right) = -6.70 \cdot 10^{-8}\ \frac{rad}{in^3}$$

Normal Stresses Due to Warping

From AISC Design Guide 9 Section 4.1.3: At midspan

$\sigma_{wm.top} := E \cdot W_{no.top} \cdot \theta''_m = -2.482\ ksi$ $\sigma_{wm.bot} := E \cdot W_{no.bot} \cdot \theta''_m = -0.62\ ksi$

$sg\_placement := 0.5\ in$ 0.5 inches from edge

$$\sigma_{wm.top} := \sigma_{wm.top} \cdot \frac{3\ in - sg\_placement}{3\ in} = -2.068\ ksi$$

$$\sigma_{wm.bot} := \sigma_{wm.bot} \cdot \frac{6\ in - sg\_placement}{6\ in} = -0.569\ ksi$$

Limit States - Service

Rotation out of Plane

$$t := w_{CIP} \cdot e = 0.054 \ \frac{kip \cdot in}{in}$$

$$\alpha := 0.5$$

$$z := 0.5 \cdot L$$

$$\theta_m := \frac{t \cdot a^2}{G \cdot J}\left(\frac{L^2}{2 \cdot a^2} \cdot \left(\frac{z}{L} - \frac{z^2}{L^2}\right) + \cosh\left(\frac{z}{a}\right) - \tanh\left(\frac{L}{2 \cdot a}\right) \cdot \sinh\left(\frac{z}{a}\right) - 1.0\right) = 1.341 \ deg$$

$\theta_m = 1.341 \ deg$ <= $\theta_{max} := 3.0 \ deg$

Vertical Deflection

$$\Delta_T := \frac{5 \cdot w_{CIP} \cdot L^4}{384 \cdot E \cdot I_x} = 0.124 \ in \quad <= \quad \Delta_{Limit} := \frac{L}{360} = 0.764 \ in$$

Stresses on Shape

$\sigma_{bx.compressive} + \sigma_{wm.top} = -5.46$ ***ksi***

$\sigma_{bx.compressive} - \sigma_{wm.top} = -1.324$ ***ksi***

$\sigma_{bx.compressive} = -3.392$ ***ksi***

$\sigma_{bx.tensile} = 2.133$ ***ksi***

$\sigma_{bx.tensile} - \sigma_{wm.bot} = 2.702$ ***ksi***

$\sigma_{bx.tensile} + \sigma_{wm.bot} = 1.564$ ***ksi***

A Shape Construction Check: Test 2

Check **edge beam** under **one-sided wet concrete load**
- **Torsionally fixed:** Design Guide 9 Case 7 - distributed torsion
- **Flexurally fixed**
- Lb = L

Limit States:
- Yielding under normal stress
- LTB
- Rotation out of plane
- Vertical deflection

Assumptions:

- Cb = 1.0
- top flange smaller than bottom flange
- top flange in compression, bottom flange in tension
- unstiffened shear design
- end conditions are flexurally and torsionally pinned (restrained from warping)
- Grade 50 steel
- E = 29,000 ksi
- G = 11,200 ksi
- Unit weight of steel is 490 pcf
- **Only considering wet concrete load, no other loads**

Steel Beam Properties:

$d := 12.1\ in$ full depth
$b_t := 6\ in$ width of top flange
$b_b := 12\ in$ width of bottom flange
$t_t := 0.605\ in$ thickness of top flange
$t_b := 0.605\ in$ thickness of bottom flange
$t_w := 0.390\ in$ thickness of web
$h := d - t_t - t_b = 10.89\ in$ height of web only
$h_0 := h + (0.5\ t_t) + (0.5\ t_b) = 11.495\ in$ center of top flange to center of bottom flange

$A_t := t_t \cdot b_t = 3.63\ in^2$ area of top flange
$A_b := t_b \cdot b_b = 7.26\ in^2$ area of bottom flange
$A_w := t_w \cdot h = 4.247\ in^2$ area of web

$A := A_t + A_b + A_w = 15.137\ in^2$ total approximate area

$f_y := 50\ ksi$
$E := 29000\ ksi$
$G := 11200\ ksi$
$C_b := 1.0$
$\gamma_s := 0.490\ \frac{kip}{ft^3}$

$L := 22.906\ ft$ span length
$s := 6\ ft$ spacing between beams
$e := 3\ in$ eccentricity of concrete panel distributed load

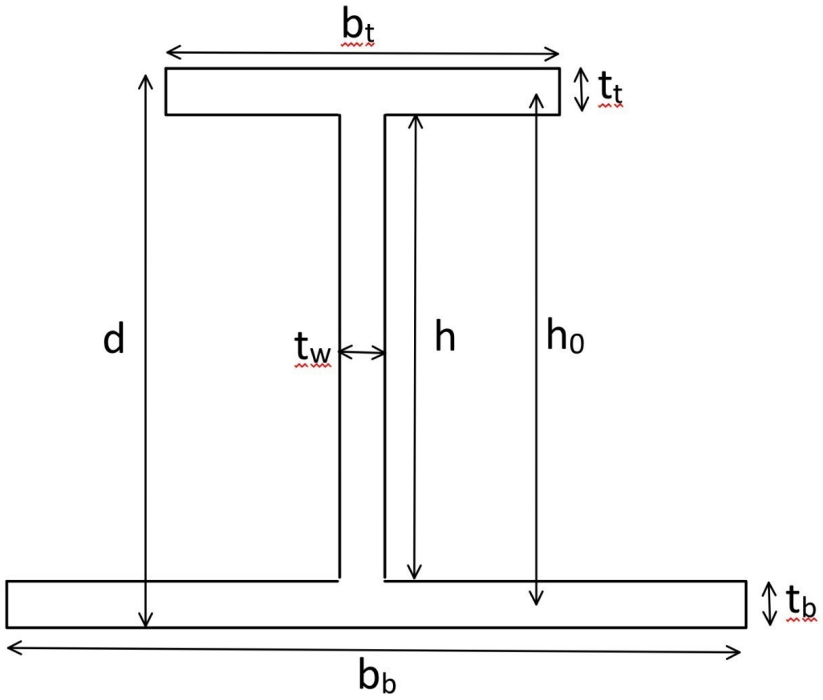

Steel Beam Section Properties:

From Eric's equations:

$$y_t := d - \frac{t_t}{2} = 11.798\ in$$

$$y_b := \frac{t_b}{2} = 0.303\ in$$

$$y_w := t_b + \frac{h}{2} = 6.05\ in$$

distances to centroids of each part of the section, measured from the bottom

$$y_{bar.bot} := \frac{(A_t \cdot y_t) + (A_b \cdot y_b) + (A_w \cdot y_w)}{A_t + A_b + A_w} = 4.672\ in$$

distance from bottom of the section to the ENA

$$y_{bar.top} := d - y_{bar.bot} = 7.428\ in$$

distance from the top of the section to the ENA

$$I_x := \left(\frac{1}{12}\ t_w \cdot h^3 + A_w \cdot \left(y_w - y_{bar.bot}\right)^2\right) \hookleftarrow \quad = 373.286\ in^4$$
$$+ \left(\frac{1}{12}\ b_b \cdot {t_b}^3 + (A_b) \cdot \left(y_b - y_{bar.bot}\right)^2\right) \hookleftarrow$$
$$+ \left(\frac{1}{12}\ b_t \cdot {t_t}^3 + (A_t) \cdot \left(y_t - y_{bar.bot}\right)^2\right)$$

$$I_y := \frac{1}{12} \cdot t_b \cdot {b_b}^3 + \frac{1}{12} \cdot t_t \cdot {b_t}^3 + \frac{1}{12} \cdot h \cdot {t_w}^3 = 98.064\ in^4$$

$$J := \frac{1}{3} \cdot b_b \cdot {t_b}^3 + \frac{1}{3} \cdot b_t \cdot {t_t}^3 + \frac{1}{3} \cdot h_0 \cdot {t_w}^3 = 1.6\ in^4$$

Find Sx for the bottom and top

$$S_{xtop} := \frac{I_x}{y_{bar.top}} = 50.252\ in^3$$

$$S_{xbot} := \frac{I_x}{y_{bar.bot}} = 79.904\ in^3$$

Torsional Properties:

$$d' := d - \frac{t_t + t_b}{2} = 11.495\ in$$

$$\alpha := \frac{1}{1 + \left(\frac{b_t}{b_b}\right)^3 \cdot \left(\frac{t_t}{t_b}\right)} = 0.889$$

$$C_w := \frac{(d')^2 \cdot {b_t}^3 \cdot t_t \cdot \alpha}{12} = 1279.067\ in^6$$

$$\alpha := \frac{{b_b}^3 \cdot t_b}{{b_t}^3 \cdot t_t + {b_b}^3 \cdot t_b} \cdot h_0 = 10.218\ in$$

$$W_{no.top} := \frac{\alpha \cdot b_t}{2} = 30.653\ in^2 \qquad W_{no.bot} := \frac{h_0 - \alpha}{2} \cdot b_b = 7.663\ in^2$$

$$S_{wt} := \frac{W_{no.top} \cdot b_t \cdot t_t}{4} = 27.818\ in^4 \qquad S_{wb} := \frac{W_{no.bot} \cdot b_b \cdot t_b}{4} = 13.909\ in^4$$

$$Q_{ft} := \left(\left(\frac{b_t}{2} - t_w\right) \cdot t_t\right) \cdot \left(y_{bar.top} - \frac{t_t}{2}\right) = 11.252\ in^3$$

$$Q_{fb} := \left(\left(\frac{b_b}{2} - t_w\right) \cdot t_b\right) \cdot \left(y_{bar.bot} - \frac{t_b}{2}\right) = 14.829\ in^3$$

$$A_{w2} := \left(y_{bar.top} - t_t\right) \cdot t_w = 2.661\ in^2$$

$$Q_w := \left(A_t + A_{w2}\right) \cdot \frac{\left(A_t \cdot \left(y_{bar.top} - \frac{t_t}{2}\right) + A_{w2} \cdot \frac{y_{bar.top} - t_t}{2}\right)}{A_t + A_{w2}} = 34.945\ in^3$$

Loads:

$A := 207.9\ in^2$

Area = 207.9 square in. (1.444 square ft.), Perimeter = 8'-6.9"
Enter an option

area of wet concrete wet beam is taking - calculated using AutoCAD

$w_{CIP} := 150\ pcf \cdot A = 216.563\ plf$ cast-in-place concrete load - only one side

Demands:

$M_u := \frac{w_{CIP} \cdot L^2}{24} = 4.734\ kip \cdot ft$

$t_u := w_{CIP} \cdot e = 0.054\ \frac{kip \cdot in}{in}$

Bending Stresses:

From AISC Design Guide 9 Section 4.5:

$\sigma_{bx.compressive} := \frac{-M_u}{S_{xtop}} = -1.131\ ksi$ $\sigma_{bx.tensile} := \frac{M_u}{S_{xbot}} = 0.711\ ksi$

Torsional Stresses:

From AISC Design Guide 9:

$a := \sqrt{\frac{E \cdot C_w}{G \cdot J}} = 46.136\ in$

Appendix B - Case 4 (Distributed Torsional Moment)

$\alpha := 0.5$

$x := \frac{L}{a} = 5.958$

Midspan (z/L = 0.5)

$z := 0.5 \cdot L$

$$\theta''_m := \frac{d^2}{dz^2}\left(\frac{t_u \cdot L \cdot a}{2\ G \cdot J}\left(\left(\frac{1+\cosh\left(\frac{L}{a}\right)}{\sinh\left(\frac{L}{a}\right)}\right)\cdot\left(\cosh\left(\frac{z}{a}\right)-1.0\right)+\frac{z}{a}\cdot\left(1-\frac{z}{L}\right)-\sinh\left(\frac{z}{a}\right)\right)\right) = -2.16\cdot10^{-6}\ \frac{rad}{in^2}$$

$$\theta'''_m := \frac{d^3}{dz^3}\left(\frac{t_u \cdot L \cdot a}{2\ G \cdot J}\left(\left(\frac{1+\cosh\left(\frac{L}{a}\right)}{\sinh\left(\frac{L}{a}\right)}\right)\cdot\left(\cosh\left(\frac{z}{a}\right)-1.0\right)+\frac{z}{a}\cdot\left(1-\frac{z}{L}\right)-\sinh\left(\frac{z}{a}\right)\right)\right) = -7.83\cdot10^{-20}\ \frac{rad}{in^3}$$

Supports (z/L = 0.0)

$z := 0.0 \cdot L$

$$\theta'_s := \frac{d}{dz}\left(\frac{t_u \cdot L \cdot a}{2\ G \cdot J}\left(\left(\frac{1+\cosh\left(\frac{L}{a}\right)}{\sinh\left(\frac{L}{a}\right)}\right)\cdot\left(\cosh\left(\frac{z}{a}\right)-1.0\right)+\frac{z}{a}\cdot\left(1-\frac{z}{L}\right)-\sinh\left(\frac{z}{a}\right)\right)\right) = \left(2.61\cdot10^{-20}\right)\ \frac{rad}{in}$$

$$\theta'''_s := \frac{d^3}{dz^3}\left(\frac{t_u \cdot L \cdot a}{2\ G \cdot J}\left(\left(\frac{1+\cosh\left(\frac{L}{a}\right)}{\sinh\left(\frac{L}{a}\right)}\right)\cdot\left(\cosh\left(\frac{z}{a}\right)-1.0\right)+\frac{z}{a}\cdot\left(1-\frac{z}{L}\right)-\sinh\left(\frac{z}{a}\right)\right)\right) = -2.01\cdot10^{-7}\ \frac{rad}{in^3}$$

Normal Stresses Due to Warping

From AISC Design Guide 9 Section 4.1.3: At midspan

$\sigma_{wm.top} := E \cdot W_{no.top} \cdot \theta''_m = -1.923\ ksi$ $\sigma_{wm.bot} := E \cdot W_{no.bot} \cdot \theta''_m = -0.481\ ksi$

$sg\_placement := 0.5\ in$ 0.5 inches from edge

$$\sigma_{wm.top} := \sigma_{wm.top} \cdot \frac{3\ in - sg\_placement}{3\ in} = -1.602\ ksi$$

$$\sigma_{wm.bot} := \sigma_{wm.bot} \cdot \frac{6\ in - sg\_placement}{6\ in} = -0.441\ ksi$$

Limit States - Service

Rotation out of Plane

$$t := w_{CIP} \cdot e = 0.054 \ \frac{kip \cdot in}{in}$$

$$\alpha := 0.5$$

$$z := 0.5 \cdot L$$

$$\theta_m := \frac{t \cdot L \cdot a}{2\ G \cdot J} \left(\left(\frac{1 + \cosh\left(\frac{L}{a}\right)}{\sinh\left(\frac{L}{a}\right)} \right) \cdot \left(\cosh\left(\frac{z}{a}\right) - 1.0 \right) + \frac{z}{a} \cdot \left(1 - \frac{z}{L} \right) - \sinh\left(\frac{z}{a}\right) \right) = 0.662 \ deg$$

$\theta_m = 0.662 \ deg$ <= $\theta_{max} := 4.0 \ deg$

Vertical Deflection

$$\Delta_T := \frac{w_{CIP} \cdot L^4}{384 \cdot E \cdot I_x} = 0.025 \ in \quad <= \quad \Delta_{Limit} := \frac{L}{360} = 0.764 \ in$$

Stresses on Shape

$\sigma_{bx.compressive} + \sigma_{wm.top} = -2.733$ ***ksi***

$\sigma_{bx.compressive} - \sigma_{wm.top} = 0.472$ ***ksi***

$\sigma_{bx.compressive} = -1.131$ ***ksi***

$\sigma_{bx.tensile} = 0.711$ ***ksi***

$\sigma_{bx.tensile} - \sigma_{wm.bot} = 1.152$ ***ksi***

$\sigma_{bx.tensile} + \sigma_{wm.bot} = 0.27$ ***ksi***

A Shape Composite System Service Check: Test 3 Case B

Check **center beam** composite section under **100 psf live load**
- **Flexurally pinned**
- Lb = 0

Limit States:
- Yielding under normal stress
- Vertical deflection

Assumptions:

- Cb = 1.0
- top flange smaller than bottom flange
- top flange in compression, bottom flange in tension
- unstiffened shear design
- end conditions are flexurally and torsionally pinned (restrained from warping)
- Grade 50 steel
- E = 29,000 ksi
- G = 11,200 ksi
- Unit weight of steel is 490 pcf
- **Only considering live load, no other loads**

Steel Beam Properties:

$d := 12.1\ in$	full depth
$b_t := 6\ in$	width of top flange
$b_b := 12\ in$	width of bottom flange
$t_t := 0.605\ in$	thickness of top flange
$t_b := 0.605\ in$	thickness of bottom flange
$t_w := 0.390\ in$	thickness of web
$h := d - t_t - t_b = 10.89\ in$	height of web only
$h_0 := h + (0.5\ t_t) + (0.5\ t_b) = 11.495\ in$	center of top flange to center of bottom flange

$A_t := t_t \cdot b_t = 3.63\ in^2$	area of top flange
$A_b := t_b \cdot b_b = 7.26\ in^2$	area of bottom flange
$A_w := t_w \cdot h = 4.247\ in^2$	area of web
$A := A_t + A_b + A_w = 15.137\ in^2$	total approximate area

$f_y := 50\ ksi$

$E := 29000\ ksi$	$L := 22.906\ ft$	span length - web bolt to web bolt
$G := 11200\ ksi$	$s := 6\ ft$	spacing between beams
$C_b := 1.0$	$seat\_width := 2\ in$	seat width of precast panels
$\gamma_s := 0.490\ \frac{kip}{ft^3}$		

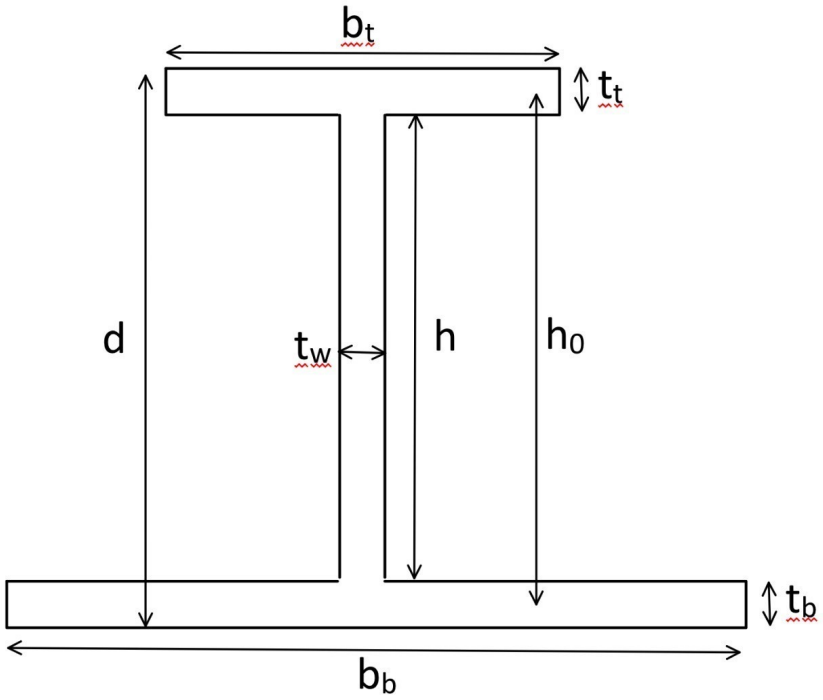

Steel Beam Section Properties:

$$y_t := d - \frac{t_t}{2} = 11.798\ in$$

$$y_b := \frac{t_b}{2} = 0.303\ in$$

distances to centroids of each part of the section, measured from the bottom

$$y_w := t_b + \frac{h}{2} = 6.05\ in$$

$$y_{bar.bot} := \frac{\left(A_t \cdot y_t\right) + \left(A_b \cdot y_b\right) + \left(A_w \cdot y_w\right)}{A_t + A_b + A_w} = 4.672\ in$$

distance from bottom of the section to the ENA

$$y_{bar.top} := d - y_{bar.bot} = 7.428\ in$$

distance from the top of the section to the ENA

$$I_{xs} := \left(\frac{1}{12}\ t_w \cdot h^3 + A_w \cdot \left(y_w - y_{bar.bot}\right)^2\right) \hookleftarrow \quad = 373.286\ in^4$$
$$+ \left(\frac{1}{12}\ b_b \cdot {t_b}^3 + \left(A_b\right) \cdot \left(y_b - y_{bar.bot}\right)^2\right) \hookleftarrow$$
$$+ \left(\frac{1}{12}\ b_t \cdot {t_t}^3 + \left(A_t\right) \cdot \left(y_t - y_{bar.bot}\right)^2\right)$$

$$I_y := \frac{1}{12} \cdot t_b \cdot {b_b}^3 + \frac{1}{12} \cdot t_t \cdot {b_t}^3 + \frac{1}{12} \cdot h \cdot {t_w}^3 = 98.064\ in^4$$

$$J := \frac{1}{3} \cdot b_b \cdot {t_b}^3 + \frac{1}{3} \cdot b_t \cdot {t_t}^3 + \frac{1}{3} \cdot h_0 \cdot {t_w}^3 = 1.6\ in^4$$

Composite Section Properties:

$f'c := 5395\ psi^2$ day-of f'c

$E_c := 57000 \cdot \sqrt{f'c} = \left(4.187 \cdot 10^6\right)\ psi$ concrete modulus of elasticity

$n := \frac{E}{E_c} = 6.927$

$y_e := y_{bar.top} = 7.428\ in$ distance to elastic neutral axis from top of steel

$D_d := 8\ in$ depth of concrete not in slab

$D_s := 5\ in$ depth of concrete slab

$A_{c1} := \left(b_b - 2 \cdot seat\_width\right) \cdot D_d = 64\ in^2$ area of concrete by steel web

$B_e := s = 6\ ft$ effective width

$A_c := D_s \cdot B_e$ area of concrete slab

$D_c := D_d + D_s - t_b - h = 1.505\ in$ depth of concrete above steel section

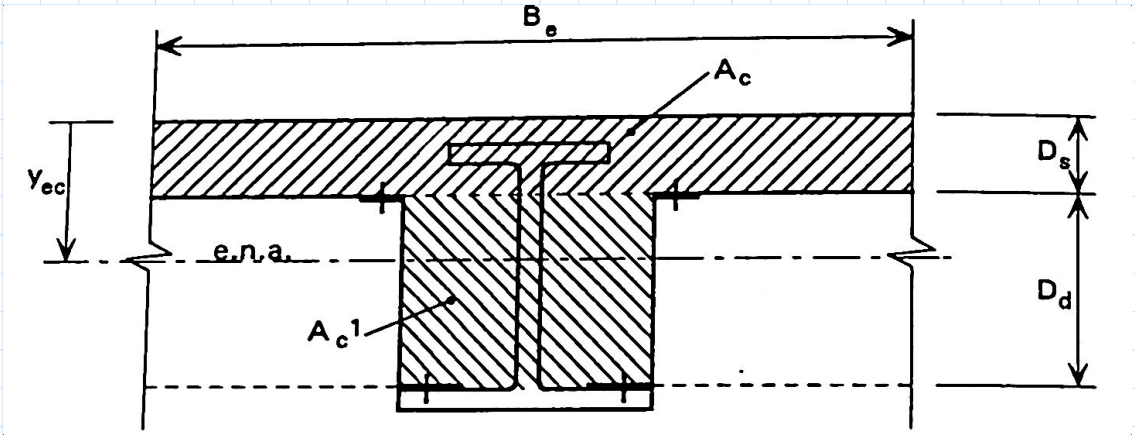

$$y_{ec} := \frac{A \cdot y_e + \left(\frac{A_{c1}}{n} \cdot \left(d - \left(0.5 \cdot D_d\right) - t_b\right)\right) + \left(\frac{A_c}{n} \cdot \left(0.5 \cdot D_s - D_c\right)\right)}{A + \frac{A_c + A_{c1}}{n}} = 3.057\ in$$

$$I_x := I_{xs} + A \cdot \left(y_e - y_{ec}\right)^2 + \frac{A_c}{n} \cdot \left(0.5 \cdot D_s - D_c - y_{ec}\right)^2 + \frac{A_c}{n} \cdot \frac{D_s^{\,2}}{12} = 1223.045\ in^4$$
$$+ \frac{A_{c1}}{n} \cdot \left(d - 0.5 \cdot D_d - t_b - y_{ec}\right)^2 + \frac{A_{c1}}{n} \cdot \frac{D_d^{\,2}}{12}$$

$$y_{ec.top} := y_{ec} = 3.057\ in$$

$$y_{ec.bot} := d - y_{ec.top} = 9.043\ in$$

Find Sx for the bottom and top

$$S_{xtop} := \frac{I_x}{y_{ec.top}} = 400.069\ in^3 \qquad S_{xbot} := \frac{I_x}{y_{ec.bot}} = 135.249\ in^3$$

Demands:

$actuator\_load := 18.6\ kip$

$dist\_factor := 0.5$

$$P_L := \frac{actuator\_load \cdot dist\_factor}{2} = 4.65\ kip$$

$$a := \frac{L - 6\ ft}{2} = 8.453\ ft$$

$$M_u := P_L \cdot a = 39.306\ kip \cdot ft$$

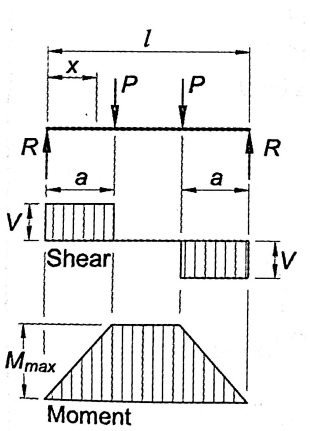

Bending Stresses:

From AISC Design Guide 9 Section 4.5:

$$\sigma_{bx.compressive} := \frac{-M_u}{S_{xtop}} = -1.179\ ksi \qquad \sigma_{bx.tensile} := \frac{M_u}{S_{xbot}} = 3.487\ ksi$$

Limit States - Service

Vertical Deflection

$$\Delta := \frac{P_L \cdot a}{24 \cdot E \cdot I_x} \cdot \left(3 \cdot L^2 - 4 \cdot a^2\right) = 0.103\ in \qquad <= \qquad \Delta_{Limit} := \frac{L}{360} = 0.764\ in$$

Stresses on Shape

$\sigma_{bx.compressive} = -1.179$ ***ksi***

$\sigma_{bx.compressive} = -1.179$ ***ksi***

$\sigma_{bx.compressive} = -1.179$ ***ksi***

$\sigma_{bx.tensile} = 3.487$ ***ksi***

$\sigma_{bx.tensile} = 3.487$ ***ksi***

$\sigma_{bx.tensile} = 3.487$ ***ksi***

A Shape Composite System Service Check: Test 3 Case B

Check **center beam** composite section under **100 psf live load**
- **Flexurally pinned**
- Lb = 0

Limit States:
- Yielding under normal stress
- Vertical deflection

Assumptions:

- Cb = 1.0
- top flange smaller than bottom flange
- top flange in compression, bottom flange in tension
- unstiffened shear design
- end conditions are flexurally and torsionally pinned (restrained from warping)
- Grade 50 steel
- E = 29,000 ksi
- G = 11,200 ksi
- Unit weight of steel is 490 pcf
- **Only considering live load, no other loads**

Steel Beam Properties:

$d := 12.1\ in$ full depth

$b_t := 6\ in$ width of top flange

$b_b := 12\ in$ width of bottom flange

$t_t := 0.605\ in$ thickness of top flange

$t_b := 0.605\ in$ thickness of bottom flange

$t_w := 0.390\ in$ thickness of web

$h := d - t_t - t_b = 10.89\ in$ height of web only

$h_0 := h + (0.5\ t_t) + (0.5\ t_b) = 11.495\ in$ center of top flange to center of bottom flange

$A_t := t_t \cdot b_t = 3.63\ in^2$ area of top flange

$A_b := t_b \cdot b_b = 7.26\ in^2$ area of bottom flange

$A_w := t_w \cdot h = 4.247\ in^2$ area of web

$A := A_t + A_b + A_w = 15.137\ in^2$ total approximate area

$f_y := 50\ ksi$

$E := 29000\ ksi$

$G := 11200\ ksi$

$C_b := 1.0$

$\gamma_s := 0.490\ \frac{kip}{ft^3}$

$L := 22.906\ ft$ span length - web bolt to web bolt

$s := 6\ ft$ spacing between beams

$seat\_width := 2\ in$ seat width of precast panels

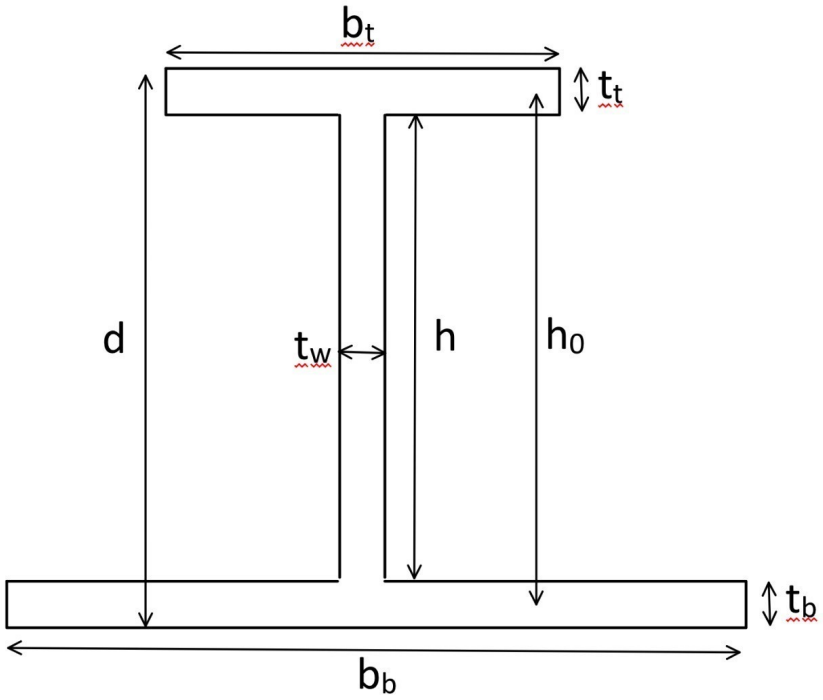

Steel Beam Section Properties:

$$y_t := d - \frac{t_t}{2} = 11.798\ in$$

$$y_b := \frac{t_b}{2} = 0.303\ in$$

distances to centroids of each part of the section, measured from the bottom

$$y_w := t_b + \frac{h}{2} = 6.05\ in$$

$$y_{bar.bot} := \frac{(A_t \cdot y_t) + (A_b \cdot y_b) + (A_w \cdot y_w)}{A_t + A_b + A_w} = 4.672\ in$$

distance from bottom of the section to the ENA

$$y_{bar.top} := d - y_{bar.bot} = 7.428\ in$$

distance from the top of the section to the ENA

$$I_{xs} := \left(\frac{1}{12}\ t_w \cdot h^3 + A_w \cdot (y_w - y_{bar.bot})^2\right) \hookleftarrow = 373.286\ in^4$$
$$+ \left(\frac{1}{12}\ b_b \cdot {t_b}^3 + (A_b) \cdot (y_b - y_{bar.bot})^2\right) \hookleftarrow$$
$$+ \left(\frac{1}{12}\ b_t \cdot {t_t}^3 + (A_t) \cdot (y_t - y_{bar.bot})^2\right)$$

$$I_y := \frac{1}{12} \cdot t_b \cdot {b_b}^3 + \frac{1}{12} \cdot t_t \cdot {b_t}^3 + \frac{1}{12} \cdot h \cdot {t_w}^3 = 98.064\ in^4$$

$$J := \frac{1}{3} \cdot b_b \cdot {t_b}^3 + \frac{1}{3} \cdot b_t \cdot {t_t}^3 + \frac{1}{3} \cdot h_0 \cdot {t_w}^3 = 1.6\ in^4$$

Composite Section Properties:

$f'c := 5395\ psi^2$ day-of f'c

$E_c := 57000 \cdot \sqrt{f'c} = \left(4.187 \cdot 10^6\right)\ psi$ concrete modulus of elasticity

$n := \frac{E}{E_c} = 6.927$

$y_e := y_{bar.top} = 7.428\ in$ distance to elastic neutral axis from top of steel

$D_d := 8\ in$ depth of concrete not in slab

$D_s := 5\ in$ depth of concrete slab

$A_{c1} := \left(b_b - 2 \cdot seat\_width\right) \cdot D_d = 64\ in^2$ area of concrete by steel web

$B_e := s = 6\ ft$ effective width

$A_c := D_s \cdot B_e$ area of concrete slab

$D_c := D_d + D_s - t_b - h = 1.505\ in$ depth of concrete above steel section

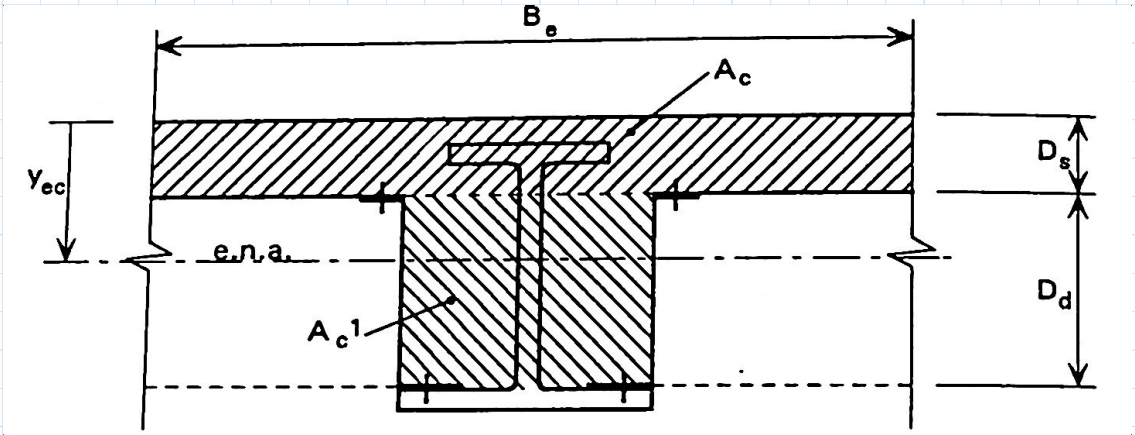

$$y_{ec} := \frac{A \cdot y_e + \left(\frac{A_{c1}}{n} \cdot \left(d - \left(0.5 \cdot D_d\right) - t_b\right)\right) + \left(\frac{A_c}{n} \cdot \left(0.5 \cdot D_s - D_c\right)\right)}{A + \frac{A_c + A_{c1}}{n}} = 3.057\ in$$

$$I_x := I_{xs} + A \cdot \left(y_e - y_{ec}\right)^2 + \frac{A_c}{n} \cdot \left(0.5 \cdot D_s - D_c - y_{ec}\right)^2 + \frac{A_c}{n} \cdot \frac{D_s^{\,2}}{12} = 1223.045\ in^4$$
$$+ \frac{A_{c1}}{n} \cdot \left(d - 0.5 \cdot D_d - t_b - y_{ec}\right)^2 + \frac{A_{c1}}{n} \cdot \frac{D_d^{\,2}}{12}$$

$$y_{ec.top} := y_{ec} = 3.057\ in$$

$$y_{ec.bot} := d - y_{ec.top} = 9.043\ in$$

Find Sx for the bottom and top

$$S_{xtop} := \frac{I_x}{y_{ec.top}} = 400.069\ in^3 \qquad S_{xbot} := \frac{I_x}{y_{ec.bot}} = 135.249\ in^3$$

Demands:

$actuator\_load := 18.6\ kip$

$dist\_factor := 0.5$

$P_L := \frac{actuator\_load \cdot dist\_factor}{2} = 4.65\ kip$

$a := \frac{L - 6\ ft}{2} = 8.453\ ft$

$b := L - a = 14.453\ ft$

$end\_moment := \frac{P_L \cdot \left(a^2 \cdot b + b^2 \cdot a\right)}{L^2} = 24.801\ kip \cdot ft$

$M_u := P_L \cdot a - end\_moment = 14.505\ kip \cdot ft$

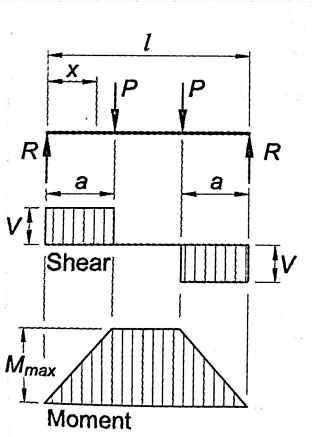

Bending Stresses:

From AISC Design Guide 9 Section 4.5:

$\sigma_{bx.compressive} := \frac{-M_u}{S_{xtop}} = -0.435\ ksi$ $\sigma_{bx.tensile} := \frac{M_u}{S_{xbot}} = 1.287\ ksi$

Limit States - Service

Vertical Deflection

$x := a$

$\Delta_t := -\frac{\frac{P_L \cdot (x)^3}{6} + \left(\left(-P_L \cdot a^2 \cdot \frac{b}{L^2} - P_L \cdot b^2 \cdot \frac{a}{L^2}\right) \cdot \frac{(x)^2}{2}\right)}{E \cdot I_x} = 0.0204\ in$

<= $\Delta_{Limit} := \frac{L}{360} = 0.764\ in$

Stresses on Shape

$\sigma_{bx.compressive} = -0.435$ ***ksi***

$\sigma_{bx.compressive} = -0.435$ ***ksi***

$\sigma_{bx.compressive} = -0.435$ ***ksi***

$\sigma_{bx.tensile} = 1.287$ ***ksi***

$\sigma_{bx.tensile} = 1.287$ ***ksi***

$\sigma_{bx.tensile} = 1.287$ ***ksi***

APPENDIX C

FLEXURAL RIGIDITY VALUES SAMPLE CALCULATION

The following is a sample calculation for finding the flexural rigidity values of the system using the deflections from Test 3.

Test 3 Beam Flexural Rigidity

Calculate flexural rigidity for **center beam** based on **experimental deflection**
- Test 3 Case B: 100 psf loading

Parameters

$L := 22.906\ ft$
$E := 29000\ ksi$

For center beam under 100 psf equivalent loading:

$dist\_factor := 0.44$
$I_x := 1223\ in^4$
$actuator\_load := 18.6\ kip$
$\Delta := 0.0891\ in$

$$P_L := \frac{actuator\_load \cdot dist\_factor}{2} = 4.092\ kip$$

$$a := \frac{L - 6\ ft}{2} = 8.453\ ft$$

$b := L - a = 14.453\ ft$

Calculate EI

$$E \cdot I_x = \left(3.547 \cdot 10^7\right)\ kip \cdot in^2$$

Pinned Equation

$$EI := \frac{P_L \cdot a}{24 \cdot \Delta}\left(3 \cdot L^2 - 4 \cdot a^2\right) = \left(3.6008 \cdot 10^7\right)\ kip \cdot in^2$$

Fixed Equation

$x := a$

$$EI := \frac{\frac{P_L \cdot (x)^3}{6} + \left(\left(-P_L \cdot a^2 \cdot \frac{b}{L^2} - P_L \cdot b^2 \cdot \frac{a}{L^2}\right) \cdot \frac{(x)^2}{2}\right)}{-\Delta} = \left(7.1333 \cdot 10^6\right)\ kip \cdot in^2$$

APPENDIX D

CRITICAL LIMIT STATE CAPACITY CALCULATIONS

The following is the calculation for the capacities of the following limit states for this system: yielding, LTB, and live load deflection.

Limit State Capacities

The capacities of the following limit states are calculated:
- Yielding
- LTB of the top flange
- Vertical deflection due to live load

The resistance factor for flexure is used for yielding and LTB.

Steel Beam Properties:

$d := 12.1\ in$ full depth

$b_t := 6\ in$ width of top flange

$b_b := 12\ in$ width of bottom flange

$t_t := 0.605\ in$ thickness of top flange

$t_b := 0.605\ in$ thickness of bottom flange

$t_w := 0.390\ in$ thickness of web

$h := d - t_t - t_b = 10.89\ in$ height of web only

$h_0 := h + (0.5\ t_t) + (0.5\ t_b) = 11.495\ in$ center of top flange to center of bottom flange

$A_t := t_t \cdot b_t = 3.63\ in^2$ area of top flange

$A_b := t_b \cdot b_b = 7.26\ in^2$ area of bottom flange

$A_w := t_w \cdot h = 4.247\ in^2$ area of web

$A := A_t + A_b + A_w = 15.137\ in^2$ total approximate area

$f_y := 50\ ksi$

$E := 29000\ ksi$

$G := 11200\ ksi$

$C_b := 1.0$

$\gamma_s := 0.490\ \frac{kip}{ft^3}$

$L := 22.906\ ft$ span length - column bolt to column bolt

$s := 6\ ft$ spacing between beams

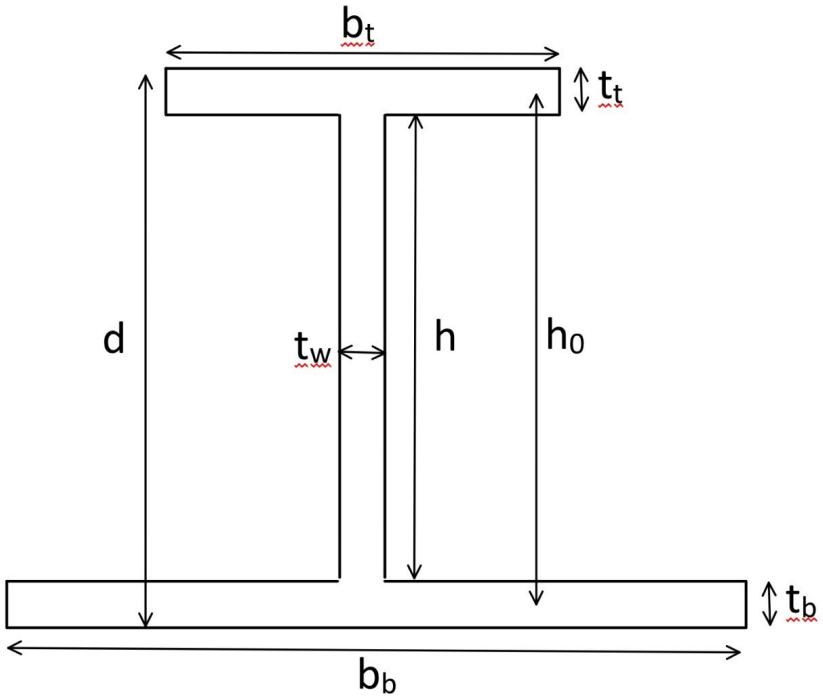

Steel Section Properties:

$$y_t := d - \frac{t_t}{2} = 11.798\ in$$

$$y_b := \frac{t_b}{2} = 0.303\ in$$

distances to centroids of each part of the section, measured from the bottom

$$y_w := t_b + \frac{h}{2} = 6.05\ in$$

$$y_{bar.bot} := \frac{(A_t \cdot y_t) + (A_b \cdot y_b) + (A_w \cdot y_w)}{A_t + A_b + A_w} = 4.672\ in$$

distance from bottom of the section to the ENA

$$y_{bar.top} := d - y_{bar.bot} = 7.428\ in$$

distance from the top of the section to the ENA

$$I_x := \left(\frac{1}{12}\ t_w \cdot h^3 + A_w \cdot \left(y_w - y_{bar.bot}\right)^2\right) \hookleftarrow = 373.286\ in^4$$
$$+ \left(\frac{1}{12}\ b_b \cdot {t_b}^3 + (A_b) \cdot \left(y_b - y_{bar.bot}\right)^2\right) \hookleftarrow$$
$$+ \left(\frac{1}{12}\ b_t \cdot {t_t}^3 + (A_t) \cdot \left(y_t - y_{bar.bot}\right)^2\right)$$

$$I_y := \frac{1}{12} \cdot t_b \cdot {b_b}^3 + \frac{1}{12} \cdot t_t \cdot {b_t}^3 + \frac{1}{12} \cdot h \cdot {t_w}^3 = 98.064\ in^4$$

$$J := \frac{1}{3} \cdot b_b \cdot {t_b}^3 + \frac{1}{3} \cdot b_t \cdot {t_t}^3 + \frac{1}{3} \cdot h_0 \cdot {t_w}^3 = 1.6\ in^4$$

Find Sx for the bottom and top

$$S_{xtop} := \frac{I_x}{y_{bar.top}} = 50.252\ in^3$$

$$S_{xbot} := \frac{I_x}{y_{bar.bot}} = 79.904\ in^3$$

Find Zx

$$A_{half} := \frac{A}{2} = 7.569\ in^2$$

$$y_p := \left\| \begin{array}{l} \text{if } A_{half} > A_b \\ \quad \left\| \frac{A_{half} - A_b}{t_w} + t_b \right. \\ \text{else} \\ \quad \left\| \frac{A_{half}}{b_b} \right. \end{array} \right. = 1.396\ in$$

PNA location from the bottom of the section

PNA is located in the web:

$$UPWA := \left(d - t_t - y_p\right) \cdot t_w = 3.939\ in^2$$

upper plastic web area
aka web area in compression

$$LPWA := A_w - UPWA = 0.309\ in^2$$

lower plastic web area
aka web area in tension

Calculate areas/centroids of compression and tension based on PNA location:

$$AC := A_t + UPWA = 7.569\ in^2$$

compression area

$$AT := A_b + LPWA = 7.569\ in^2$$

tension area

$$yC := \frac{\left(UPWA \cdot \frac{d - t_t - y_p}{2}\right) + \left(A_t \cdot \left(d - \frac{t_t}{2} - y_p\right)\right)}{AC} = 7.616\ in$$

distance to centroid of compression area

$$yT := \frac{\left(LPWA \cdot \frac{y_p - t_b}{2}\right) + \left(A_b \cdot \left(y_p - \frac{t_b}{2}\right)\right)}{AT} = 1.065\ in$$

distance to centroid of tension area

$$Z_x := \left(AC \cdot yC\right) + \left(AT \cdot yT\right) = 65.706\ in^3$$

Calculate capacity for LTB of top flange

From AISC F4:

$L_b := L = 22.906\ ft$ braced at each end

$S_{xc} := S_{xtop} = 50.252\ in^3$ top is in compression

$S_{xt} := S_{xbot} = 79.904\ in^3$ bottom is in tension

$$F_L := \left\| \begin{array}{l} \text{if } \frac{S_{xt}}{S_{xc}} \geq 0.7 \\ \quad \| 0.7 \cdot f_y \\ \text{else} \\ \quad \| \max\left(f_y \cdot \frac{S_{xt}}{S_{xc}}, 0.5 \cdot f_y\right) \end{array} \right\| = 35\ ksi$$

$h_c := \left(y_{bar.top} - t_t\right) \cdot 2 = 13.647\ in$ hc and hp equations from AISC Table B4.1b

$h_p := \left(d - y_p - t_t\right) \cdot 2 = 20.198\ in$

$a_w := \frac{h_c \cdot t_w}{b_t \cdot t_t} = 1.47$ aw calculated with compression values - top flange in this case

$r_t := \frac{b_t}{\sqrt{12 \cdot \left(1 + \frac{1}{6}\ a_w\right)}} = 1.553\ in$ effective radius of gyration for I-shaped members (approximation from what we did earlier)

$L_p := 1.1 \cdot r_t \cdot \sqrt{\frac{E}{f_y}} = 41.133\ in$

$F_{cr} := \frac{C_b \cdot \pi^2 \cdot E}{\left(\frac{L_b}{r_t}\right)^2} \cdot \sqrt{1 + 0.078 \cdot \frac{J}{S_{xc} \cdot h_0} \cdot \left(\frac{L_b}{r_t}\right)^2} = 25.152\ ksi$

$L_r := 1.95 \cdot r_t \cdot \frac{E}{F_L} \cdot \sqrt{\frac{J}{S_{xc} \cdot h} + \sqrt{\left(\frac{J}{S_{xc} \cdot h_0}\right)^2 + 6.76 \cdot \left(\frac{F_L}{E}\right)^2}} = 17.5\ ft$

$M_p := Z_x \cdot f_y = \left(3.285 \cdot 10^3\right)\ kip \cdot in$

$M_y := min\left(f_y \cdot S_{xc}, f_y \cdot S_{xt}\right) = \left(2.513 \cdot 10^3\right)\ kip \cdot in$

$M_{yc} := f_y \cdot S_{xc} = \left(2.513 \cdot 10^3\right)\ kip \cdot in$

$$\lambda := \frac{h_c}{t_w} = 34.991$$

λ equations from AISC Table B4.1b

$$\lambda_{rw} := 5.70 \cdot \sqrt{\frac{E}{f_y}} = 137.274$$

$$\lambda_{pw} := min\left(\frac{\frac{h_c}{h_p} \cdot \sqrt{\frac{E}{f_y}}}{\left(0.54 \cdot \frac{M_p}{M_y} - 0.09\right)^2}, \lambda_{rw}\right) = 42.872$$

$$I_{yc} := \frac{1}{12} \cdot t_t \cdot {b_t}^3 = 10.89\ in^4$$

$$R_{pc} := \left\| \begin{array}{l} \text{if } \frac{I_{yc}}{I_y} > 0.23 \\ \quad \left\| \begin{array}{l} \text{if } \lambda \le \lambda_{pw} \\ \quad \left\| \frac{M_p}{M_{yc}} \right. \\ \text{else} \\ \quad \left\| min\left(\frac{M_p}{M_{yc}} - \left(\frac{M_p}{M_{yc}} - 1\right) \cdot \left(\frac{\lambda - \lambda_{pw}}{\lambda_{rw} - \lambda_{pw}}\right), \frac{M_p}{M_{yc}}\right) \right. \end{array} \right. \\ \text{else} \\ \quad \left\| 1.0 \right. \end{array} \right. = 1$$

$$M_{nLTB} := \left\| \begin{array}{l} \text{if } L_b \le L_p \\ \quad \left\| M_p \right. \\ \text{else if } L_b > L_r \\ \quad \left\| min\left(C_b \cdot F_{cr} \cdot S_{xc}, R_{pc} \cdot M_{yc}\right) \right. \\ \text{else} \\ \quad \left\| min\left(C_b \cdot \left(R_{pc} \cdot M_{yc} - \left(R_{pc} \cdot M_{yc} - F_L \cdot S_{xc}\right)\left(\frac{L_b - L_p}{L_r - L_p}\right)\right), R_{pc} \cdot M_{yc}\right) \right. \end{array} \right.$$

$$M_{nLTB} = 105\ kip \cdot ft$$

nominal moment due to LTB

$$f_{LTB.top} := \frac{M_{nLTB}}{S_{xtop}} = 25.152\ ksi$$

Resistance Factor for Flexure

$\phi_b := 0.90$

Yielding

$f_y := 50\ ksi$

$\phi f_y := \phi_b \cdot f_y = 45\ ksi$

LTB

$f_{LTB.top} = 25.152\ ksi$

$\phi f_{LTB} := \phi_b \cdot f_{LTB.top} = 22.637\ ksi$

Deflection

$\frac{L}{360} = 0.764\ in$

APPENDIX E

ULTIMATE LOAD CAPACITY CALCULATION

The following calculation finds the ultimate load capacity of the system if it were fully composite. It also calculates the moment the beam experienced at failure.

Composite Capacity

Steel Section Properties:

$d := 12.1\ in$
$b_t := 6\ in$
$b_b := 12\ in$
$t_t := 0.605\ in$
$t_b := 0.605\ in$
$t_w := 0.390\ in$
$h := d - t_t - t_b = 10.89\ in$
$h_0 := h + (0.5\ t_t) + (0.5\ t_b) = 11.495\ in$

$A_t := t_t \cdot b_t = 3.63\ in^2$
$A_b := t_b \cdot b_b = 7.26\ in^2$
$A_w := t_w \cdot h = 4.247\ in^2$

$A_s := A_t + A_b + A_w = 15.137\ in^2$

$L := 22.906\ ft$

$f_y := 50\ ksi$
$E := 29000\ ksi$
$G := 11200\ ksi$
$C_b := 1.0$
$\gamma_s := 0.490\ \frac{kip}{ft^3}$

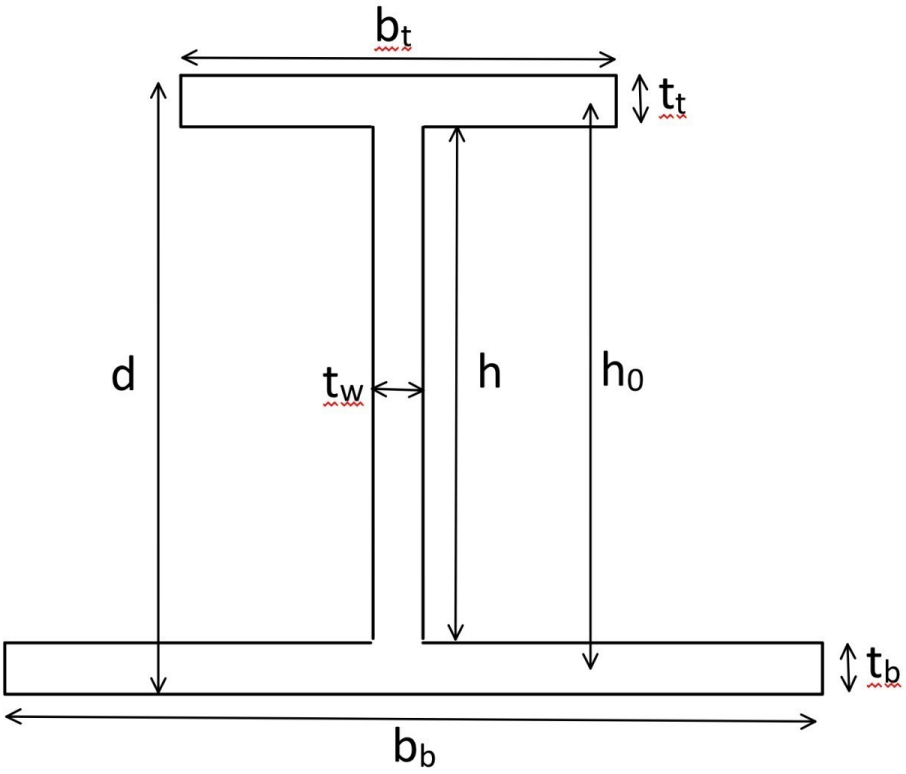

Concrete Section Properties:

$D_d := 8\ in$

$D_s := 5\ in$

$D_c := D_d + D_s - t_b - h = 1.505\ in$ depth of concrete slab on top of steel

$f'c := 5395\ psi$

$B_e := 6\ ft$

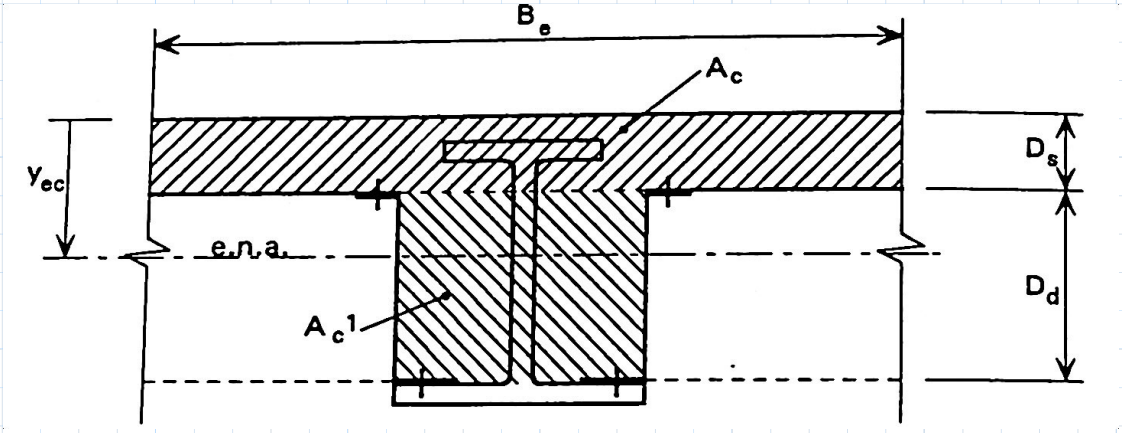

Calculate composite capacity

Check if plastic neutral axis (PNA) lies in concrete slab above the steel, hence no steel is in compression

$$a := \frac{A_s \cdot f_y}{0.85 \cdot f'c \cdot B_e} = 2.292\ in \qquad > \qquad D_c = 1.505\ in$$

PNA will lie within steel section

Check if PNA is in concrete slab and steel top flange.
Guess where the PNA is and iterate until C and T match

$y_{PNA} := 1.793\ in$ from top of concrete slab

$C_c := 0.85 \cdot f'c \cdot \left(\begin{matrix} \left\langle B_e \cdot D_c \right\rangle \\ + \left(\left\langle B_e - b_t \right\rangle \cdot \left\langle y_{PNA} - D_c \right\rangle \right) \end{matrix} \right) = 584.078\ kip$ force of concrete in compression

$C_s := f_y \cdot \left(b_t \cdot \left\langle y_{PNA} - D_c \right\rangle \right) = 86.4\ kip$ force of steel in compression

$C := C_c + C_s = 670.478\ kip$ total compressive force

$T := A_s \cdot f_y - C_s = 670.455\ kip$ force of steel in tension

Calculate moment arms and moment capacity

$$T_{centroid} := \frac{d + D_c - y_{PNA}}{2} + y_{PNA} = 7.699\ in$$

$$C_{c.centroid} := \frac{\left(B_e \cdot D_c \cdot \frac{D_c}{2} \right) + \left\langle B_e - b_t \right\rangle \cdot \left\langle y_{PNA} - D_c \right\rangle \cdot \left(\frac{y_{PNA} - D_c}{2} + D_c \right)}{B_e \cdot D_c + \left\langle B_e - b_t \right\rangle \cdot \left\langle y_{PNA} - D_c \right\rangle} = 0.886\ in$$

$$C_{s.centroid} := \frac{y_{PNA} - D_c}{2} + D_c = 1.649\ in$$

$d_c := T_{centroid} - C_{c.centroid} = 6.813\ in$

$d_s := T_{centroid} - C_{s.centroid} = 6.05\ in$

$M_c := C_c \cdot d_c + C_s \cdot d_s = 375\ kip \cdot ft$

Mc is the moment capacity under all loads. In order to find the capacity under live load only, the moment due to dead loads must be subtracted out.

$$w_C := 64\ psf \cdot 6\ ft = 384\ plf$$

$$w_{CIP} := 150\ pcf \cdot 415.3\ in^2 = 432.6\ plf$$

$$M_D := \frac{w_C \cdot L^2}{8} + \frac{w_{CIP} \cdot L^2}{8} = 53.6\ kip \cdot ft$$

$$M_L := M_c - M_D = 322\ kip \cdot ft$$

Calculate moment experienced due to failure

$$actuator\_load := 94\ kip$$

$$dist\_factor := 0.44$$

$$P_L := \frac{actuator\_load \cdot dist\_factor}{2} = 20.68\ kip$$

$$a := \frac{(L - 6\ ft)}{2} = 8.453\ ft$$

$$M_{exp} := P_L \cdot a = 175\ kip \cdot ft$$

$$\frac{M_{exp}}{M_L} = 0.544$$